ISSN 1810-0384

ADVANCES IN ELECTROMETALLURGY

No. 2 Volume 12 2014

CAMBRIDGE INTERNATIONAL SCIENCE PUBLISHING

Advances in Electrometallurgy is a cover-to-cover English translation of *Sovremennaya Elektrometallurgiya*, published four times a year by International Association 'Welding' at the E.O. Paton Electric Welding Institute, National Academy of Sciences of Ukraine, 11 Bozhenko Street, 03680 Kyiv, Ukraine

Published by

Cambridge International Science Publishing Ltd
7 Meadow Walk, Great Abington, Cambridge CB21 6AZ, England
Tel: +44 (0) 1223 893295; Fax: +44 (0) 1223 894539
email: ver@cisp-publishing.com; http://www.cisp-publishing.com

Advances in Electrometallurgy 2014 ***12*** *(2) 77–85*
Translated from Sovremennaya Elektrometallurgiya 2014 ***12*** *(2) 3–9*

ELECTROSLAG TECHNOLOGY

Alloying titanium with carbon in the process of chamber electroslag remelting

A.D. Ryabtsev[1], A.A. Troyanskii[1], B. Friedrich[1], V.V. Pashinskii[2], F.L. Leokha[1] and S.N. Ratiev[1]

[1]Donetsk National Technical University; [2]RWTH Aachen University, Aachen, Germany

The feasibility of titanium hardening by its alloying with carbon in the process of chamber electroslag remelting (CESR) was considered. It was shown experimentally that adding carbon to titanium in the form of powder of different fractions increases greatly its strength whilst retaining a sufficient level of ductility. CESR as a metallurgical process allows adding of carbon into the metal and providing its uniform distribution throughout the ingot body. Ref. 20, Table 1, Figures 13.

Key words: *titanium; alloying; carbon; powder; nanoparticles; chamber electroslag remelting; properties*

Titanium and its alloys occupy as structural materials an important position in the human activity. The unique properties of these materials (high specific strength and resistance to impact loading, corrosion resistance) allow to use these materials for the manufacture of structural components in aviation and rocket construction and also in many other areas of the industry [1, 2].

There are also a large number of applications of titanium in medicine. At the present time, alloys VT-6S (Grade 5) and unalloyed titanium VT1-0, VT-1-00 (Grade 1-2) are used quite widely for prosthetic applications in medicine [2–6]. Vanadium and aluminium in the VT-6S alloy greatly increase the strength properties of titanium. At the same time, the products of oxidation of vanadium, present in titanium, are very dangerous for the health of people [3, 7].

The titanium of the grades VT-1-0, VT-1-00 presents no risks to the health of people. However, the parameters of the strength properties of these materials are almost 50% lower than those of the VT-6S alloy. Therefore, the increase of the strength parameters of this type of titanium as a result of alloying with elements 'safe' from the medical viewpoint is a very important task.

One such safe element is obviously oxygen [8–12]. Carbon is also interesting in this case [13].

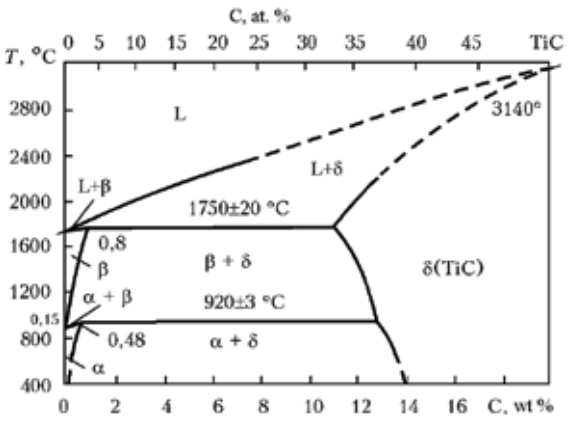

Fig. 1. Equilibrium diagram of the Ti–C binary system.

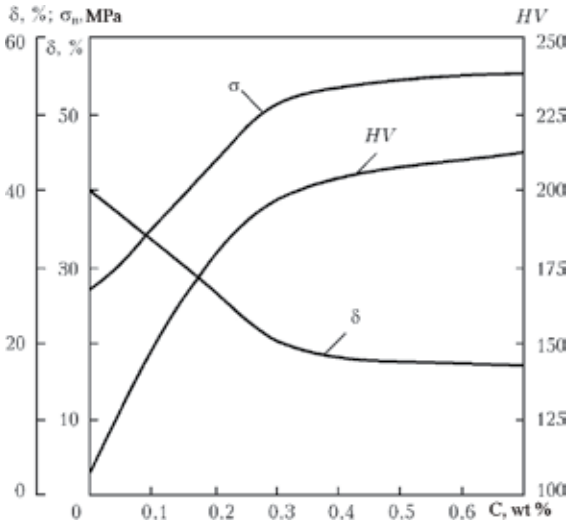

Fig. 2. Effect of carbon on the hardness, strength and ductility of titanium.

Carbon belongs in the group of the elements stabilising the α-phase increasing the polymorphous transformation temperature of titanium. Titanium, interacting with carbon, forms narrow ranges of β-and α-solutions and a chemically stable compound – titanium carbide (Fig. 1).

The solubility of carbon in β-Ti at the eutectic temperature is equal to 0.138 wt.% (0.55 at.%) and is almost constant at low temperatures. The maximum solubility of carbon in the α-titanium at 920°C is approximately 0.5 wt.% (2 at.%) and decreases with the reduction of temperature to 0.05 wt.%

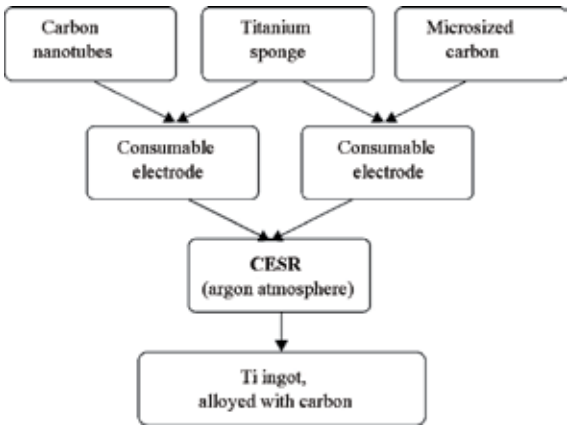

Fig. 3. Diagram of the introduction of carbon to titanium in chamber electroslag remelting.

Fig. 4. Blocks of titanium sponge with the carbon powder pressed into the axial orifice.

(0.2 at.%) at 20 °C. At the carbon content greater than 0.05 wt.% carbides may precipitate in the structure of titanium [14].

Carbon, like oxygen is an efficient element hardening titanium (Fig. 2). The hardening coefficient of carbon is 7...8 MPa per 0.01 wt.% C [14].

The carbon content of titanium of up to 0.35 wt.% can be regarded as an economic alloying element greatly changing the strength and ductility characteristics of titanium. A further increase of the carbon concentration of the metal changes only slightly the mechanical characteristics.

Fig. 5. The chamber electroslag furnace based on equipment A-550.

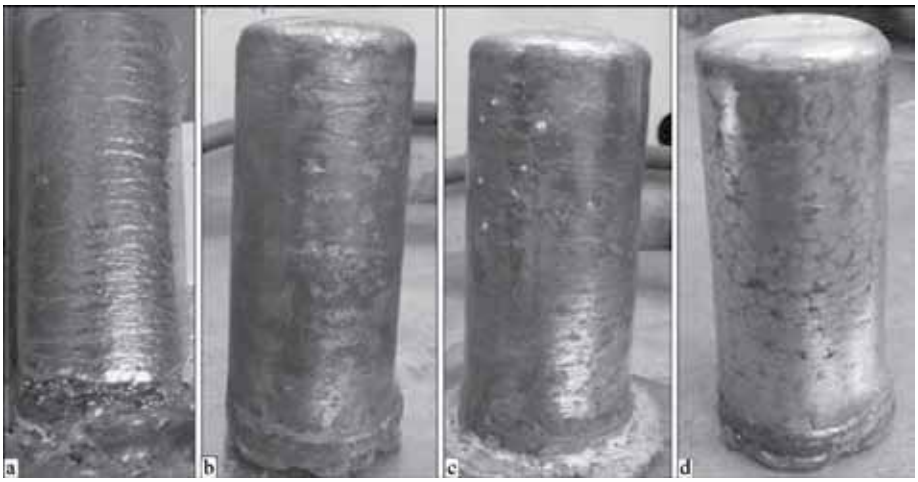

Fig. 6. General view of titanium ingots: *a*) without addition of carbon; *b–d*) with the addition of carbon, wt.%; here and in Fig. 9, 10, 13: *a*) 0.0 19; *b*) 0.130; *c*) 0.340; *c*) 0.300.

Thus, varying the carbon content of titanium in the range from 0 to 0.35 wt.% it is possible to obtain the required ratio of the values of the strength and ductility characteristics, and also increase the strength as a result of the toughness margin of the metal.

An important factor from the metallurgical viewpoint is the uniform distribution of carbon as the alloying element in the volume of the ingots and castings. To a certain extent, this can be achieved by remelting processes in electrometallurgy, including chamber electroslag remelting (CESR) [15–19].

The carbon material for alloying titanium was the powder of carbon (approximately 15 μm) and carbon nanotubes (CNT) (approximately 15 nm), mainly on the basis of the considerations of purity with respect to the impurities. In addition to this, the addition of dispersed refractory particles into the metal in chamber electroslag remelting is interesting also from the viewpoint of the effect of these particles on the structure of the cast titanium ingot.

In the investigations, attention was given to the method of introduction of carbon to titanium, shown in Fig. 3.

The following experimental procedure was used. Blocks with a diameter 41 mm and 150...200 mm long, compacted from the titanium sponge TG-100, were drilled through along the axis. The required amount of the carbon powder of different fractions was placed in the orifice with a diameter of 4.0 and 6.5 mm (Fig. 4). The blanks were welded in consumable electrodes 550...650 mm long by argon-shielded arc welding.

Experimental melts were produced in the argon atmosphere in a chamber electroslag furnace with a power of 724 kW in a copper watercooled solidification mode with a diameter of 70 mm (Fig. 5).

The electrodes with the carbon powder were remelted under a flux produced from pure

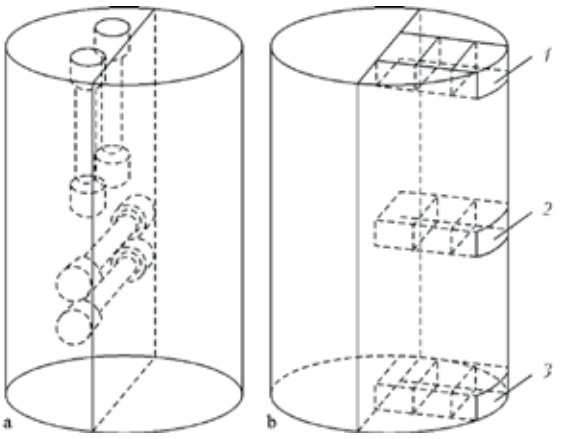

Fig. 7. Diagrams of cutting ingots into specimens for mechanical tests (*a*), four metallographic studies (*b*): *1*) the top; *2*) the centre; *3*) the bottom.

Table 1. Variants of melts and carbon, oxygen and nitrogen content in the produced metal

Melt no.	Electrode composition	Calculated C content, wt.%	Content in ingot, wt.%		
			C	O	N
1	TG-100 titanium sponge	–	0.030 0.019	0.04 0.06	0.020 0.013
2	TG-100+CNT titanium sponge	0.140	0.030 0.130	0.04 0.10	0.020 0.021
3	TG-100 + CNT titanium sponge	0.350	0.030 0.340	0.04 0.14	0.020 0.021
4	TG-100 titanium sponge + carbon micro-powder	0.350	0.030 0.300	0.04 0.14	0.020 0.019

Comment. The numerator gives the distribution of elements in Ti sponge, the denominator – in ingot.

CaF_2 of grade Ch, and the reference specimens (without carbon) – under the flux CaF_2 +2.5 wt.% Ca. The flux was melted directly in the solidification mode, using the 'solid' start. The starting mixture was produced from titanium shavings and the working flux.

The electrical parameters of remelting were maintained at U = 36.0 V; I = 2.0...2.5 kA ensuring the high quality of the surface of the ingots (Fig. 6).

Specimens were taken from the produced ingots in accordance with the method shown in Fig. 7 chemical analysis, metallographic examination and mechanical tests.

The chemical composition of the metal was determined in a Spectromax optical emission spectrometer manufactured by Spectro (Germany), the gas content was determined in the laboratories of the E.O. Paton Electric Welding Institute, the Zaporozh'e Titanium-Magnesium Concenr and the Aachen University (Germany) in TN-114, RO-316 and RH-2, RH-3 gas analysers manufactured by LECO (USA).

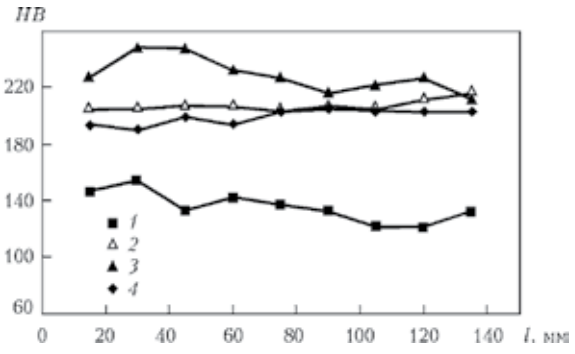

Fig. 8. Hardness HB of titanium ingots produced by chamber electroslag remelting, here and in Nos. 11 and 12: No. 1–4 – numbers of melts (Table 1); *l is* the distance from the base to the line of head trimmings of the ingot.

The metallographic studies of the metal were carried out in optical microscopes Axiovert 40 MAT (Carl Zeiss) and Neophot-2 (magnifications from 50 to 5000), and also a JEOL JSM-6490LV scanning electron microscope (JEOL, Japan), fitted with an energy dispersing spectrometer INCA Penta FET ×3 (Oxford Instruments, England), a INCA Wave wave spectrometer (Oxford Instruments, England) and a detector of the diffraction of backscattered electrons HKL (Oxford Instruments, England).

The mechanical tests and hardening measurements were carried out in accordance with the standard procedures (GOST 1497–84).

The results analysis of the characteristic ingots are presented in Table 1.

It may be seen that the carbon content in the experimental ingots (melt No. 2–4) is close to the calculated values and equals 0.13...0.34 wt.%. The degree of pickup of carbon, introduced in the form of the carbon

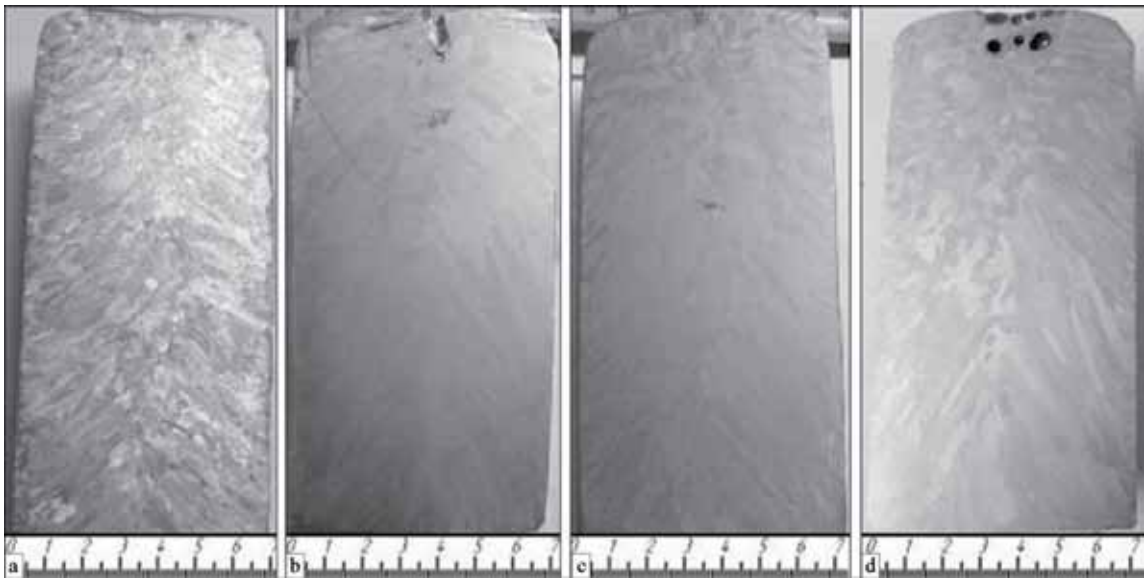

Fig. 9. Microstructure of titanium of ingots produced by chamber electroslag remelting; for *a–d* see Fig. 6.

nanotubes and the micro powder, was high and equalled respectively 92 and 86 wt.%.

The metal of the experimental ingots also showed, in comparison with the reference specimens, the enquiries of the oxygen content by a factor of 2.5–3 which in turn may also increase the strength of titanium [14, 20]. The increase of the mass fraction of oxygen

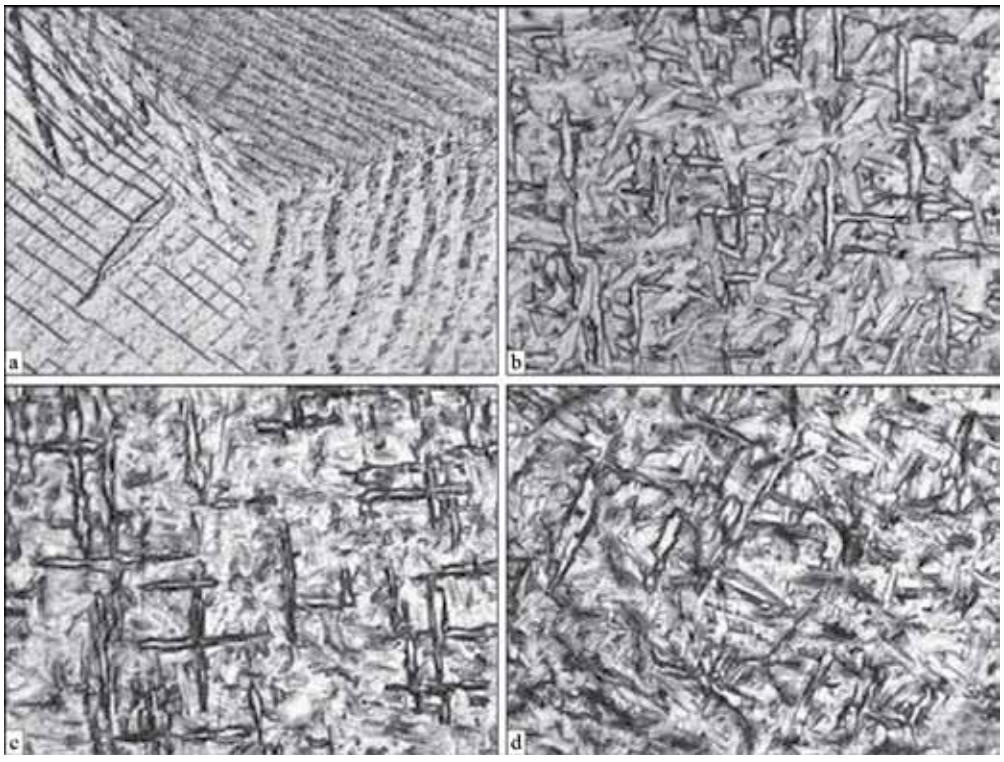

Fig. 10. Structure (×200) of titanium, alloyed with carbon; for the designations *a–d* refer to Fig. 6.

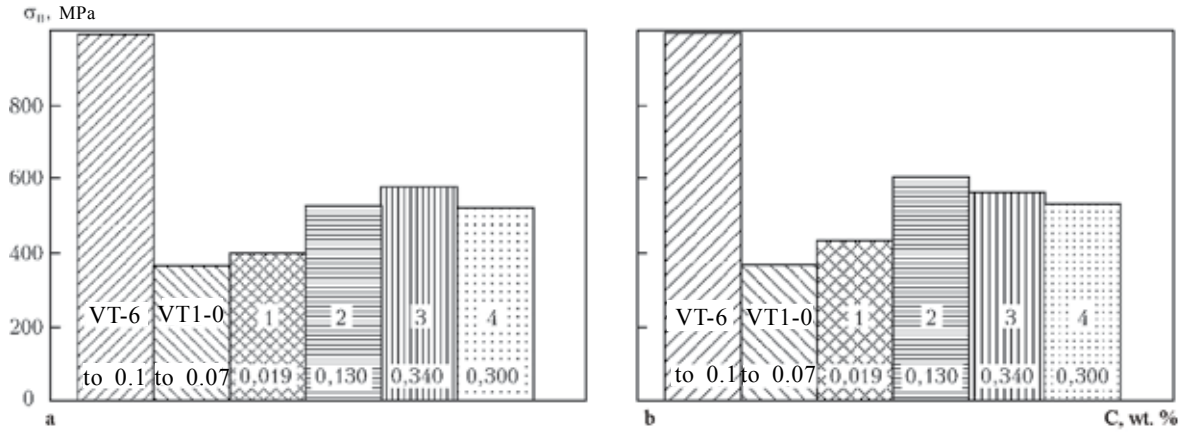

Fig. 11. Ultimate strength of failure of titanium with different carbon content in the horizontal (*a*) and vertical (*b*) planes of the ingot.

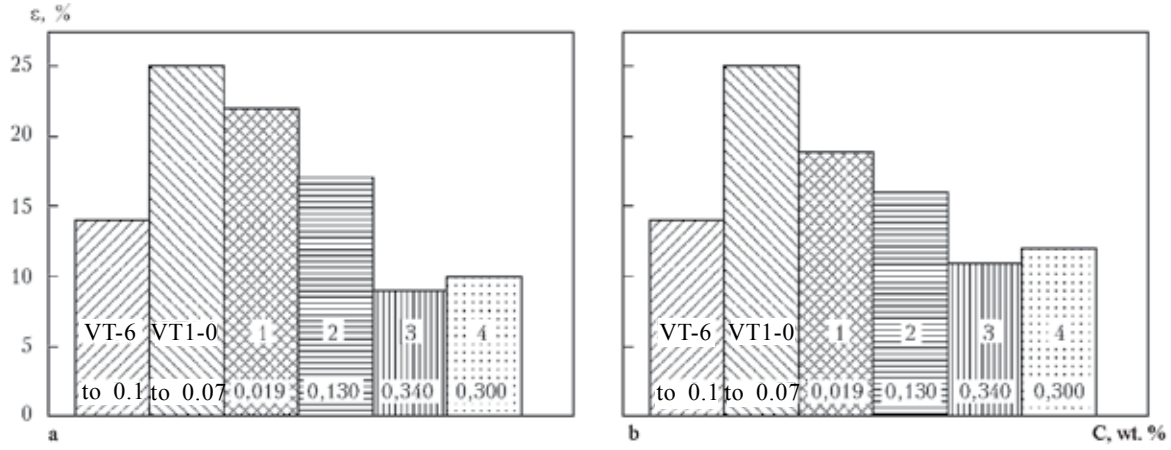

Fig. 12. Elongation of titanium with different carbon content in the horizontal (*a*) and vertical (*b*) planes of the ingot.

is evidently associated with the adsorption capacity of carbon nano powders and micro powders and also with the partial surface oxidation of carbon in the stages of preparation of the electrode blocks followed by melting them. The more developed surface of the nano tubes also results in the supply of a large amount of oxygen to titanium.

One of the indirect indicators of the presence of impurities in titanium and of the distribution is the hardness of titanium. Figure 8 shows the values of hardness, measured along the axis in the height of the experimental ingots. It may be seen that the hardness of titanium correlates with the carbon content of titanium and increases with increase of the mass fraction of carbon in the metal. An exception is the melt No. 4 in which the carbon was introduced in the form of a micropowder. Evidently, this is associated with the lower oxygen content in comparison with the melt No. 3.

Figure 9 shows the macrostructures of the experimental titanium ingots. It may be seen that the metal, with the exception of the top parts of the ingots, is dense, without visible defects. Attention should be given to the reduced (in comparison with variant 1) contrast of etching the dendritic structure of titanium, alloyed with carbon in the form of nanotubes (melt 2 and 3). This may be associated with the change of the morphology

of the microstructure of the metal (Fig. 10). The addition of carbon to titanium in the form of the micropowder (melt 4) results in a slight expansion (in comparison with the melts 2 and 3) of the central zone of the equiaxed crystals.

The characteristic microstructures of titanium are presented in Fig. 10. It may be seen that the structure of the titanium of melt No. 1 (0.019 wt.% C) consists of larger grains of α-titanium with regular grain boundaries. This type of structure is characteristic of the alloys of unalloyed titanium. The addition of carbon (melts No. 2–4) results in the refining of the structure which becomes more fine-dispersed in comparison with the plate-shaped structure of commercial titanium (melt 1). When adding carbon in the form of nano powders and micro powders, the structure of the metal becomes acicular, with the random orientation of the needles. The structure is typical of the alloys in which the β–α transformation takes place in the conditions of inhibition of the transformation by the kinetic factors. The reason for this inhibition may be the higher carbon concentration of the β-phase.

The special feature of the structure formation in the titanium alloys with a higher carbon content is the formation of the excess second phase which is darker on the sections after etching. The morphology of the second phase differs and depends on the concentration and type of carbon, added to titanium. For example, the melt No. 2 (0.13% C) is characterised by the structure consisting of the non-oriented, approximately equiaxed crystals and of the elongated second phase distributed mostly in the form of thin interlayers at the grain boundaries, and also in the form of individual coalesced particles of the circular form.

The metal of the melt No. 3 (0.34 wt.% C) is characterised by the increase of both the amount of the second phase and also the thickness of the interlayers between the grain boundaries, leading to a reduction of the ductility. To determine the nature of the second phase, it is necessary to carry out additional investigations. However, the results

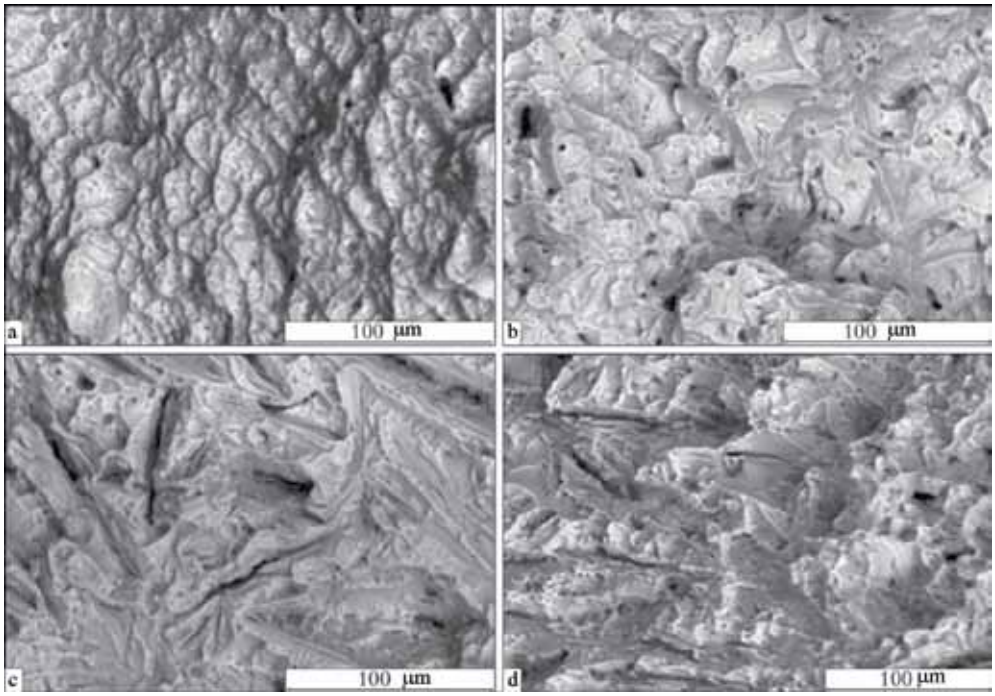

Fig. 13. Fractographs of fracture surfaces of the titanium specimens after mechanical tests, for *a–d* refer to Fig. 6, *a–c*) × 500; *c*) × 400.

of x-ray spectrum microanalysis indicate that the second phase is the high-carbon phase of the non-stoichiometric composition. The needles of the second phase intersect and the right-hand (Fig. 10). The structure may form due to the fact that the nanotubes, which did not react with titanium, act as unique 'nuclei' of the formation of the structure.

The structure of the metal of the melt No. 4 (0.300 wt.% C) is characterised by the random distribution of the needles of the second phase. The precipitates of this phase are thicker and susceptible to coalescence.

Important indicators of titanium as the structural materials are the mechanical properties of titanium. Figures 11 and 12 so the results of mechanical tests of the specimens taken from the experimental ingots. The mechanical properties of the VT6 and VT1-0 titanium in the deformed and annealed conditions are presented [2].

It may be seen that the metal of the comparison melt No. 1 is characterised by the highest ductility characteristics and the lowest strength properties. For example, the relatively elongation of this alloy is 22 and 19%, and tensile strength 400 and 435 Pa in the horizontal and vertical direction, respectively.

The strength of titanium of melt No. 2 equals 530 MPa across the axis of the ingot and is slightly higher (600 MPa) along the axis of the ingot. The relatively elongation, characterised in the ductility of the metal, decreases to 17 and 16%, respectively.

The specimen, produced from titanium melt No. 3, has the lowest ductility in the horizontal and vertical planes (9 and 12%, respectively) and the strength of this metal (580 and 564 MPa) is comparable with the values for the metal of the melt No. 2, in which the carbon content is 2.6 times smaller.

As regards the metal of melt No. 4, its ductility characteristics are lower than in the titanium melt No. 2, but slightly higher than in the titanium melt No. 3, and equal 10 and 15%. The strength is equal to 520 and 535 MPa in the horizontal and vertical direction, respectively.

It should also be mentioned that the large increase of the carbon content in the titanium of melts No. 3 and 4 does not lead to any large increase of the strength characteristics.

The above differences in the variation of the mechanical properties of the metal of the experimental melts No. 2–4 are evidently associated with the changes in the structure of the ingots alloyed to different degrees with carbon. For example, with increasing carbon content the structure of the metal transforms from plate -shaped to random needle structure with the formation of the second phase at the grain boundaries. With the increase in the metal of the thickness of the intergranular layer and circular inclusions of the second phase the mobility of dislocations the creases, and this has a negative effect on the ductility properties of the investigated metal.

Fractographic studies of the specimens of titanium after the mechanical tests (Figure 13) show that the fracture surface of the specimen of melt No. 1 consists of a system of micropores with circular boundaries, indicating that this metal is characterised by intragranular failure.

The structure of the fracture surfaces of the melts 3 and 4 consists of a set of flat faces, coinciding with the grain boundaries or slip planes. Therefore, the structure can be characterised as brittle.

The fractograph of the specimen of melt No. 2 has the intermediate structure with typical features of both fractures.

The results of investigations of the structures and fractographs of titanium, alloyed with carbon, its hardness and mechanical properties, indicate that the effect of carbon additions on the processes of structure formation depends not only on the carbon concentration but also the nature of the added particles.

Conclusions

1. It has been shown possible to alloy titanium with carbon in order to increase the strength characteristics without affecting the ductility characteristics.

2. Chamber electroslag remelting as a metallurgical process can be used for adding carbon to the metal and ensure the uniform distribution of the carbon in the body of the ingot.

3. The results of investigation of the structure and mechanical tests show that the increase of the carbon content of titanium results in the refining of the structure from the single-phase equiaxed structure, typical of commercial titanium, having the morphology of α-titanium (0.019 wt.% C) to the random needle-shaped two-phase structure and in the increase of the strength on average from 430 (0.019 wt.% C) to 560 MPa (0.130 wt.% C) whilst retaining the ductility at the level of 17 wt.%. A further increase of the carbon content in titanium to 0.34 wt.% does not leave to any significant increase of strength. The experiments also show that the application of carbon in the form of nanotubes for alloying of titanium is more efficient from the viewpoint of the pickup of the alloying element and obtaining the required degree of strengthening of the metal.

References

1. Aleksandrov, A.V., Titan, 2011, No. 1, 44–50.
2. Il'in, A.A., et al., Titanium alloy. Composition, structure, properties, VILS-MATI, Moscow, 2009.
3. Leyens, Ch. Titanium and titanium alloys. Fundamentals and applications, Wiley-VCH, Weinhem, 2003.
4. Disegi, J.A., Injury, 2000, **31**, suppl. 4, 4–17.
5. Hanawa, T., Materials Science Forum, 2006, **512**, 243–248.
6. Kolobov Yu.R., Nanotechnologies in Russia, 2009, **4**, No. 11–12, 758–775.
7. Oshida, Y. Bioscience and bioengineering of titanium materials, Elsevier, Amsterdam, 2007.
8. Ryabtsev, A.D., et al., Sovremen. elektrometallurgiya, 2007, No. 3, 3–6.
9. Ratiev, S.N., et al., Sovremen. elektrometallurgiya, 2010, No. 2, 8–12.
10. Ryabtsev, A.D., et al., Proc. 2011 Int. Symp. on Liquid Metal Proc. and Casting, LMPC, Nancy, 2011, 39–42.
11. Ryabtsev, A.D., et al., Sovremen. elektrometallurgiya, 2012, No. 1, 7–10.
12. Snizhko, O.A., et al., Titan, 2013, No. 1, 14–19.
13. Panotskii D.A., Boreslavskii, A.L., Titan, 2006, No. 1, 20–23.
14. Kornilov, I.I., Titaniu. Sources, properties metal chemistry and application, Nauka, Moscow, 1975.
15. Ryabtsev, A.D., et al., Slags and fluxes in modern metallurgy, Proc. Int. Workshopon metal-slag interactions, Aachen, Verlag, 2011, 175–188.
16. Ryabtsev, A.D., et al., in: , LMPC, Santa Fe, USA, 2005, 120–136.
17. Ryabtsev, A.D., Troyanskii, A.A., Elektrometallurgiya, 2005. No. 4, 25–32.
18. Troyanskii A.A., Ryabtsev, A.D., Titan, 2007, No. 1, 28–31.
19. Reitz J., et al., Proc. Europ. Metallurgical Conf. EMC 2007, Dusseldorf, 2007, 17–23.
20. Eremenko, V.N. Titanium and its alloys, Academy of Sciences of the UkrSSR, Kiev, 1960.

Submitted 3.3.2014

Advances in Electrometallurgy 2014 ***12*** *(2) 86–91*
Translated from Sovremennaya Elektrometallurgiya 2014 ***12*** *(2) 10–14*

Electroslag melting of titanium billets with pulsed electric power supply

I.V. Protokovilov[1], A.T. Nazarchuk[1], V.B. Porokhon'ko[1], YU.P. Ivochkin[2] and I.O. Teplyakov[2]

[1]E.O. Paton Electric Welding Institute, Kiev;
[2]Joint Institute of High Temperatures, Russian Academy of Sciences, Moscow

Presented are the results of experiments on electroslag melting of titanium ingots at pulsed supply of process with electric power. To carry out the experimental melting, the power transformer TShP-10-1 was subjected to modification, that allowed realizing the electroslag process at a pulsed mode, adjusting the frequency and amplitude characteristics of pulses of operating voltage during melting. Experimental investigations were carried out in melting of 84 mm diameter ingots of titanium of Grade 4. From the experimental results the stability of electroslag process, its electrical conditions, formation of surface of ingots, their macrostucture and distribution of hardness in longitudinal section were evaluated. Two schemes were studied for pulsed supply of electroslag process at different duration of pulses and pauses of electric supply and voltage level at the pool during the pause. During experiments the feasibility of electroslag melting of titanium ingots at pulsed mode, keeping the stability of electroslag process and good formation of lateral surface of ingot, dense macrostructure without metallurgical defects was shown. Possibility of control of solidification of titanium ingots and refining of their cast structure by pulsed electric supply and appropriate potion heat input was established. Ref. 9, Table 1, Figures 5.

Key words: *electroslag remelting; pulsed electric supply; ingot; macrostructure; portion heat input*

The promising direction of increasing the efficiency of the process of electroslag remelting (ESR) is the development of different methods of influencing heat and mass transfer and solidification of the metal which make it possible to control the properties of the melted alloys already in the stage of melting the billet. One of these methods is the pulse power supply to the electroslag process supplying electric energy. The efficiency of application of the method for controlling the process of electroslag melting was described in [1, 2]. Since the slag and metal pools are characterised by the high level of thermal inertia, it is possible to change in a wide range of the conditions of pulsed supply to the electroslag process and, consequently, influence the heat and mass transfer and solidification of the ingot, whilst retaining the high-quality of formation of the ingot. However, the complicated nature of pulsed supply of high current (tens of kiloamperes) and expensive equipment greatly restricted the possibility of application of this method of influencing the electroslag process.

With the development of the advanced elemental base, in particular, the powerful power thyristors with the working current up to 6 kA and higher [3, 4], the possibilities of application of the pulsed supply of power for controlling the process of electroslag remelting have been greatly expanded. In addition to reducing the specific consumption of electric energy, the pulsed power supply

makes it possible to influence the formation and separation of the droplets of electrode metal, thermal and hydrodynamic processes in the slag and metal pool, and also control the solidification of the metal of the billet [1, 2, 5, 6].

The aim of the present work is the examination of the technological and metallurgical special features of the ESR process of titanium in the conditions of the pulsed supply of electric energy. It was required to develop equipment for the pulsed power supply in the electroslag process, and also investigate the relationships governing the formation of the ingot and its solidification structure.

In [7, 8] the authors indicated the efficiency of application of the external electromagnetic effect for controlling the structure formation of titanium ingots in the electroslag remelting process. The experimental results show that of the pulsed effect of the longitudinal magnetic

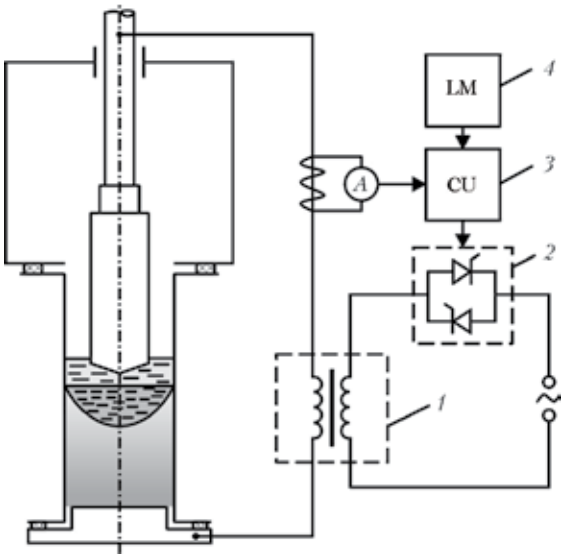

Fig. 1. Diagram of electroslag melting of titanium ingots with pulsed electric power supply: *1*) the TShP-10-1 power transformer; *2*) the thyristor block; *3*) the thyristor control block; *4*) the programmable logic module.

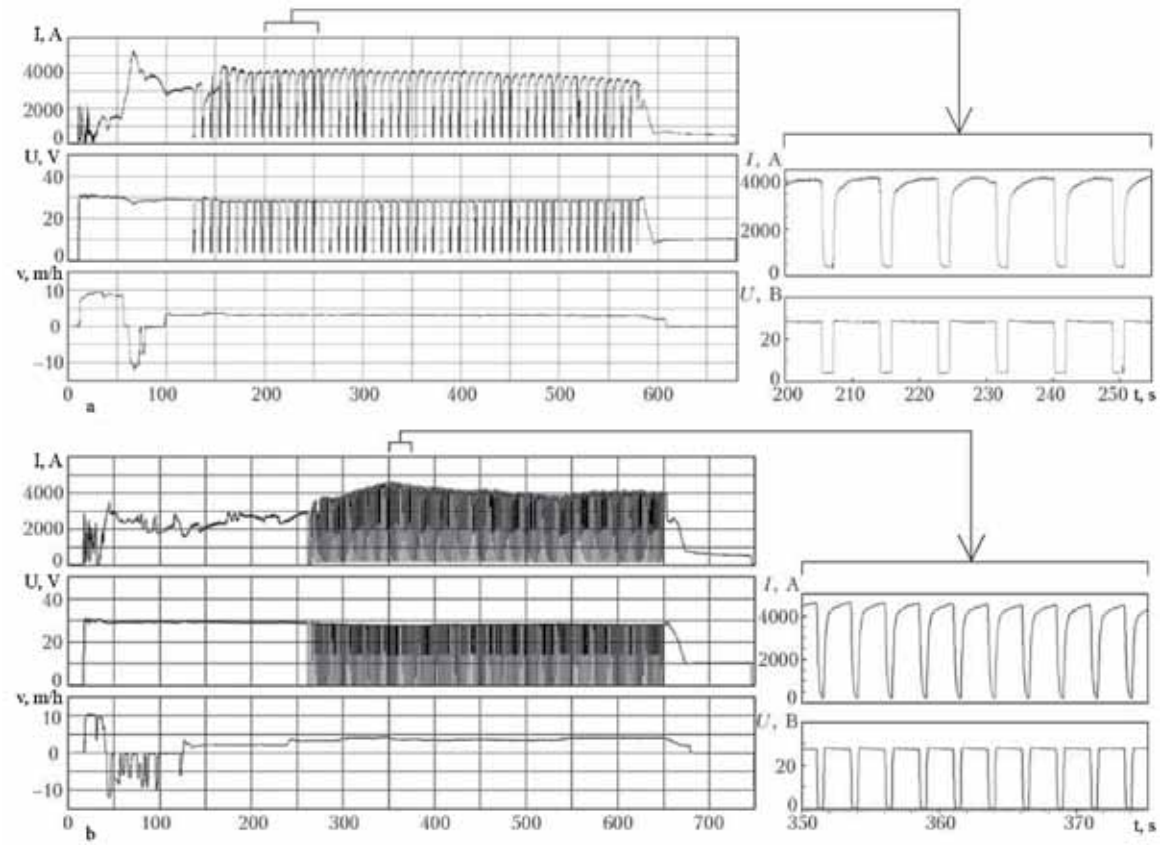

Fig. 2. Recording of the melting processes with pulsed electric power supply, s: *a*) t_{pulse} = 7, t_{break} = 1.4 (melt No. 825); *b*) t_{pulse} = 2, t_{break} = 0.5 (melt No. 826).

Table 1. Conditions of experimental melts with pulsed power supply

Melt No.		d, mm		t, s		U, V		I, A	
		electrode	ingot	pulse	break	pulse	break	pulse	break
825	3.0...3.5	48	84	7	1.4	28	4	3900....4100	400
826	3.0...3.7	48	84	2	0.5	28	0	4000...4150	0

Comment. Flux AN-T4, the depth of the slag pool 40 mm

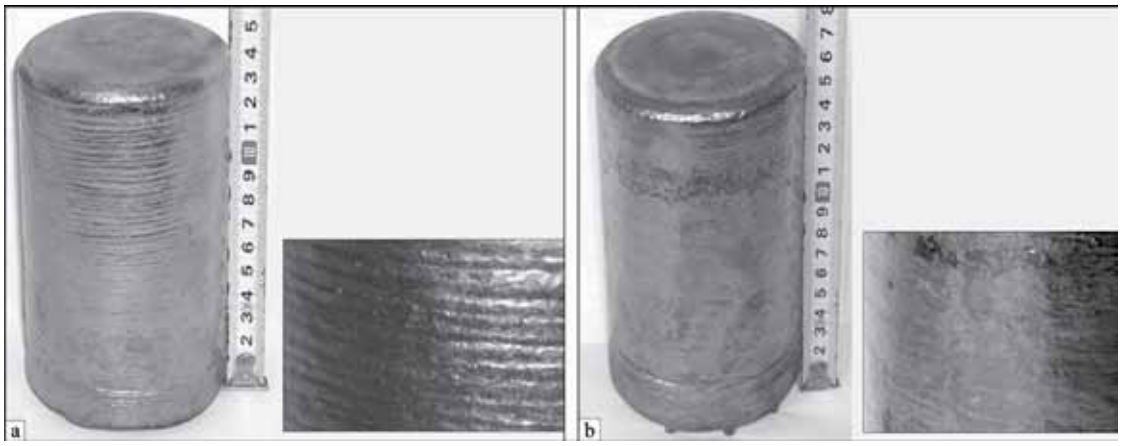

Fig. 3. External appearance and the side surface of titanium ingots, melted with pulsed electric pass supply: *a*) melt No. 825; *b*) melt No. 826.

field with a sufficiently high induction results in the spontaneous periodic changes of the melting current which is caused probably by the deformation of the surface of the slag pool and by the increase of the electrical resistance of the section of the consumable electrode – metal pool circuit. During the pulse of the magnetic field, the melting current decreases by approximately 30…70%, and during the break it is restored to the initial value, i.e., pulsed (discrete-portional) heat generation takes place in the slag pool.

Fig. 4. The macrostructure of the titanium ingots, melted with the electric pass supply: *a*) melt No. 825; *b*) melt No. 826.

In the melting of the billets with a diameter of 80–100 mm and the induction of the external magnetic field of the 0.16–0.24 T, the best results in the refining of the structure of the metal and the formation of the surface of the ingot were obtained in the case of the pulse and break time of the electromagnetic effect of respectively 1–2 and 6–15s. This effect resulted in a reduction of the melting current during the pulse of the magnetic field to 70% [7].

Thus, it was interesting to carry out experiments using the Aalst electric power supply, reproducing the similar nature of variation of the melting current but in this case as a result of the change of the voltage of the power source. Also, to obtain resonance oscillations, experiments were carried out with the application of a higher frequency of current modulation, similar to the frequency

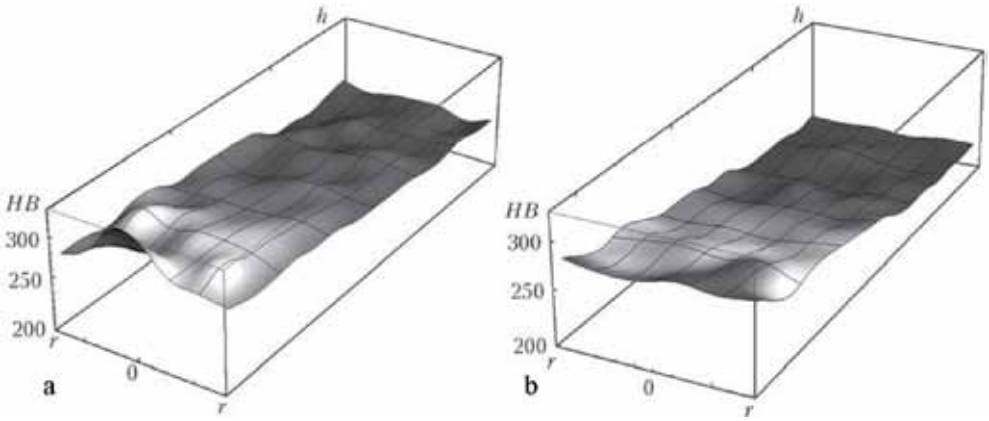

Fig. 5. Distribution of hardness HB in the longitudinal section of the ingots: *a*) melt No. 825; *b*) melt No. 826, *h*, *r* – the height and radius of the ingot, respectively.

of natural oscillations of the metal pool [1].

Experiments with the melting of billets of titanium of Grade 4 type with the diameter of 84 mm were carried out in a chamber-type electroslag furnace (Fig. 1). The power was supplied to the equipment using the modernised power transformer TShP-10-1, fitted with a block of controlling thyristors connected by the antiparallel connection in the primary winding circuit. The control system of the thyristors makes it possible to control smoothly the voltage during melting in the range 0–72 V at a current of up to 10 kA and ensure efficient protection against overloading. To realise the pulsed operating regime of the transformer, the programmable logic module SR2 B1218D was connected to the thyristor control circuit which made it possible to regulate the duration of the pulses and breaks of the voltage in the secondary circuit of the power transformer with a discreteness of 0.1 s in a wide range (0.1…999 s), applying different methods of pulsed power supply to the ESR process (pulse – breaks, a group of pulses – breaks with different depth of modulation, etc).

The conditions of the experimental melts are presented in Table 1 and Fig. 2. The experimental results were used with you earlier the stability of the electroslag process, its electrical parameters, formation of the surface of the ingots, the macrostructure of the ingots and the distribution of hardness in the longitudinal section.

Two methods of pulsed bar supply to the electroslag process were investigated. In the first method (melt No. 825), the power was supply by the pulses of alternating voltage with the duration of 7 s with a break of 1.5 s during which the voltage was reduced to 4 V (Fig. 2 a). In the second method (melt No. 826), the duration of the voltage pulses in the pool was 2 s with a break of 0.5 s during which the voltage was completely switched off (Fig. 2b).

In the investigated range of the conditions of the pulsed power supply the electroslag process was stable, without any disruption of stability. In accordance with the variation of the electrical voltage in the pool, the melting current was changed cyclically (Fig. 2). The front of current increase was flatter in comparison with the front of voltage increase which is evidently associated with the cooling of the slag pool during the break in the pulsed supply and the non-linear form of the electrical resistance of the slag.

The reduction of the supplied power in the melts produced in the past conditions resulted in a small (by 3...5%) reduction of the melting rate of the electrode and the corresponding increase of the duration of the process. However, on the whole, the specific consumption of electric energy, in comparison with melting in the stationary conditions (with continuous electric power supply) decreased

by 7...10%. Evidently, this is associated with the intensification of droplet formation and heat and mass processes at the end of the consumable electrode as a result of the vibrations caused by electrodynamic forces which in the final analysis increases the thermal efficiency of melting [6, 9].

The external appearance of the melted billets it shown in Fig. 3. In both cases, the billets are characterised by the efficiently formed side surface. The surface of the ingot No. 825 showed small corrugations caused by the pulsed heat input (Fig. 3a). The mechanism of formation of these corrugations is associated with the increase of the cooling rate of the metal during the break-in the electric power supply and with the appropriate cyclic variation of the thickness of the slag skull on the surface of the ingot. The depth of the corrugations was on average 0.1...0.15 mm, which did not impair the surface quality of the ingot. In the case of the duration of the break of 0.5 s, the surface of the ingot was almost completely free from corrugations (Fig. 3b).

The macrostructures of the longitudinal section of the produced ingots are shown in Fig. 4. In both cases, the metal is characterised by a dense structure, the absence of slag inclusions, no lack of fusion defects, shrinkage porosity and other metallurgical defects.

The peripheral areas of the ingots (in the vicinity of the side surface) are characterised by a fine-grained globular structure, with the mean size of the globules being 0.5...1.5 mm. The width of this zone in the ingot No. 825 reached 13 mm, which is slightly greater than in the ingot No. 826 (11 mm).

The central part of the ingots contained both globular grains and columnar grains, elongated in the direction of heat transfer, with the mean size of 1.87×8.50 mm (ingot No. 825) and 1.95×10.15 mm (ingot No. 826). The distinctive 'weak' zone was not detected at the axis of the ingots.

On the whole, analysis of the macrosections of the produced ingots indicates both refining and homogenising of the macrostructure of the ingots, in comparison with the metal of the titanium ingots melted in the stationary conditions which are characterised by the distinctive 'firtree' structure of the metal with the size of the dendrites comparable with the radius of the ingot.

Evidently, the observed effect is determined by a number of factors, in particular, the variation of the temperature gradient at the solidification from as a result of breaks in the electric power supply and hydrodynamic 'impacts' on the crystals growing in the two-phase zone during activation and disconnection of voltage. The pulsed electric pass supply also resulted mechanical solutions of the melt in the metal pool resulting in breaking of the dendrites.

The distribution of hardness HB in the longitudinal section of the ingots (Fig. 5) indicates the relatively high degree of homogeneity of the cast metal. The enquiries of the hardness of the metal of the root part of the ingot is typical of the majority of metallurgical processes and is associated with the higher content of the impurities in the given zone.

The experiments showed that it is possible to control the solidification of titanium ingots in electroslag the melting by the pulsed supply of electric energy. The further investigation should be carried out to determine the relationship between the parameters of the structure of the cast metal and the influence conditions, such as the frequency of the pulses, the on-off ratio of the pulses and the level of modulation of the voltage four different standard dimensions of the melted ingots.

Conclusions

1. The TShP-10-1 power transformer was modernised for the use in the pulsed supply for the electroslag process with the possibility of regulation of frequency and amplitude characteristics of the pulses of working voltage during melting.

2. It has been shown possible to carry out electroslag melting of titanium ingots with

the pulsed supply of electric energy whilst retaining the stability of the electroslag process ensuring high quality of the formation of the side surface of the ingot with a dense structure, without metallurgical defects.

3. The application of the pulsed power supply has reduced the specific consumption of electric energy by 7...10% in comparison with melting in the stationary conditions.

4. New experimental data were obtained for the special features of the formation of the macrostructure of the titanium ingots in the conditions of pulsed electric power supply. The refining of the structure of the metal in comparison with the metal of the ingots produced by conventional electroslag remelting was observed.

References

1. Control of the process of solidification of the electroslag ingot, in: Problems of steel ingots, proceedings of the 5th conference for ingots, Kiev, September 1974, Metallurgiya, Moscow, 1974, 707–714.
2. Paton, B.E., Medovar, B.I. Electroslag furnaces, Naukova Dumka, Kiev, 1976.
3. Element-Preobrazovatel': Thyristors, low-frequency tablet design; www.element.zp.ua/products/list.php?category=29.
4. Railton electronics: thyristor disc. www.railtonelectronics.com/powerelectronics.html.
5. Abramov, A.V., et al., Probl. Spets. Elektrometall., 1993, No. 4, 10–12.
6. Patent 2337979, RF, MPK S 22 V 9/18; A method of controlling the operating conditions of equipment for electroslag remelting and systems for this purpose, Abramov, A.V., et al., 10.11.2008, Bull. No. 31.
7. Kompan, Ya.Yu., Sovremen. elektrometallurgiya, 2007, No. 4, 3–7.
8. Nazarchuk, A.T., et al., ibid, 2013, Nol. 4, 21–26.
9. Ivanenko, O.G., et al., Izv. VUZ, Chern. Metall., 1984, No. 4, 15–18.

Submitted 29.1.2014

Advances in Electrometallurgy 2014 ***12*** *(2) 92–98*
Translated from Sovremennaya Elektrometallurgiya 2014 ***12*** *(2) 15–20*

ELECTRON BEAM PROCESSES

Effect of alloying with boron and tantalum on the structure and properties of an alloy based on the TiAl intermetallic compound

G.M. Grigorenko, S.V.Akhonin, A.Yu. Severin, V.A. Berezos and S.G. Grigorenko

E.O. Paton Electric Welding Institute, Kiev

Presented are the results of investigations of alloys on base of intermetallic compound TiAl. Ingots were produced by the method of electron beam cold hearth melting. The effect of additional alloying with boron and lanthanum, as well as thermal deformation and heat treatment on structure formation, mechanical properties and high-temperature strength of model alloys was studied. Adding of boron and lanthanum into alloy contributes to refining of structural components, as well as to increase in its hardness, high-temperature strength and mechanical properties. It was found that the structure, produced after additional heat treatment, will provide the best combination of mechanical and technological properties of alloy being studied. Ref. 7, Tables 2, Figures 4.

Key words: *intermetallic; titanium aluminide; alloying; structure; thermal deformation; heat treatment; hightemperature strength*

The intermetallic alloys based on titanium aluminides belong in the group of important structural materials. Because of the unique set of the physical and mechanical properties – high-strength, low density, heat resistance, high values of the corrosion resisting properties, high resistance to fatigue failure and creep – these alloys are promising for aviation and aerospace industry, automobile industry, chemical and power engineering.

The alloys based on TiAl are divided into two groups: γ-alloys with the aluminium content 50...52 at.% and two-phase ($\gamma + \alpha_2$) alloys with 44...49 at.% [1] (Fig. 1). However, it should be noted that the alloys with the structure of both γ and $\gamma + \alpha_2$ are referred to as the γ-alloys [1–4].

The single-phase γ-alloys are not used widely because of the very high values of the technological properties. The amount of aluminium in the two-phase alloys ensures the maximum ductility of not only binary but also multi-component alloys [2]. Therefore, these alloys are most promising for producing satisfactory relationships of the mechanical properties imposed on the structural materials. The largest increase in the activities obtained in these alloys by adding elements such as molybdenum, chromium, vanadium, manganese, niobium, and the favourable effect of the latter remains unchanged up to relatively high concentrations.

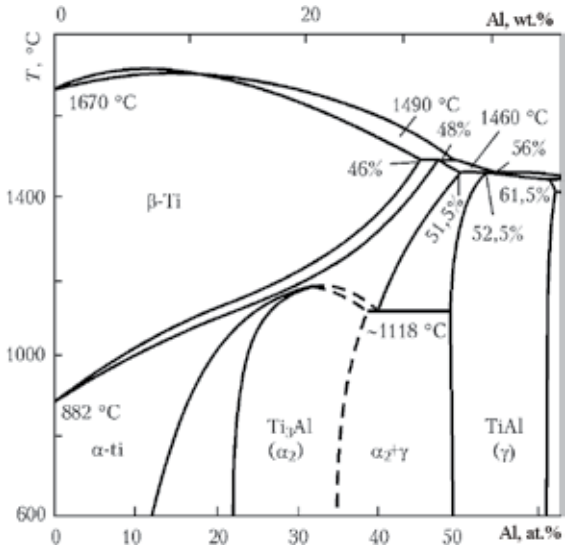

Fig. 1. Equilibrium diagram of the Ti – Al system.

Boron, carbon and silicon, if they are situated mostly in the solid solution, increase the values of the ductility characteristics of the alloys. At the same time, the borides and carbides in the form of excess phases greatly refined grains and this may also increase the ductility. The strength and resistance talks relation of the alloys with the $(\gamma + \alpha_2)$-structure are increased by 1...3% of niobium, tantalum, manganese, zirconium, hafnium or tungsten [3].

Table 1. Chemical composition of the alloys, wt.%

Sample No.	Chemical composition of alloys, wt.%	Condition
1.	Ti–28, 8Al–11, 7Nb–3, 5Cr–3, 1Zr	Cast
2.	Ti–29, 3Al–11, 9Nb–2, 8Cr–2, 9Zr–0, 3B–0, 01La	Cast
3.	Ti–29, 3Al–11, 9Nb–2, 8Cr–2, 9Zr–0, 3B–0, 01La	After HDT
4.	Ti–29, 3Al–11, 9Nb–2, 8Cr–2, 9Zr–0, 3B–0, 01La	After HDT+HT

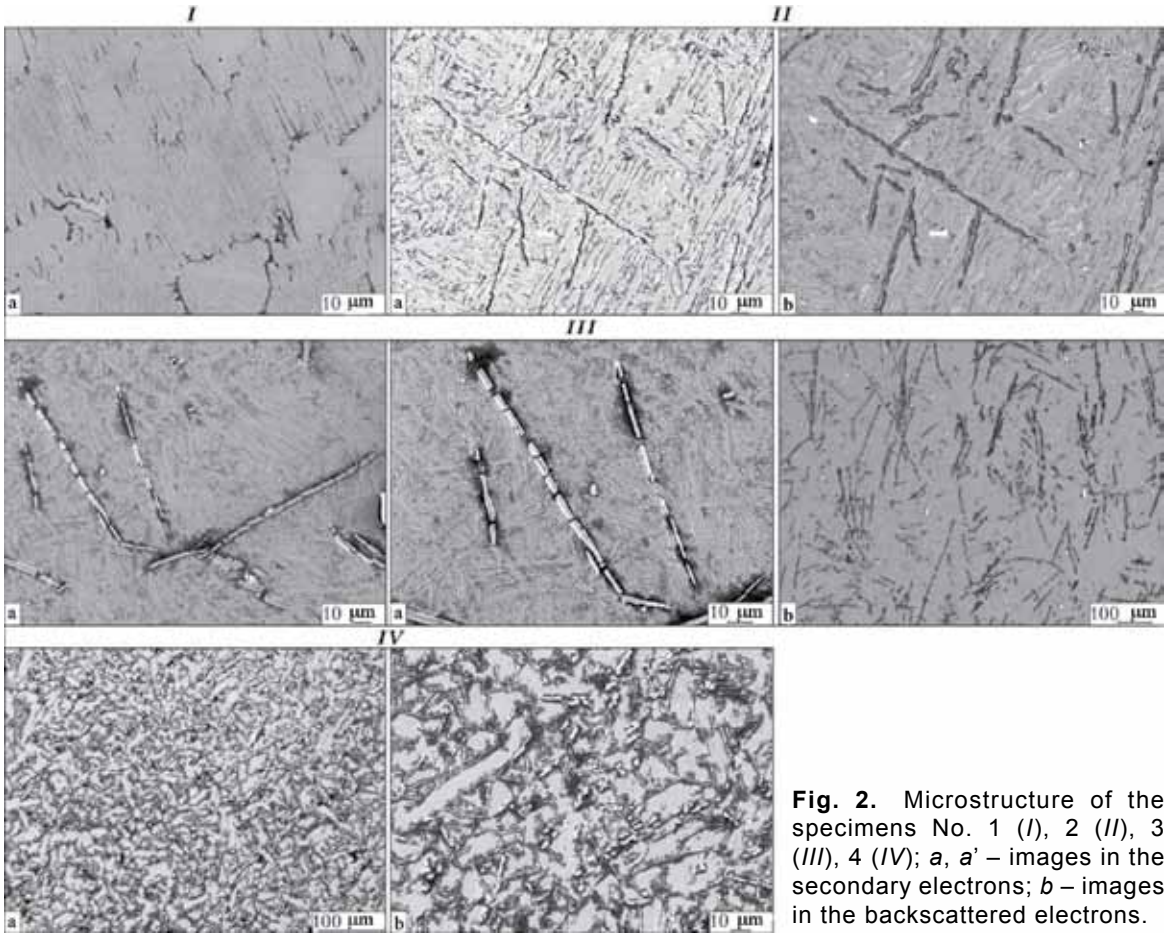

Fig. 2. Microstructure of the specimens No. 1 (*I*), 2 (*II*), 3 (*III*), 4 (*IV*); *a*, *a*' – images in the secondary electrons; *b* – images in the backscattered electrons.

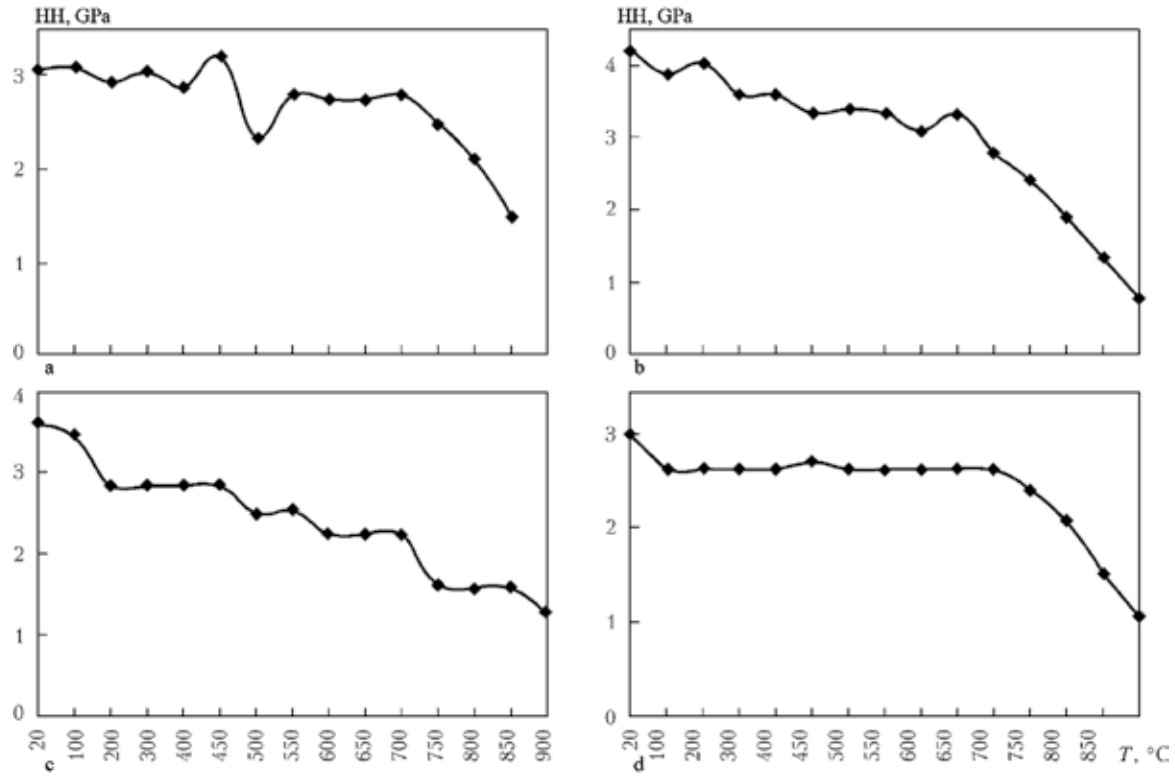

Fig. 3. Dependence of hot hardness (HS) on temperature for the specimens No. 1 (*a*), 2 (*b*), 3 (*c*), 4 (*d*).

The efficient control of the structure of the γ-alloys is one of the main conditions of producing the required properties of these alloys. Different technologies of producing blanks, the condition of the hot deformation and subsequent heat treatment are used to produce three made types of the structure of the TiAl intermetallic compound: lamellar (plate-shaped), recrystallised (globular) and bimodal (duplex). The characteristics of the creep strength of the highest values in the case of the lamellar structure. The globular structure ensures a higher level of the mechanical properties (strength and ductility) at room temperature in comparison with the lamellar structure, but the creep strength is lower. At room temperature, the alloy with the bimodal structure is characterised by the highest mechanical properties [4].

At present, work is being carried out to increase the parameters of the strength, ductility, creep strength and other characteristics of the alloys based on TiAl by producing in them special structural-phase states as a result of alloying, thermal and thermomechanical treatment.

DM of the present work is the examination of the effect of alloying with boron and lanthanum and also thermal deformation and thermal treatment of the structure and properties of the intermetallic alloy based on titanium aluminides.

The ingots were produced by electron beam melting (EBR) with an intermediate container [5]. This method is highly promising ensuring the high degree of removal of harmful inclusions. The application of the intermediate container (cold hearth) improve the efficiency of refining, resulting averaging of the chemical composition and the removal of high- and low-density inclusions [6]. Difficulties in electron beam remelting are associated with the introduction of boron into the ingots to be produced because under the effect of electron-beam heating in vacuum the melting of boron, characterised by the very high vapour tension, is accompanied by its evaporation and also dispersion and removal

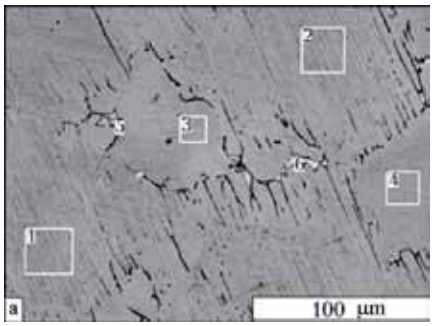

Spectrum No.	Al	Si	Ti	Cr	Fe	Zr	Nb
1	29.99	0	52.07	2.99	0	1.89	11.51
2	30.75	0	51.65	2.62	0	2.49	11.13
3	32.35	0.07	47.66	2.82	0	7.24	9.12
4	33.20	0	47.23	2.42	0.31	7.33	8.73
5	19.39	0.23	52.11	14.98	1.14	1.15	10.19
6	19.10	0.15	52.03	15.99	1.98	1.02	8.84

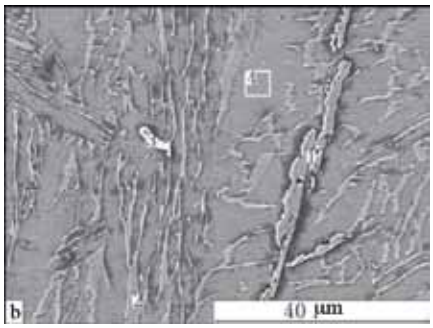

Spectrum No.	B	O	Al	Si	Ti	Cr	Ni	Zr	Nb	La
1	21.01	0	3.50	0.04	50.14	0.49	0.32	1.32	20.21	1.12
2	0.45	0	14.68	0.23	55.63	3.24	1.36	4.64	17.04	1.41
3	0	3.78	9.97	0.03	1.89	0	1.72	0.41	0.81	80.52
4	0	0	15.05	0.26	67.24	0.85	0.75	3.28	11.59	0

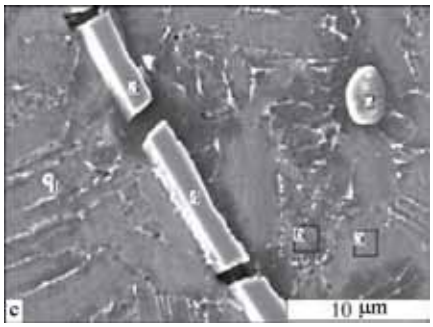

Spectrum No.	B	O	Al	Ti	Cr	Zr	Nb	La
1	0.94	21.53	1.24	5.00	0	0.51	1.09	57.90
2	0.62	16.59	0.21	1.93	0	0.30	0.51	78.72
3	17.09	0	0.15	57.75	0.34	0.09	21.13	0.41
4	16.63	0	0.22	58.96	0.73	0.67	21.33	0.36
5	0	0	13.94	68.44	0.69	3.62	12.17	0.16
6	1.99	0.90	10.90	58.26	2.29	4.43	15.45	1.07

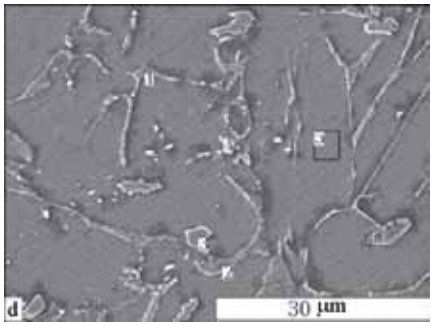

Spectrum No.	B	O	Al	Ti	Cr	Fe	Zr	Nb	La
1	3.91	2.65	8.40	43.71	7.61	1.86	5.72	16.21	0.72
2	1.82	2.17	9.18	49.08	6.60	2.19	5.05	20.48	0.13
3	14.77	0	0.24	58.68	0	0	0.22	24.24	0.98
4	0.76	14.17	0.94	3.91	0	0.22	0	0.10	76.93
5	0	0	15.07	67.93	0.64	0	3.91	11.71	0

Fig. 4. Results of EDS analysis of the specimens No. 1 (*a*), 2 (*b*), 3 (*c*), 4 (*d*) (the content of the element is given in wt.%).

of the particles when boron is added to the charge in the form of powder. Therefore, a chemical compound, lanthanum hexaboride LaB_6, characterised by the considerably lower vapour density in comparison with pure boron, was used for this purpose [7].

The experimental mouse of the ingots of γ-aluminide of titanium, aluminium niobium, zirconium, chromium and also additionally with boron and lanthanum were carried out in equipment UE-208M. The charge materials were in the form of sheets of commercial titanium of grade VT1-0, according to GOST 22178–76, aluminium of grade A8 according to GOST 11070–74, metallic niobium 99.9% in the form of pipes, electrolytic chromium

and zirconium iodide 99.97%. The lanthanum hexaboride was added to the charge in the form of cylindrical pressings of the LaB_6 powder in a special pressing mode. The boron content in the powder was approximately 32 wt.%.

A new method of producing the ingots of titanium aluminide was proposed. The addition of the all refractory following elements, and also a boron and lanthanum, was carried out in the first stage of producing the ingot. The lanthanum hexaboride in the first remelting cycle was placed between the refractory components of the charge in order to avoid direct effect of the electron-beam heating on them. In the first remelting cycle the aluminium was not added. In the second remelting cycle, aluminium was added taking into account the losses due to evaporation. The produced ingots had a diameter of 165 mm, length 200...250 mm.

The content of the elements and the condition of the alloys from which the specimens were produced, are shown in Table 1.

According to the equilibrium diagram of the Ti – Al system (Fig. 1), the alloys consist of two phases ($\gamma + \alpha_2$).

One of the alloys (specimen No. 3) was subjected to thermal deformation treatment after melting. This treatment consisted of the following procedure.

The blank, placed in a jacket of a low carbon steel 5 mm thick, was heated in a furnace to 1220°C and held for 40 min. Subsequently, the specimen was compressed in a hydraulic press with a force of 200 t with the degree of the formation of 50%. The specimen was subsequently reheated to 1100°C and held for 30 minutes followed by rolling in a reversing mill. The initial thickness of the blank was 35 mm, the final thickness 7 mm. The total relative compression was 80%. The rolling was followed by thermal treatment, heating to 900°C, holding for 2 hours, cooling in the furnace.

After thermal deformation treatment, specimens No. 4 was subjected to additional heat treatment. The deformed alloy was heated in the vacuum furnace to 1260°C and held for 30 minutes. This was followed by cooling to 900°C in the furnace and then by cooling to room temperature in. The next stage was reheating to 900°C, holding for 2 hours, cooling in the furnace.

Table 2. Mechanical properties of the investigated alloys at a temperature of 20 °C

Sample No.	$\sigma^c_{0.2}$, MPa	σ^c_B, MPa	ε, %
1	655	1600	9.33
2	1078	1660	11.5
3	975	1680	11.0
4	980	1750	14.0

The structure of the produce specimens was studied in a multifunctional advanced system with the high technical characteristics JAMP 9500F (JEOL Ltd, Japan), fitted with an Oxford EDS INCA Energy 350 energy-dispersing spectrometer (EDS) for the analysis of the elements (from beryllium to uranium), with the energy resolving power of 133 eV and the electron probe diameter of 1 μn. The investigations were carried out in a superhigh vacuum of $5 \cdot 10^{-8}$ Pa. The hardness of the specimens was measured in a M-400 hardness measuring equipment manufactured by LECO (USA) at a load of 9.8 N. The creep strength of the alloys was investigated by the hot hardness (HH) method. To reduce the thermal stresses, the specimens were subjected to preliminary annealing for 1 hour at a temperature of 900°C. The hot hardness of the specimens was determined in the temperature range 20...900°C using an HPQ 250 microhardness metre under a load of 9.8 N, duration 1 min. The compression test was carried out on rectangular specimens with a size of 3.5 × 3.5 × 5 mm in equipment U22-52 in accordance with GOST 8817–82 and GOST 25.503–97.

The structure of the metal of the specimen No.1 consists of various with the globular and plate-shaped (lamellar) structure). In some cases, precipitates with the eutectoid-type structure were detected in some areas at the boundaries. The microstructure of the metal and the analysis of the results ob-

tained in the microstructure are presented in Fig. 2, *I*, *a*, 4, *a*.

Examination of the structural component showed that the boundary zones are enriched with chromium (Fig. 4*a*, spectra No. 5, 6) and the support the preferential precipitation of the $TiCr_2$ intermetallic compound. The hardness of the alloy is 3.05–3.16 GPa. The dependence of the hot hardness of the metal on the temperature is shown in Fig. 3a. In the temperature range 20...750°C the softening of the alloy is almost completely negligible.

Examination of the structure of the alloy, alloyed with the lanthanum hexaboride

LaB_6 (Specimen No. 2) shows that the alloy has the (α_2 + γ) plate -shaped structure with a small number of areas of the γ-phase. The structure also contained rod-like crystals and light dispersed particles (Fig. 2, *II*).

The analysis results show that these crystals are enriched with boron and they can be identified as right (Fig. 4b, spectrum No. 1), and the light particles contain lanthanum and oxygen (Fig. 4b, spectrum No. 3). In comparison with the specimen No. 1, the hardness increases and equals 3.53...3.74 GPa. Hot hardness also increases and then remains almost constant up to 650°C (Fig. 3b).

After thermal and the formation treatment of the alloy (specimen No. 3) the following changes to place in the structure. The relief of the structure decreased, the particles became smaller and the distance between them also decreased, and rod-like crystals fragmented into individual particles (Fig. 2, *III*, *a*, *a*'). As in the structure of the specimen without deformation, light dispersed particles appeared over the entire surface (Fig. 2, *III*, *b*).

The results of EDS analysis are presented in Fig. 4c. The fragmented crystals are the borides of titanium and niobium (Fig. 4c, spectra No. 3, 4), and the light particles, as in the previous case, can be identified as the lanthanum oxide (Fig. 4c, spectra No. 1, 2). The hardness of the alloy is 3.58...3.75 GPa. The temperature dependence of the hot hardness is shown in Fig. 3c.

After heat treatment (specimen No. 4), the specimens contained the bimodal (duplex) structure, consisting of the areas represented by recrystallised grains, and the areas with the lamellar structure. Small inclusions of different shape (Figure 2, *IV*) were distributed over the entire investigated surface.

More detailed examination of the structural components showed that the inclusions of the fragmented form are fragmented borides, the branched areas are the remnants of the intermetallic phase based on $TiCr_2$ and the light dispersed globular inclusions represent the lanthanum oxide (Fig. 4b). The hardness of the structure is 3.90...3.95 GPa. Analysis of the graph of the dependence shown in Fig. 3d shows the creep strength of the alloy is high, as indicated by the relatively high and stable values of hot hardness in the temperature range 100...750 °C.

The bimodal structure, produced after a treatment of the alloy, belongs to the structures characterised by the acceptable combination of strength and ductility. Therefore, the next stage of this work was the determination of the mechanical properties, characterised in the strength and ductility of the investigated alloys. The tests were carried out in compression, because the thickness of the sheet from which the samples No. 3 and No. 4 were taken, did not make it possible to produce the tensile specimens. In the investigation of the specimens with the relatively small geometrical dimensions, the compression test is preferred and is characterised by the highest accuracy and information content. The results of the mechanical tests are presented in Table 2.

As shown in Table 2, the addition to the alloy of the boron and lanthanum increases the strength parameters $\sigma_{0.2}$, σ_B and the degree of deformation ε (activity). After additional heat treatment the degree of deformation and the ultimate strength of the material increases even further, and the yield limit remains relatively high.

Conclusions

1. Alloying of the investigated intermetallic

alloy with boron and lanthanum by adding the lanthanum hexaboride LaB_6 to the melt refines the structural components, results in the formation of the almost completely ductile (lamellar) (α_2 + γ)-structure with small areas of the γ-phase, and also in the precipitation of rod-like borides and fine lanthanum oxides.

2. The thermal deformation treatment results in even greater refining of the structure and fragmentation of the boride bars.

3. After additional heat treatment of the alloy the structure was bimodal (duplex) characterised by the uniform distribution of the particles of borides, lanthanum oxide and the intermetallic phase based on $TiCr_2$, forming the so-called hardening frame. The alloy with such a structure is characterised by sufficiently high and stable values of hot hardness in the temperature range 100...750 °C.

4. The proposed method of alloying with the chemical compound LaB_6 with the low vapour tension in electron beam remelting produces the alloys based on titanium aluminide with the required contend of boron and lanthanum, greatly reduces the losses of the components with high vapour tension and increases the uniformity of the distribution of these following elements in the cross-section and along the length of the ingot.

5. Complex alloying of the alloy with boron and lanthanum and subsequent heat treatment make it possible to increase and obtain the best combination of hardness, strength and mechanical properties.

References

1. Boyer, R., et al., Materials properties, handbook, The Material Information Society, USA, 1994.
2. Povarova, K.B., Bannykh, O.A., The principles of development of new materials for service at high temperatures, in: Processing of light and special alloys, Research Institute of Light Alloys, Moscow, 1996, 56–70.
3. Bannykh, O.A., et al., MiTOM, 1996, No. 4, 11–14.
4. Il'in A.A., et al., Titanium alloys. Composition, structure, properties, VILS-MATI, Moscow, 2009.
5. Paton, B.E., et al., Electron-beam melting of the refractory and high reactivity alloys, Naukova dumka, Kiev, 2008.
6. Grigorenko, G.M., et al., Recrystallisation of titanium aluminide, Titan v SNG 2010, Proc. Conf., Ekaterinburg, 2010, 132–130.
7. Samsonov, G.V., Refractory compounds, a handbook, Metallurgizdat, Moscow, 1963.

Submitted 27.1.2014

Advances in Electrometallurgy 2014 ***12*** *(2) 99–104*
Translated from Sovremennaya Elektrometallurgiya 2014 ***12*** *(2) 21–25*

Electron-beam melting of the surface of titanium alloy ingots

[1]S.V. Akhonin, [1]V.A. Berezos, [1]A.N. Pikulin, [1]A.Yu. Severin and [2]A.G. Erokhin

[1]E.O. Paton Electric Welding Institute, Kiev
[2]Titan Scientific and Production Centre, E.O. Paton Electric Welding Institute, Kiev

At the E.O. Paton Electric Welding Institute of the NAS of Ukraine the specialized electron beam installations UE-185 and UE-5810 with a complex of technological equipment have been designed and manufactured, which allow realizing the process of melting of surface layer of ingots both of cylindrical and rectangular sections. Feasibility of wasteless removal of local surface defects of ingots of titanium alloys by the method of electron beam melting is shown, thus reducing the losses of base metal and alloying elements. Schemes of surface electron beam melting of ingots of round and rectangular sections are given. It is shown that the developed technology of electron beam surface melting of ingots of titanium alloys can produce a surface layer which differs negligibly from base metal by chemical composition and corresponds to the requirements of standards. Determined are the technical-economical parameters of electron beam treatment of ingots of titanium alloys, at which the technology and specialized equipment for electron beam of melting of lateral surface of ingots of titanium alloys, developed at the E.O. Paton Electric Welding Institute of the NAS of Ukraine, allow increasing the yield of efficient metal by 4...15 % depending on the assortment of ingots and providing the significant economic efficiency. Ref. 11. Tables 2, Figures 7.

Key words: *Electron beam melting; ingot; titanium; alloy; electron beam surface melting; surfaced layer; electron beam installation*

The main methods of producing titanium-based alloys are vacuum-arc (VAM), electron-beam (EBM) and plasma-arc (PAM) melting messes. As a result of the special physical-chemical properties of titanium (high melting point, very high chemical activity in relation to the gases of the atmosphere at elevated temperatures, sensitivity to contamination with interstitial impurities, et cetera), the production of titanium is accompanied by a number of difficulties. For example, in producing the titanium-based alloys by the conventional melting methods, large defects – cracks, breaks, folds, skins, cavities, corrugations, and other defects, form in the surface layer of the ingots and blanks. The reasons for the formation of the the phase have been studied sufficiently but it is almost impossible to prevent the formation of these defects on the given level of production.

At present time, the required quality of the surface of ingots and blanks is obtained as a result of removing the surface layer by machining. However, the operations of cleaning in dressing the ingots are very labour- and energy-consuming. It should be mentioned that in the machining the surface of the ingots of titanium-based alloys in the currently available machines, the productivity is 3...6 times lower than in the machining of alloyed structural

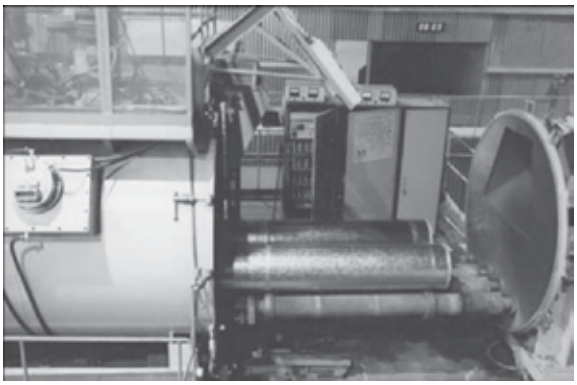

Fig. 1. Ingots with a diameter of 400 mm, surface melted in the UU-185 electron-beam equipment.

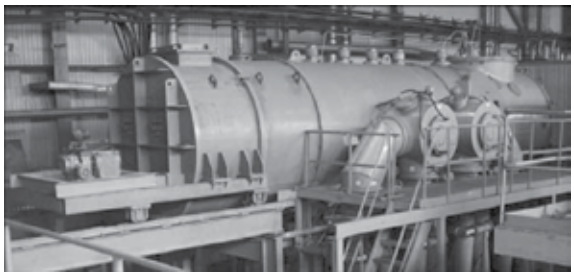

Fig. 2. External appearance of the UE-5810 universal multipurpose electron-beam equipment.

steels [1]. Also, the low heat conductivity of the titanium-based alloys results in local of heating of the metal in the area of contact with the cutting tool in machining and, correspondingly, to the oxidation of shavings and increased consumption of the cutting tools. In the production of titanium-based alloys as a result of the more stringent requirements on the purity of the initial charge materials, only a small part of the shavings is used repeatedly.

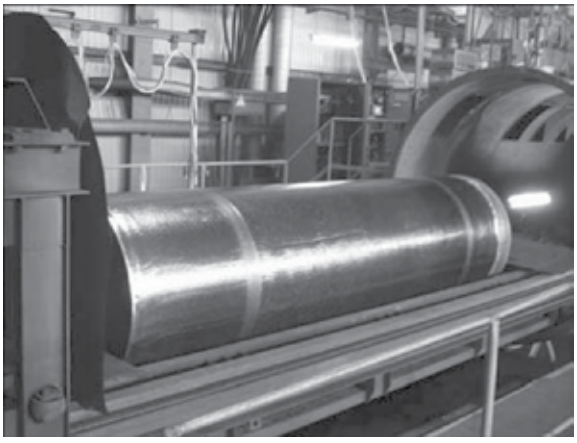

Fig. 3. Ingot with a diameter of 840 mm, surface melted in the UE-5810 electron-beam equipment.

The process of increasing the quality of the side surface of the ingots and blanks as a result of removing the defective surface layer is one of the limiting members of the metallurgical cycle, characterised by the high-level of the metal losses in the form always (shavings, abrasive slurry) which may equal up to 20% [2–4].

The solution of the problem of waste free removal of the local surface defects makes it possible to reduce the losses of parent metal and valuable alloying elements greatly improving the economic parameters of the process.

An alternative to the standard technology of removing the defective surface layer of the ingots and blanks of titanium alloys by mechanical methods is the application of the methods of treatment of the surface with the concentrated heat sources – plasma arc, laser and electron-beams, – and also electroslag dressing which make it possible to avoid large losses of the metal [5–8].

The most efficient source of concentrated heating in treatment of the surface of the ingots and blanks of high-reactivity metals and alloys, including titanium, is the electron-beam which has a number of significant advantages: the presence of vacuum in the furnace space – shielding and refining medium; high density of supplied energy; precision, easy control and regulation of the technological parameters.

The E.O. Paton Electric Welding Institute, Kiev use electron-beam melting (EBM) of ingots instead of machining [6]. UE-185 [9] pilots planned equipment was designed, constructed and introduced into service for the electron-beam treatment of the surface layer of cylindrical and the rectangular ingots (Fig. 1). The UE-185 equipment consists of a vacuum chamber with the mechanisms, devices and systems for realising the technological process.

Technical characteristics of UE-185 electron-beam equipment

Type of gun	Axial
Total power, kW	1200
The power of the EB volotage, kW	900
Accelerating voltage, kV	30
Number of guns	3
Largest dimensions of the ingots, m:	
Length	2
Diameter	0.85
Width to thickness	1.0 × 0.42
Working vacuum in the melting chamber, Pa	$(6.6...13.0)\cdot10^{-2}$

In a single vacuum cycle, the UE-185 electron-beam equipment can be used to process three ingots with a diameter of 110...250 mm, two ingots with a diameter of 300...500 mm, a single ingot with a diameter of 600...850 mm, or a single ingot – slab.

The UE-5810 multipurpose electron-beam equipment has been constructed and introduced into service for the melting of large diameter ingots at the E.O. Paton Electric Welding Institute, Kiev (Fig. 2).

Technical characteristics of UE-5810 electron-beam equipment

Type of gun	Axial
Total power, kilowatt	5400
Power of EB voltage, kilowatt	1200
Accelerating voltage, kV	30
Number of guns	4
Largest dimensions of the ingots, m:	
Length	4
Diameter	1.2
Working vacuum in the melting chamber, Pa	$(6.6...13.0)\cdot10^{-2}$

The UE-5810 multipurpose electron-beam equipment can be used for melting the ingots with a diameter of 600...1200 mm, up to 4000 mm long (Fig. 3).

The process of melting the surface of the cylindrical ingots is carried out by the procedure according to which the electron-beam is stationary and the ingot rotates around its axis (Fig. 4).

Surface melting of the rectangular ingots is carried out using the procedure in which the ingot is stationary and the beam travels around the surface to be melted, and the displacement of the beam is realised using a program or manually. The surface is melted in one or two passes, and after processing one surface the ingot is tilted and then the remaining surfaces are processed (Fig. 5).

The process of electron-beam treatment of the surface of the ingots and blanks is realised in high vacuum and, therefore, the application of the method for titanium alloys in which the alloying components consist of highly volatile elements (aluminium, chromium, and others) is associated with problems in maintaining the required composition of the melted surface layer. Therefore, the technology of electron-beam melting the surface of the ingots of titanium and its alloys was developed on the basis of the mathematical models of thermal processes in cylindrical ingots [10] and the processes of evaporation of alloying elements from the surface of the liquid metal full in electron-beam melting [11], developed at the E.O. Paton Electric Welding Institute, Kiev, and also on the bases of the experimental processing of the conditions of melting the ingots of titanium alloys, carried out by electron-beam melting with a cold hearth, obtained as a result of modelling.

The proposed authority produces the molten layer with the chemical composition differing only slightly from that of the parent metal and satisfying the standard requirements (Table 1).

After melting, the side surface of the ingots acquires the flat microrelief, has a smooth mirror-like appearance without visible cracks, fractures and other defects. The surface roughness is in the range 3...4 grades with the waviness of the surface equal to 0.2...0.6 mm (Fig. 6).

Thus, the technology of electron-beam surface melting and equipment for the process, developed at the E.O. Paton Electric Welding Institute, Kiev, make it possible to remove efficiently surface defects to a depth of 10 mm, ensuring the required quality of the side surface and the correspondence of the

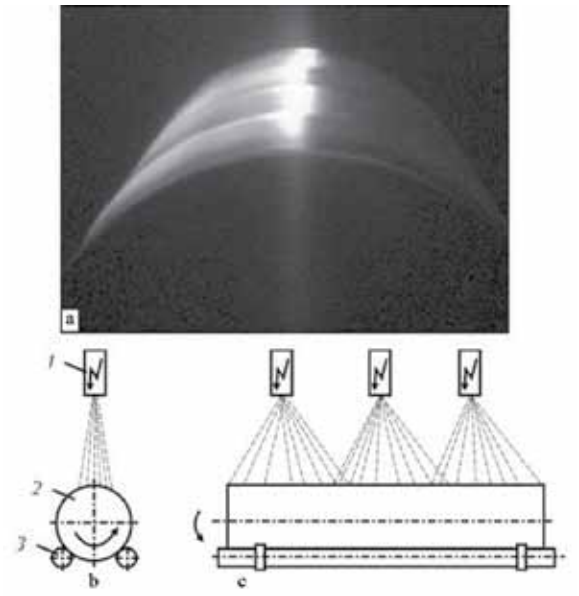

Fig. 4. Process of melting the ingot with a cylindrical cross-section: *a*) external appearance; *b*) the diagram; *1*) electron-beam gun; *2*) the ingot; *3*) the rollers of the mechanism for rotating the ingot.

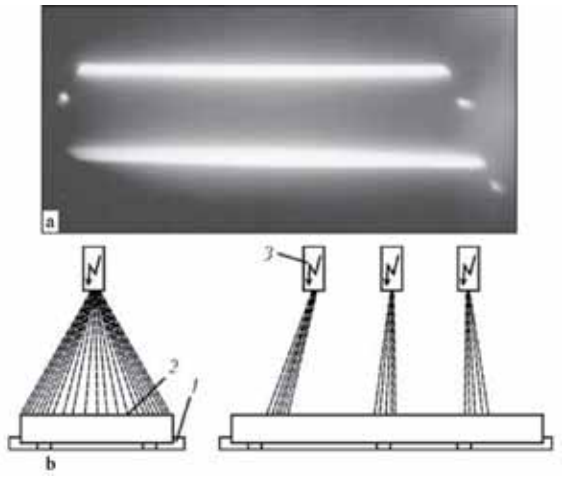

Fig. 5. The process of melting a flat ingot: *a*) external appearance; *b*) the diagram; *1*) electron-beam done; *2*) the ingot; *3*) the frame of the rotation mechanism.

chemical composition of the molten layer to the standard requirements (Fig. 7).

Experiments were carried out on the Uc-185 specialised electron-beam equipment for melting ingots to determine the technical and economic parameters of electron-beam treatment of the ingots of titanium alloys with the cylindrical cross-section and a diameter of 165, 400 and 600 mm, and also 940×165 mm rectangular section.

The technical and economic efficiency of the technology of electron-beam melting of the ingots of titanium alloys was evaluated by comparing the specific consumption of electric energy and the yield of suitable metal of the ingot for different methods of surface treatment (Table 2). The parameters of the consumption of electric energy in the machining and electron-beam melting of

Table 1. Content of chemical elements in the multilayer of the ingots of the investigated titanium alloys, wt.%

Ti alloy	Al	Cr	v	Mo	Zr	Nb	O	N
VT6 alloy, 600 mm dia:								
GOST 19807-91	5.3...6.8	–	3.5...5.3	–	≤0.3	–	≤0.20	≤0.05
Initial	6.18	–	3.86	–	–	–	0.024	0.018
EB melting	5.74	–	4.02	–	–	–	0.046	0.031
VT6 alloy, 400 mm dia:								
GOST 19807-91	5.5...7.0	–	0.8...2.3	0.5...1.8	1.4...2.5	–	≤0.15	≤0.05
Initial	6.9	–	2.05	1.57	1.81	–	0.066	0.011
EB melting	6.48	–	2.14	1.63	1.78	–	0.078	0.019
VT22 alloy, 150 mm dia:								
GOST 19807-91	4.4...5.7	0.5...1.5	4.0...5.5	4.0...5.5	≤0.3	–	≤1.18	≤0.05
Initial	5.6	0.78	4.24	4.1	–	–	0.050	0.011
EB melting	5.22	0.51	4.31	4.53	–	–	0.062	0.014

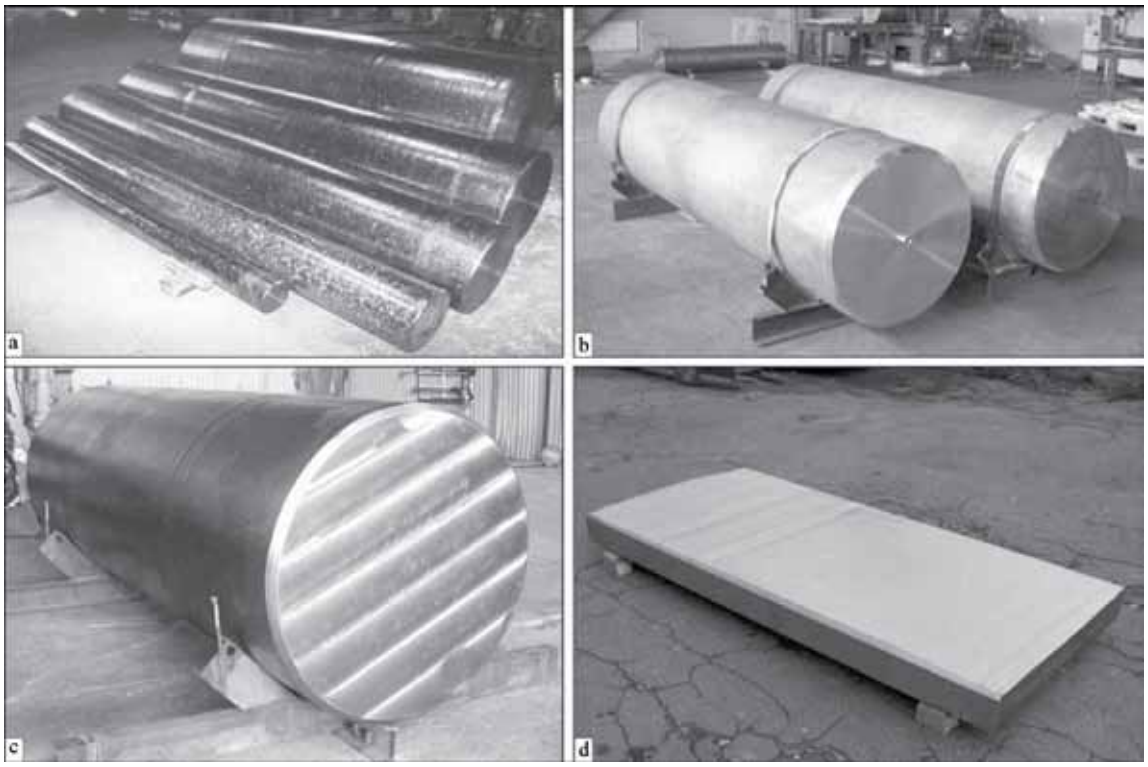

Fig. 6. External appearance of the ingots of titanium alloys with the melted surface with a diameter of 110...600 (*a*); 840 (*b*); 1100 (*c*); ingot-slab 960×165×2000 mm (*d*).

Fig. 7. External appearance of the surface of titanium ingots: *a*) melted; *b*) machined; *c*) the cast ingot.

the surface layer were determined on larger datasets. They corresponded to the actual data obtained in pilot plant production of the ingots of titanium alloys.

Comparative analysis of the technologies of removing the defective surface layer of the ingots of the titanium alloys shows that the consumption of electric energy in machining is 2...3 times lower than in the proposed technology of electron-beam surface melting. However, the latter technology increases the yield of suitable metal by 4 – 15% (depending on the grade of ingots) which counterbalances the consumption of electric energy and in the

Table 2. Technical-economic parameters of the surface treatment of ingots of titanium alloys

Ingot dimensions, mm	Weight of 2 m ingot, kg	Specific electric energy consumption kW h/kg		Yield of finished metal, %		Saving of metal in EBM, kg
		Machining	Melting	Machining	Melting	
165	195	0.62	0.71	85....90	100	20...30
400	1130	0.20	0.39	94...95.5	100	50...70
600	2540	0.10	0.18	94.5...96	100	100...140

treatment of the titanium alloys results in a significant economic effect.

References

1. Sozinov, A.I., Stroshkov, A.N., Increasing the efficiency of machining blanks of titanium alloys, Metallurgiya, Moscow, 1990.
2. Al'perovich, M.E., Vacuum arc remelting and its economic efficiency, Metallurgiya, Moscow, 1978.
3. Koryagin, S.I., et al., Methods of processing materials, a textbook, Kaliningrad, 2000.
4. Zykin, A.S., Effect of the chemical composition of titanium alloys on some parameters of machinability by cutting, Ufa, 1982, 3–8
5. Shilov, G.A., et al., Problemy Spets. Elektrometall., 1993, No. 3, 58–63.
6. Paton, B.E., et al., Electron-beam melting of titanium, Naukova dumka, Kiev, 2006.
7. Latash, Yu.L., et al., Problemy Spets. Elektrometall., 1983, No. 18, 75–79.
8. Pomarin, Yu.M., et al., ibid, 1992, No. 2, 102–106.
9. Trigub, N.P., et al., Sovremen. elektrometall., 2003, No. 2, 12–14.
10. Paton, B.E., et al., Electron-beam melting, Naukova dumka, Kiev, 1997.
11. Akhonin, S.V., Sovremen. elektrometall., 2005, No. 3, 32–35.

Submitted 28.2.2014

Advances in Electrometallurgy 2014 ***12*** *(2) 105–117*
Translated from Sovremennaya Elektrometallurgiya 2014 ***12*** *(2) 26–35*

Structure and physical-mechanical properties of vacuum condensates of VT6 titanium alloy

I.S. Malashenko, V.V. Kurenkova, I.V. Belousov and V.I. Biber

E.O. Paton Electric Welding Institute, Kiev

Producing of condensates of titanium alloy VT6, being one of leading structural materials in aircraft and turbine construction, represents a rather important direction in modern metallurgy. The rational metallurgical method of producing of alloy VT6 condensates is the high-speed electron beam evaporation using intermediate molten-metallic pool-intermediary. Selection of alloying components, added into molten pool, creates not only favorable technological conditions for evaporation of material Ti–6Al–4V, but also affects the structure and properties of the condensates being produced. It was found that the application of "soft" pool-intermediary of Zr–Mo system gives an opportunity to adjust the rational rates of condensation, influencing the mechanical properties and structure of produced condensates VT6, depending on composition of intermediate pools-intermediaries. Ref. 14, Figures 14.

Key words: *electron beam evaporation; alloy VT6; vacuum condensate; pool-intermediary; rate of deposition; substrate; temperature of condensation; microlamination; distribution of components; microdrop transfer; elongation*

Titanium alloys, in particular Ti–6Al–4V (VT6), are used widely for the manufacture of blades of compressors of gas turbine engines. The VT6 alloy has an efficiently developed chemical composition and is one of the leading structural materials in aviation and turbine construction [1].

The VT6 alloy with the reduced content of the interstitial impurities is recommended for application in components in which high values of fracture toughness and resistance to salt corrosion are required, and is also highly suitable for applications in cryogenic technology [2, 3].

There are a large number of technological (metallurgical) measures which make it possible to produce different types of semi-finished products from the Ti–6Al–4V alloy with a wide range of the microstructures. The technology of electron-beam evaporation and vacuum condensation is an advanced metallurgical process which can be used to produce both foil [1] and thick components (condensates) with the ultrafine grains and the high values of the strength characteristics [3]. The deposition of the vapour flow on the specially prepared surface (substrate) made of a titanium alloys produces a material for efficient constructional coatings used, for example, for the restoration of the geometrical dimensions of the components of the compressors, aviation, ship and power engineering systems.

A rational metallurgical method of producing the condensates of the VT6 alloy is the high-speed electron-beam evaporation using an intermediate liquid metal pool – intermediary pool. To increase the melt temperature, refractory metals are added to the pool [4] which make it possible to regulate the supplied power in the volume of the melt. For this reason, the conditions of evaporation of the components of the alloys (titanium, aluminium, vandium), with different vapour

tension, change at the melt temperature, together with the microstructural parameters of the vacuum condensates and also their physical-mechanical properties.

When selecting the system of the alloying additions, forming the intermediary bath for the evaporation of VT6 alloys, it was necessary to take into account the possible positive effect of the microadditions of the added components on the properties of the produced condensates (coatings). According to [5], these elements include molybdenum and zirconium. In the evaporation of alloys based on titanium, nickel, aluminium and iron, it is recommended to use tungsten, molybdenum, their or materials from the group of rhenium, tantalum, niobium and hafnium [6, 7].

In this study, investigations were carried out into the possibilities of application of the intermediate pools of refractory components with a high melting point – niobium and tantalum, the 'light' pool-intermediary of the Zr–Mo system for producing rational condensation rates, and also attention is given to the dependence of the mechanical properties and structure of the produced VT6 condensates on the condensation rates, determined by the composition of the intermediate pools.

Experimental methods

To compare the mechanical properties of the condensates of the VT6 alloy, investigations were carried out on annealed sheets of Ti–6.4V alloy with a thickness of 0.65 mm (supplied by an American company), and the evaporated materials was in the form of ingots of Ti–6Al–4V alloy, produced by double electron-beam remelting with a diameter of 70 mm.

The vacuum condensates were produced in the experimental electron-beam equipment of the UE-193 type, designed at the E.O. Paton Electric Welding Institute, Kiev, with the application of intermediate pools Zr–Mo which were produced on the surface of the billet by consecutive enrichment of the pool with zirconium and molybdenum. For easy separation of the vacuum condensates from the flat substrate of the VT6 alloy, the alloy was deposited with a layer of CaF_2, which was evaporated from the main evaporator. The substrate temperature was varied in the range 620...720°C at a cooling rate of the vapour flow of 13...25 mm/min.

After separating the condensate from the substrate, specimens were produced from the condensate for different types of tests. The properties of the condensates were determined in the initial condition and after vacuum and healing at temperatures of 450...650°C, 2 h and 700°C, 1 h.

The microstructure and chemical composition of the condensates were investigated in a CamScan4 electron microscope using an Energy 200 energy-dispersing analyser (INCA software).

Experimental section

The VT6 alloy belongs in the group of the two-phase α + β alloys of the martensitic class with a small amount of the β-phase with the BCC lattice which predetermines the susceptibility of the of the material to the hardening heat treatment. Aluminium is a stabiliser of the α-phase with the hexagonal dense-packed lattice. At a temperature of 882.5°C, the allotropic transformation of the α- to the β-phase takes place.

The mechanical properties of the titanium alloys are determined by the technology of melting and subsequent heat treatment. In the case of a stable chemical composition, the strength and ductility of the titanium alloys depend on the grain size, the ratio of the volume fractions of the α- and β-phases and the presence of the hardening phases. In most cases, the alloys used in the industry are characterised by a slightly oriented polyhedral structure with the mean grain size of 25...40 μm after annealing at a temperature of 600...650°C for 2...4 hours [8].

It is important to know the effect of the structure of the titanium condensates on the fracture toughness and fracture resistance under alternating loading. This depends on the type of structure, the homogeneity of the

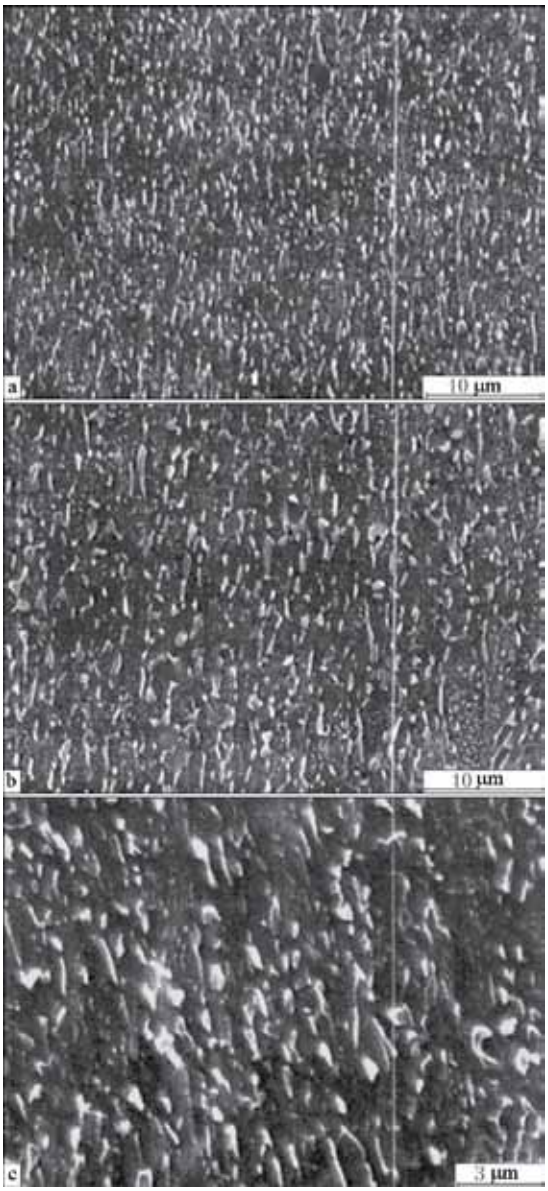

Fig. 1. Microstructure of the VT6 vacuum condensate in the initial condition (a) and after vacuum annealing at 650°C for 2 hours (a, b, c).

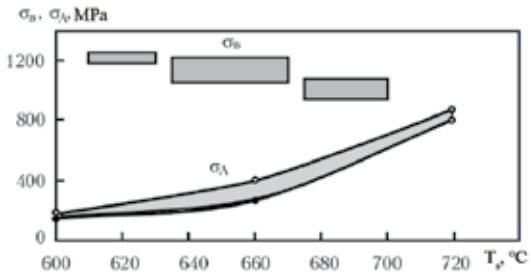

Fig. 2. Effect of the substrate temperature on the tensile strength σ_B and adhesion strength σ_A of the VT6 vacuum condensates on the substrate of VT6 alloy.

structure in the thickness, the dispersion of the structural components, and the phase composition of the condensates. It is assumed that the increase of the deformation temperature or annealing temperature to the temperature of the (α + β) ↔ β-transition increases the fracture toughness parameters. On the other hand, the formation of the globular structure by deformation below the temperature of the β (α + β)-transition reduces the fracture toughness which the creases with the reduction of temperature and the increase of the degree of deformation. Consequently, as the degree of super cooling of the Ti–6.4 vapour flow in condensation increases, the toughness of the resultant condensate increases. In the case vacuum condensates, important parameters include the condensation rates and the substrate temperature, which determine the degree of super cooling of the vapour flow on the surface, the size of the single grains in the thickness of the condensates, the ratio of diameter to the length of the grain, etc.

The structure of the equilibrium condensate of the VT6 alloy, produced at T_c = 650°C (T_c is the condensation temperature) was analysed by scanning electron microscopy (Fig. 1). The structure consists of a composition of two phases, α and β. The distribution of the components between the α- and β-phases was recorded, together with the enrichment of the boundary regions of the α-phase with vanadium (2.6–5.8 wt.%) in comparison with the centre of the grain (1.9...3.5 wt.%). The particles of the β-phase contain up to 10...14 wt.% of vanadium at

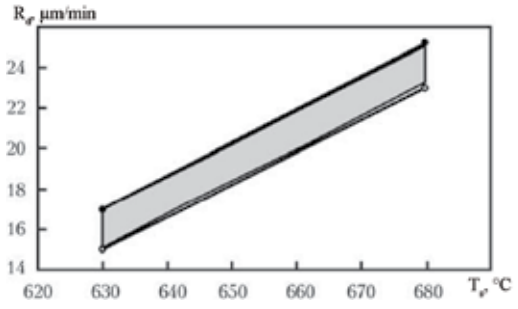

Fig. 3. The relationship of the condensation rate R_d and the substrate temperature T_s resulting in the formation of high functional properties of the the VT6 vacuum condensates.

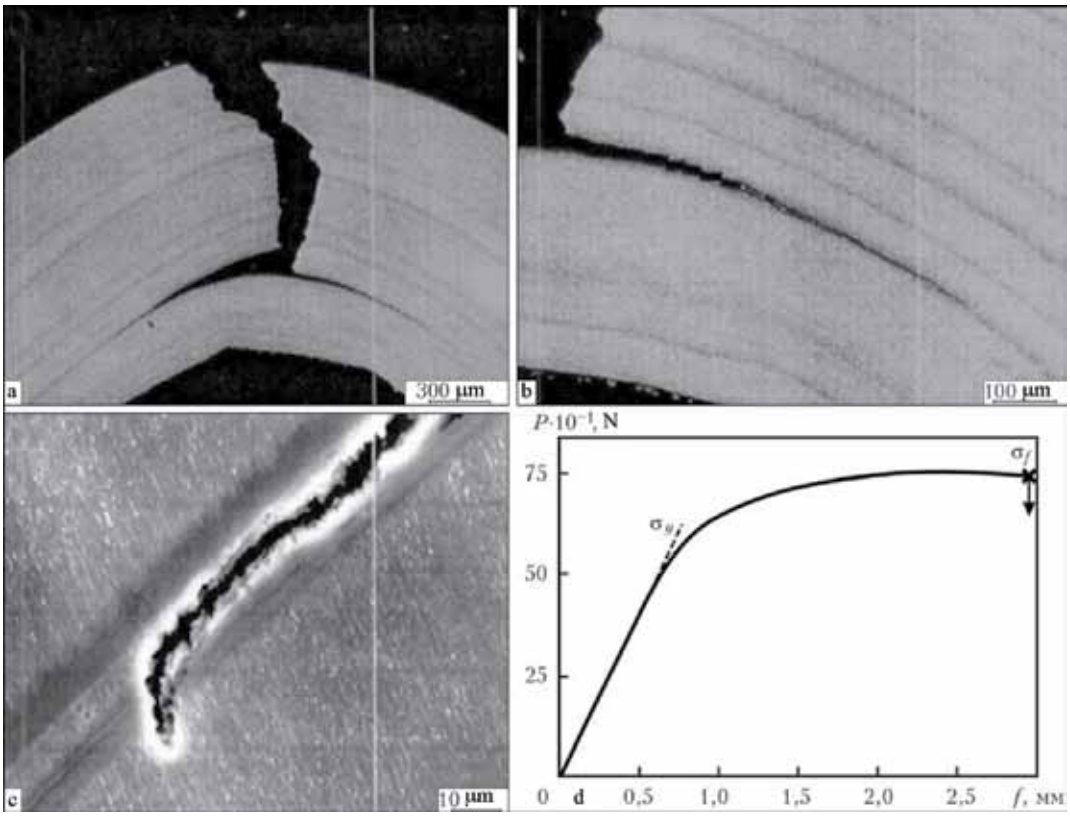

Fig. 4. Microstructure (*a* – *c*) and the deformation diagram (*d*) of the VT6 condensate after the bend test: *f* is the deflection.

2.8...4.5 wt.% of aluminium, and as regards the α-phase, 4.6...6.47 wt.% of aluminium and 1.9...3.8 wt.% of vanadium.

The reduction of the size of the initial α-grains and, at the same time, the distance between the particles of the globular β-phase increases the fracture toughness of the titanium alloys with the globular structure after quenching and ageing. In the vacuum condensates, the primary structure after cooling is the α-phase, which forms at temperatures lower than the polymorphous transformation temperature. With increasing annealing temperature, the particles of the β-phase form in the matrix and coalesce. The reduction of the distance between the particles of the β-phase should increase the frequency of arrests of the propagating crag during loading. This increases the fracture toughness. For this reason, the increase of the temperature or annealing time in the range 500...600°C should reduce the fracture toughness of the vacuum condensates, because the distance between the particles of the β-phase increases due to the coalescence of the particles (Fig. 1b). At the same time, the increase of the grain size results in the weakening of the anisotropic of the crystallographic growth, which indicates the positive effect of the structural changes on the fracture toughness values.

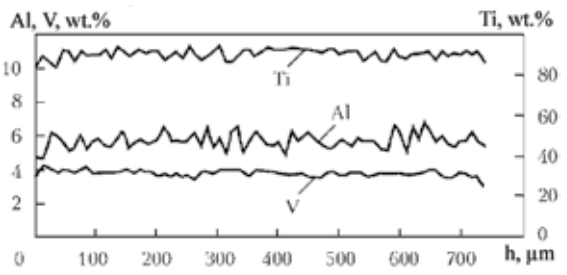

Fig. 5. Distribution of aluminium, titanium, vanadium in the the T6 vacuum condensate (after deposition) using the intermediate pool M_{pool} = 44 g Zr + 25 g Mo, T_d = 650°C, R_t = 14.9 μm/min); *h* is the thickness of the condensate.

The strength properties of the condensates of the VT6 alloy after heat treatment are similar to those of the industrial sheets. The ductility of the sheets was 1.5–2.0 times higher as a result of the different textures of growth (polycrystalline material).

The existence of a large number of the structures of the two-phase titanium alloys determines the large variation of the mechanical properties (Fig. 2). The strength and ductility of the vacuum condensates of the VT6 alloy depend greatly on the temperature of the substrate and the condensation rate, which are determined by the power supply to the evaporator and by the amount of the refractory element introduced into the intermediate pool (Fig. 3).

In the case of the α + β titanium condensates, the reduction of the limit should result in an increase of impact toughness, and the maximum values of the impact toughness should correspond to the structural state resulting in the largest difference between the values of the yield limit and the ultimate resistance of the condensate. However, in accordance with the deformation diagrams this difference is usually minimal (Fig. 4c).

In the course of the investigations of the mechanical properties of the condensates, the micro laminated nature of the structure as a result of the instability of the self-oscillatory process of evaporation had almost no effect on the tensile properties of the VT6 alloy. In the case of high homogeneity of chemical composition in the cross-section ($\Delta Al/Al \rightarrow 0.1$) at a deposition rate of R_d = 16.2 μm/min, the relatively elongation of the condensates was 4...13% (Fig. 5), and the impact bending resistance was maximum, 46...68.9 J/cm^2 (Fig. 3).

The equilibrium nature of the structure of the condensates is ensured by the efficiency of the diffusion processes in the deposited material during its production. The nonequilibrium nature of the structure is retained with increasing the deposition rate of the VT6 vapour flow and the reduction of the substrate temperature. Consequently, to obtain the equilibrium structure of the condensates, it is necessary to use a relatively low condensation rates of R_d = 15...18 μm/min at temperatures of 620...630°C. The deposition rate at a temperature of 650...660°C should 18...22 μm/min, and at (680 + 10)°C it may reach 23...25 μm/min. The increase of the evaporation current (supplied power) and also of the volume and degree of superheating of the intermediary pool increases the instability of the process evaporation of the VT6 alloy microporosity appears in the structure of the condensates, and its development is determined by the material of the intermediary pool, its mass and evaporation current (Fig. 2, 3).

The generalised data on the mechanical properties (tensile properties) of the condensate of the VT6 alloy indicate that the level of strength that not depend greatly on the average chemical composition and the nature of micro laminated structures. The strength of the condensates with a low (3 wt.%) and optimum (6 wt.%) aluminium content confirms the controlling role of the growth texture in the condensates with fine grains in reaching the strength of the matrix at the level of 1150...1200 MPa (Fig. 2). The results show a monotonic decreased of the yield limit, ultimate strength, and also an increase of the ductility of the condensates with the increase of the substrate temperature in the temperature range from 620...630 to 680...690°C.

Heating to the maximum temperature of the substrate of VT6 (650°C) was insufficient

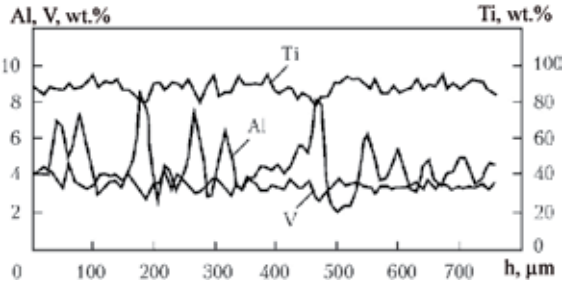

Fig. 6. Distribution of aluminium, titanium, vanadium in the VT6 vacuum condensate (after deposition) using the intermediate pool (M_{Ta} = 73 g, T_d = 650 – 660°C, R_d = 21.5 μm/min).

for obtaining high-strength joints between the alloy and the condensate in adhesion tests. However, the deposition of the the VT6 vapour flow in short-term (8...10 min) heating of the substrate to 715...720°C and is subsequent reduction to 650°C resulted in a stable high level of adhesion (more than 600 MPa) of the condensate with the base (Fig. 2).

The lower condensation rate of the vapour flow (15...18 μm/min) at the periphery of the substrate resulted in a higher level of strength (1125...1300 MPa) in comparison with the material condensed directly above the evaporator where, with other conditions being equal (in one experimental), the rate was 21...23 μm/min, and the ultimate strength 1040...1070 MPa.

These differences in the mechanical properties may be attributed to the extent of the diffusion processes in the volume of the condensate during its formation. At lower deposition rates, the non-equilibrium nature of the structure of the produce condensate is less pronounced, the material may reach the thermodynamic equilibrium in every separately considered microlayer. The concentration of the non-equilibrium vacancies which form in subsequent stages micro pores was relatively low in this case. Consequently, the VT6 condensate with the satisfactory level of the strength at the substrate temperature of 620...630°C was produced.

The higher (23...25 μm/min) deposition rate of the vapour flow also result in the release of a large amount of the hidden condensation heat on the substrate, but it does not ensure the formation of the equilibrium structure of the alloy, condensed on the substrate at 620...630°C. The substrate material and its heat conductivity are important in this case. The condensates, produced on the steel substrate with the high level of heat conductivity are susceptible to ageing in subsequent vacuum annealing in the conditions for 450...560°C.

At the condensation rate of 12...14 μm/min, the difference in the maximum and minimum values of the yield limit of the specimens, measured in different areas of the substrate, was relatively large (200 MPa) at the ultimatum strength of 1180...1200 MPa. When the condensation rate was 25 μm/min, the difference between the highest and lowest values of the limit was less than 50 MPa. This indicates the higher susceptibility of the vapour flow to quenching effects at R_t = 24...25 μm/min. Consequently, the materials, produced at high deposition rates (and low condensation temperature) are sensitive to the ageing effects and the loss of ductility in heating which is undesirable for the structural coatings, deposited on actual components.

The increase of the cooling rate of the vapour flow from 16 to 25 μm/min results in a monotonic reduction of the fracture toughness of the vacuum condensates VT6 from 45...0 to 24...35 J/cm^2. This effect is associated with the formation of micro porosity in the material in the non-equilibrium cooling conditions of the vapour flow. The rational conditions of subsequent heat treatment increase the fracture toughness. The maximum fracture toughness was obtained in the case of the uniform distribution of the components in the thickness of the condensate when the values of Al do not exceed 0.5% at the mean aluminium content of 5.2…6.5 weight percent (Fig. 6). The importance of the result is the fact that the increase of the evaporation current results in superheating of the pool, increase of the volume of the pool, and also the increase in the extent of the microlayers in the structure of the material

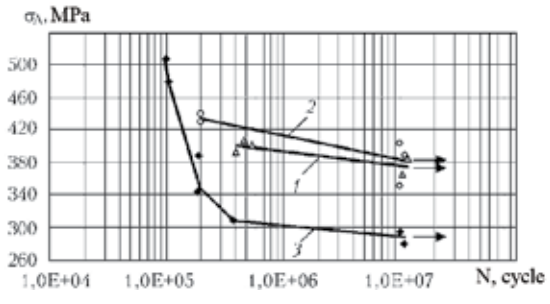

Fig. 7. High cycle fatigue of the VT6 condensates at a temperature of 20°C: *1*) Ti – 6.4 (1.35 mm sheet); *2*) VT6 after deposition at Ts = 650°C; *3*) VT6 after deposition in vacuum annealing at 650°C, 2h.

[ΔA (max–min) = 3%] (Fig. 6). However, this does not have any significant effect on the physical-mechanical properties (ultimate strength and ductility of the condensates). The physical micro-heterogeneity influences the mechanism of failure of the laminated condensates in the band test, and also results in early failure through the brittle interlayers of the α-phase (Fig. 4a, b, d).

The generalised results of high-cycle fatigue of the condensates in relation to the deposition temperature (substrate temperature) indicate that the maximum endurance is obtained in the case of the condensates produced at 650°C. Subsequent equalising annealing of the condensates at this temperature for 2 hours does not lead to any changes in the endurance limit of the material (Fig. 7).

The following conclusions was made on the bases of the comparison of the fatigue endurance of the VT6 condensates with the metallurgical conditions of production of the condensates (M_{Ta} = 73 g). At a substrate temperature of 650...660°C, the reduction of the condensation rate of the Ti...6.4 vapour flow resulted in a small reduction of the endurance limit of the condensate. The increase of the substrate temperature, which determines the grain growth and increase of the size of the particles of the β-phase, reduced unambiguously the endurance limit of the condensate from 370...400 to 285...305 MPa at $1 \cdot 10^7$ cycles.

The low substrate temperature (620...630°C) results in the quenching effect and, consequently, the increase of the values of the yield limit and tensile strength as a result of the formation of the solid solution of the Ti–6.4 condensate, saturated with aluminium and vanadium, reduces the endurance limit at high stress amplitudes, stabilising it at 320...330 MPa in the range of $1 \cdot 10^6 \ldots 1 \cdot 10^7$ load cycles.

The formation of the microlayered structure (Fig. 8 a) of the VT6 condensed alloy

Fig. 8. Microstructure of the VT6 condensate in the cross-section, produced using the intermediate pool made of 73g of (*a*) and 44 g Zr +15 g Mo (*b*).

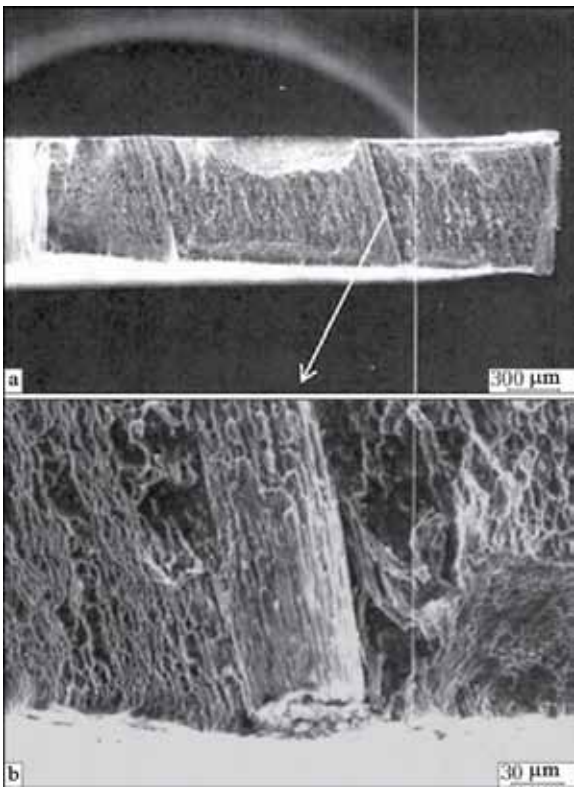

Fig. 9. Fracture surface of the VT6 condensate (*a*) with the ??? of growth from the microdroplet (*b*).

is associated primarily with the selective evaporation of aluminium from the superheated pool through the non-equilibrium layer of the vapour. The pool is heated by the electron-beam, scanned on the surface of the melt. The application in the first stage of the investigations of the refractory additions of niobium and tantalum for the formation of the intermediary pool and reaching the higher rate evaporation conditions did not ensure the homogeneity of the structure of the condensed material (Fig. 8a, 7, 4).

When producing relatively thick condensates (up to 3...5 mm), the duration of condensation of the vapour flow was relatively long and reached 5 hours at a deposition rate of 12...13 μm/min. Increasing the deposition rate to 18 μm/min by increasing the supplied power reduce the evaporation time but this resulted in the occurrence of the microdroplet transfer. As the power, supplied to the evaporating increase, the evaporation rate/condensation rate increase together with the probability of formation of the spectrum of the microdroplets in the volume and on the surface of the deposited layer. This is unacceptable (Fig. 9).

The main reason for the splashing of the evaporated materials (ingot) is the reactive effect of the vapour jets, i.e., the local increase of the vapour pressure on the liquid pool accompanied by the formation of closures of the melt with the increase of the size of the local meniscus. Splashing is also caused by local differences in the vapour pressure and movement of the melt.

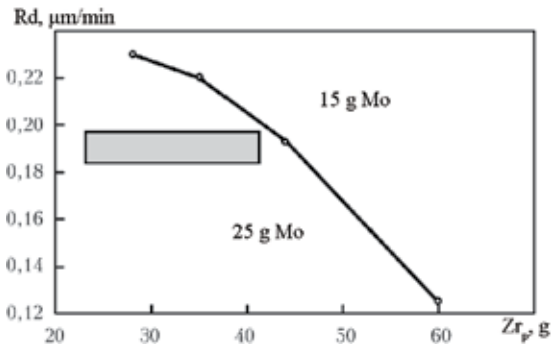

Fig. 10. Dependence of the oxygen content of the hot zone of the VT6 vacuum condensates after adding zirconium to the intermediate pool Zr – Ti – Zr – Mo – V – Al; dark field – initial oxygen content of the Ti – 6.4 ingots 0.173 – 0.187 wt.%.

The susceptibility to splashing is determined not only by the surface power but also by the quality of the evaporated materials – oxygen content, and density of the ingot metal, minimum porosity, temperature gradients in the melts pool. In many materials, the higher rate of splashing is detected at a specific surface power of 10...100 kW/cm^2 [4].

An important factor, influencing the mechanical properties of the produce condensates is the oxygen content (Fig. 10). As indicated by the diagrams, shown in Fig. 11, at the minimum oxygen content (0.13 in wt.%), the VT6 material has a certain ductility reserve. In the foreign foil, the oxygen content was 0.10...0.14 wt.%. This oxygen content, taking into account the small grain size, did not influence the reduction of the yield limit and ultimate strength of the HCP matrix. The mass fraction of oxygen, which is an alloying addition, in the VT6 alloy should not exceed 0.2% to ensure the sufficiently high ductility of the the material (weldability and the deformation capacity).

The rate of evaporation and the accompanying microdroplet transfer are influenced by the energy parameters of the evaporation process (the frequency of scanning in program ???, the level of the melt in the evaporator). At a constant rate of supply to the pool, ensuring partially the stable conditions of evaporation of a long period of time, the microdroplet transfer is influenced by the refining reaction of the evaporated pool at the liquid phase – vacuum interface.

The evaporation of the VT 6 alloy with the electron-beam in vacuum is accompanied by the scattering of aluminium in the surrounding space and by the preferential deposition of aluminium on the substrate at the periphery. According to the data published in [8], in the presence in the centre of the hotspot of 6% of aluminium the Ti...6.4 condensate contains 8.5 wt.% of aluminium at a distance of 250 mm from the centre. In all likelihood, this phenomenon is caused by the

considerable axial superheating of the melt when the boundary of contact of the melt with the solid evaporated ingot has a distinctive parabolic shape (at a possible depth of 30 mm).

The application of the intermediate pool, containing components with a high binding energy with excision in comparison with the titanium, results in the interaction of these components with oxygen, dissolved in the evaporated ingot. This results in the formation, on the surface of the melt of oxide slag films, ensuring a reduction of the oxygen content of the condensates. The results also show a monotonic reduction of the oxygen content in the VT6 condensates in relation to the increase of the amount of the additions added to the melt (Fig. 10).

The metallurgical methods of preventing the splashing of the liquid metal pool in evaporation included the restriction of the amount of the gas impurities and the increase of the density of the evaporated alloy; application of the intermediate pools made of the refractory metals of the groups IV...VIa.

In [9], investigations were carried out into the effect of the additions of yttrium, titanium, vanadium, zirconium, niobium, iron used as the filler material in the intermediate pool in evaporation and condensation of copper.

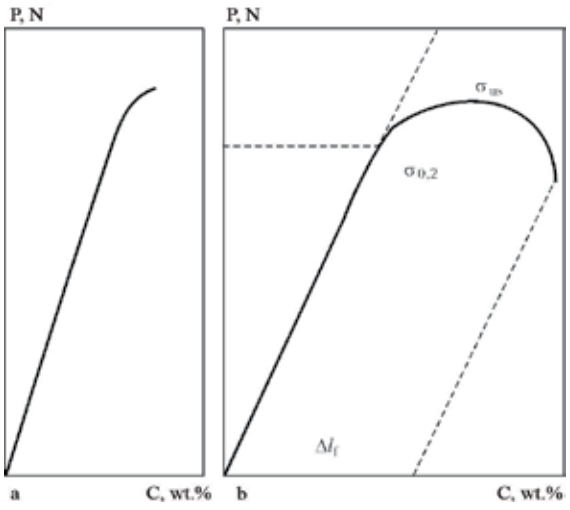

Fig. 11. Typical deformation diagrams of the VT6 condensates at a mass fraction of oxygen of 0.16...0.25 (*a*) and <0.13% (*b*).

The material, used for the formation of the intermediate pool in evaporation of a pure metal should satisfy a number of requirements. The density (specific weight) of the added metal should be lower than the density of the evaporated metal; the vapour tension of the filler material should be lower than the vapour tension of the evaporated alloy, and the melting point should be higher [10].

There are methods of regulating the rate of electron-beam evaporation of the materials in vacuum using widget is possible to restrict the extent of splashing of the metal in high-speed evaporation from the liquid pool. The refractory pool (intermediate pool) in the evaporation of the titanium alloy was initially niobium and tantalum characterised by low values of the vapour tension and a high melting point of niobium. The latter was 2468°C, and in the case of tantalum 3000°C. The increase of the temperature of the VT6 melt in the formation of the intermediate pool resulted in the increase of the evaporation rate, and also the condensation rate (R_d 25–35 μm/min), and the formation of a micro laminated structure of the condensate (Fig. 8a, 4, 6). In this case, the microlayers, enriched with aluminium alternated with the layers of the condensate enriched with vanadium and depleted in aluminium. The maximum aluminium concentration in the individual microlayers reached 12 wt.%. This heterogeneity of the structure and the large scatter of the data for aluminium caused embrittlement and delamination of the condensates during bending or under alternating loading (high cycle fatigue).

The principle of the alloying method, investigated in [10, 11] is the application of a special intermediate pool made of zirconium which is produced in a crucible on the surface of the copper melt. The intermediate pool was produced using the melt of a zirconium charge (up to 10 volume percent of the pool volume), which was dissolved in the melt of evaporated copper thus increasing the temperature of the pool surface. This resulted in a large increase of the evaporation rate of the metal (copper chromium) whilst restrict-

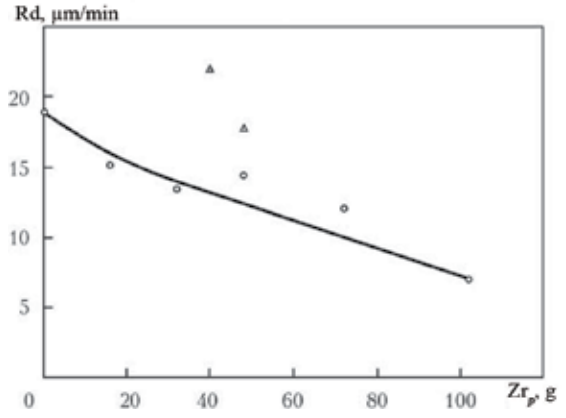

Fig. 12. Dependence of the condensation rate on the amount of zirconium (o) and molybdenum (Δ) in the molten pool in the evaporation of the VT6 ingot (I_{evap} = 2.3 A).

ing the extent of the microdroplet process.

In the present study, in the optimisation of the chemical composition of the intermediate pool it was necessary to take into account the need for the restriction of the scattering of the highly volatile aluminium in the vapour flow [12] which increases when the ratio of the masses Mo/Zr at the eutectic point, initially accepted as 3/7, increases. Excess molybdenum increases the surface temperature of the pool and, according to the bent meniscus of the melt, reduces the surface tension of the pool. Consequently, the condensation rate increases and a tendency for the scattering of aluminium at the periphery becomes stronger [12]. This also takes place when the total mass of the additions increases. For example, the scattering of aluminium (the difference of the absolute values of the aluminium content in the centre of the hotspot above the evaporator and at the periphery of the substrate and the angle greater than 30°) reached 0.9 wt.%, is the amount of the addition to the melt was 60 g Zr + 25 g Mo (Σ = 85g).

In the intermediate pool with a lower degree of alloying the deviation in the aluminium content in the individual microlayers of the condensate was smaller (Fig. 8b, Fig. 5).

The determination of the amount of the additions added to the VT6 melt was linked with two main problems: obtaining the high quality of the condensate (coating), i.e., the reliability of the technological process, and the time required to produce a high quality condensate or the condensation rate, which determines the economic efficiency of the process. The quality of the condensate is expressed by the minimisation of the microdroplet process and by the absence of microlaminated structures in the condensed material whilst maintaining its chemical composition.

The problem of optimisation of the content of the liquid metal pool – intermediate pool for the evaporation of the Ti–Al–V alloy was solved by adding to the melt of the evaporated materials components reducing the sensitivity of the evaporation surface to temperature variations (gradients) and enabling homogeneous evaporation/condensation of a long period of time without the formation of microlayers in the deposited material and the restriction of the microdroplet transfer (with the size of the microdroplets in the condensate not greater than d_{spit} = 50 μm on the surface area of 10 cm^2).

The addition of zirconium to the melt reduce the condensation rates (Fig. 12) at the constant thermophysical evaporation conditions (as a result of reducing T_L according to the equilibrium diagram [13] and the increase of the surface tension of the melt). In turn, the addition of molybdenum increased the evaporation/condensation rate of the Ti–6.4 ingot as a result of the increase of T_L of the liquid metal pool of the evaporated ingot.

The proposed composition consists of the alloying elements, added to the evaporated Ti–Al–V melt, which in interaction with the melt form on the end surface of the ingot, placed in the watercooled crucible, the evaporated pool – intermediate pool. The pool is used for the evaporation of the main components of the VT6 alloy, including high-purity zirconium and electron-beam remelted molybdenum, containing the minimum amount of interstitial impurities (C ≤ 0.2 and O ≤ 0.1 wt. %), at a mass ratio of zirconium/molybdenum, corresponding to the eutectic composition. This ratio is approximately 7:3, which corresponds to 71 wt.% of zirconium and 29 wt. % of molyb-

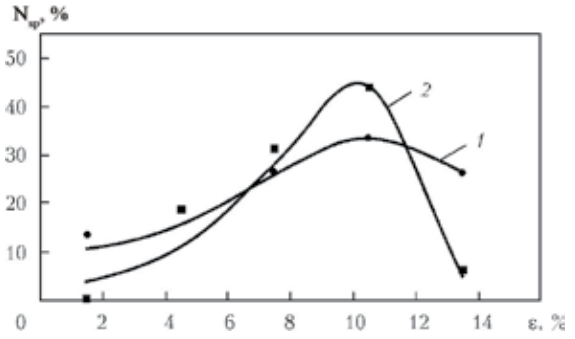

Fig. 13. Elongation of the specimens-condensates of the VT6 alloy, produced using the intermediate pools on the titanium substrate: *1*) 28 g Zr +12 g Mo; *2*) 35 g Zr +15 g Mo.

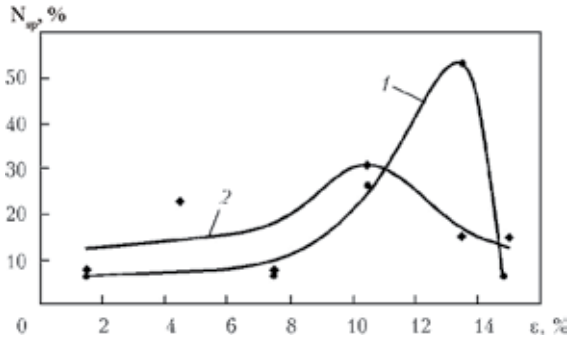

Fig. 14. Elongation of the specimens-condensates of VT6 alloy, produced using the intermediate pools deposited on the titanium substrate: *1*) 44 g Zr +25 g Mo; *2*) 44 g Zr +15 g symbol.

denum at T_{eut} = 1553°C, according to [13].

The main approach to this problem is based on the formation of the intermediate pool with the melt temperature lower than the melting point of the evaporated VT6 alloy. This is a completely different approach, in contrast to that proposed in [6] where T_m of the material of the intermediate pool (niobium, tantalum), place in the crucible on the evaporated ingot (nickel or titanium alloys) is always higher than the melting point of the evaporated metal. The addition to the Ti–Al–V melt of zirconium and molybdenum at a ratio, corresponding to the Zr–Mo eutectic system with the reduced level of the surface tension of the melt, made it possible to create favourable conditions for evaporation in electron-beam heating of the ingots of the VT6 and produce a shallow pool (at constant conditions of scanning of the electron-beam on the surface of the melt).

The addition of these elements to the melt made it possible to restrict the extent of liquation of the melt and support the formation of the flat melting front of the solid phase under the pool of the ingot, redistributed the Marangoni collective flows in the subsurface layers of the melt as a result of the restriction of the temperature gradients and due to the increase of the heat conductivity of the melt. Thus, the transfer of aluminium from the solid phase of the VT6 ingots through the layer of the Ti–Zr–Mo–V–Al melt to the surface of the liquid – vacuum interface was simplified.

When using the intermediate pool, the Ti–Zr–Mo–V–Al melt was almost completely homogeneous throughout the entire volume of the pool of the VT6 alloy. Evaporation of vanadium and aluminium took place is a result of the washing out, by the collective flows of the liquid metal, of the components of the VT6 alloy from the solid phase of the ingot and transfer of the components of the subsurface layers of the melt, bordering with the gas phase (vacuum). Consequently, the evaporation of the main components of the Ti–6Al–4V alloy took place in a still manner from the surface of the intermediate pool, without any significant enrichment of the vapour flow with zirconium and molybdenum. Zirconium was found in the condensate in the content of 0.035–0.100 wt.%, depending on the amount of the addition added to the intermediate melt.

In most cases, the values of the yield limit and tensile strength of the condensates, produced using the intermediate pool of different chemical composition, where approximately identical, but the parameters of the relative elongation differed which is evidently associated with the different intensity of the microdroplet process.

The maximum values of the relative elongation of the produce condensates were obtained in the range 12.5...14.0%. In all cases, when in tensile loading of the specimens they were equal to 3...5%, the examined

fracture surface contained 'stems' of growth from the microdroplets formed in a very small number on the substrate (Fig. 9). The presence of foreign growth inclusions in the condensates is unacceptable because of the limited (weak) cohesion bond with the matrix of the condensates/coating and, consequently, the act as notches in mechanical loading of the material.

The vacuum condensates of the VT6 alloy, produced on the stationary substrate, in comparison with the industrial alloys (0.2% O, 0.05% N) showed a lower content of the interstitial impurities, primarily oxygen and nitrogen (0.120%, 0.007% N). In the process of evaporation of the ingot the peripheral regions of the vapour flow screen the penetration of the residual atmosphere to the internal volume (cone-shaped) of the vapour flow and, consequently, result in the relatively high purity with respect to the gas impurities in the material condensed on the substrate.

Analysis of the fracture surfaces of the condensates, produced using the Zr + Mo pool with a total mass of 40...45 g, did not show any microlamination, characteristic of the case of application of intermediate pools based on niobium or tantalum in evaporation of the Ti–6Al–4V alloy (Fig. 8b, 4).

The increase of the total mass of the Zr + Mo mixture, added to the evaporated pool of the titanium alloy, starting at a certain amount reduces the evaporation/condensation rate of the Ti–6.4 ingot in the stabilised conditions of heating the melt. Regardless of the increase of the volume fraction of the mixture with low T_L (in the Mo–Zr eutectic system the minimum T_L = 1553°C), the fraction of zirconium with T_L = 1855°C and with a low vapour tension in the melt increases. For example, when adding to the melt 100g of the mixture, consisting of 71g of zirconium and 29g of molybdenum, the condensation rate of the Ti–6.4 alloy on the substrate positioned at a distance of 330 mm from the outlet of the evaporator, was not greater than 8 μm/min. This was accompanied by a reduction of the amount of aluminium, transferred by the vapour flow to the centre of the condensates, because molybdenum increases the degree of scattering of the aluminium at the periphery of the vapour flow.

The efficiency of different intermediate pools in producing the maximum level of the ductility of the Ti–6Al–4V condensed alloy is shown in Fig. 13, 14 which give the histograms of the elongation of the specimens with a cross-section of 3 × 1 mm and the gauge length of 10 mm, produced from a sheet of the condensate, corresponding to the so-called hotspot. The mostly high values of the relative elongation (ε = 10...15%) of the condensates at uni axial tensile loading with the strain rate of ($\varepsilon' = 1.7 \cdot 10^{-3}$ 1/s) confirmed the absence of microlayers in the structure. These condensates with a thickness of 1 mm were produced at condensation rates of R_d = 14–16 μm/min.

Thus, the depth of the evaporated pool in the crucible required for the formation of the homogeneous structure of the con the coating with the constant Al/V ratio in the thickness of the deposited layer should be 9...12 mm. Evaporation of the Ti–Al–V alloy takes place by the electron-beam scanned on the periphery of the surface of the cylindrical pool without the central heating spot to produce the flat melt – solid-phase front. The mixture of the metals, added to the liquid metal pool of the vacuum evaporated VT6 titanium alloy, consisting of the high-purity zirconium and aluminium, is characterised by the fact that the mass ratio of the components of the mixture corresponds to the eutectic concentration according to the equilibrium diagram [14]. The amount of the mixture of the metals (Mo + Zr), added to the Ti–6 Al–4V melt, should be 23–30% of the mass of the metal (liquid pool).

Conclusions

1. The investigations were carried out to determine the possibilities of electron-beam evaporation of VT6 alloy, containing components with different vapour tension (vanadium, aluminium), in the prepara-

tion of the vacuum condensates. This was carried out using the intermediate tool of heavy elements (niobium, tantalum) with a high melting point, and also the 'light' intermediate pool of the eutectic composition of the Zr–Mo system with the melting point of 1553°C to obtain the rational solidification rates.

2. The application of the 'heavy' intermediate pools based on niobium and tantalum increases the condensation rate R_d to 21–25 μm/min which supports the formation of the microlaminated structure of the condensate and the results in the acceptable enrichment of the individual layers of the condensates with aluminium. This reduces the relatively elongation of the deposited material to 3–5–8% and results in the brittle fracture in the bend test.
3. An intermediate pool based on zirconium and molybdenum with the mass ratio of the components of 7:3 was developed. The pool ensures the high evaporation rate at a limited microdroplet transfer of the vapour flow and the minimum microlaminated nature of the structure of the produce condensates of the VT6 alloy.
4. The experimental results show that the microlaminated structure of the vacuum condensates (as the results of the self-oscillatory process of electron-beam evaporation) has almost no effect on the strength properties of the condensates in the tensile tests.
5. The increase of the amount of the additions of zirconium and molybdenum, added to the evaporated pool, result in a monotony reduction of the density of splashes in the VT6 condensate. The ultimate strength of the condensates that the depend on the chemical composition of the intermediate pool, the relative elongation of the condensates reaches 10.5–13.5% with the Ti achievement of the maximum values of strength by 50% of the investigated specimens. The increase of the amount of the additions of zirconium and molybdenum added to the intermediate pool (up to 60 g of zirconium and 25 g of molybdenum) results in a reduction of the mass fraction of oxygen in the hot zone. The minimum amount of oxygen in the vacuum condensates is 0.13 wt.%.
6. The highest physical and mechanical properties of the condensates of the VT6 alloy were obtained when using the 'light' intermediate pool in the variant 44 g Zr + 25 g Mo (Zr/Mo = 1.76) with the increase of the molybdenum content in comparison with the Zr/Mo eutectic ratio, equal to 2.45. This corresponds to the optimum content of the additions of zirconium and molybdenum in the pool, equal to 20–24 wt.% Zr and 13–14 wt.% Mo, when the Zr/Mo ratio is equal to 1.54–1.70.

References

1. Arzamasov, B.N. (editor), Structural materials, a handbook, Mashinostroenie, Moscow, 1990.
2. Smith, H.R., et al., Journal of Vacuum Science Technology, 1970, vol. 7, No. 6, 48–51.
3. Pat. 8.329436B2 USA, IC17 C23C16/00, Vapour deposition of dissimilar materials, Belousov, I.V., et al., 16.10.2012.
4. Schiller, Z., et al., Electron-beam technologies, Energiya, Moscow, 1980.
5. Moiseev, V.N., et al., Welded joints in titanium alloys, Metallurgiya, Moscow, 1980.
6. Pat. 5474809 USA, IC16B05D, Evaporation method, Skelly, D.W., Jackson, M.R., 12.12.95.
7. Glazunov, S.G., Kalachev, B.A., Metallography of titanium alloys, Metallurgiya, Moscow, 1980.
8. Physical vapour deposition, Airco Temescal, Berkeley.
9. Mochan, B.A., et al., Probl. Spets. Elektrometall., 1991, No. 3, 58–61.
10. Pat. 3356487 USA, IC13 C23C 13/00, Prevention of splattering during vaporization processing, Hunt, C.d.A., Merrill, J.D., 5.12.1967.
11. Pat. 2156005 France, IC13 C23C 13/00 H01J, 19/00. Source de vapour et procode de d'epo't sous vide, Cock, H.G., Hallen, P.A., 27.9.1972.
12. Makhotkin, A.V., et al., Sovremennaya Elektrometallurgiya, 2005, No. 3, 36–43.
13. Lyakishev, N.P., Molybdenum-zirconium. Equilibrium diagrams of the binary metallic systems, vol. 3, book 1, Moscow, Mashinostroenie, 1999, 470–473.
14. Lyakishev, N.P., Titanium–zirconium. Equilibrium diagrams of the binary metallic systems, ibid, 872.

Submitted 11.3.2014

Advances in Electrometallurgy 2014 ***12*** *(2) 118–126*
Translated from Sovremennaya Elektrometallurgiya 2014 ***12*** *(2) 36–43*

Structure of titanium dioxide condensates produced by vacuum electron-beam deposition

L.A. Krushinskaya

E.O. Paton Electric Welding Institute, Kiev,

Investigated are the morphology of the surface, microstructure, element and phase composition of thick condensates TiO_2, produced by EB PVD method, depending on temperature of condensation T_s. Experimental investigations of condensates were carried out using X-ray diffraction method, optic, scanning and transmission microscopy. In formation of condensates TiO_2 within the interval of 120...1200 °C temperatures of condensation the laws were observed that are also same for the majority of inorganic materials: formation of nanodimensional up to Ts < $0.3T_m$ and columnar structures within the interval $0.3T_m < T_s < 0.5T_m$. Polymorphous transformations make an additional contribution to the size and morphology of the structure. Presence of the nanostructural component of different morphology and phase composition within the wide interval of temperatures of deposition was revealed. Within the interval T_s 120...700°C the fractal structure is formed with dimension 2.92...2.95. The results of measurements of electrical strength of titanium dioxide condensates are given. Different forms of TiO_2 (coatings, condensed materials, nanoparticles) produced by the method of vacuum deposition with preset morphology and functional properties are promising for many directions in engineering and also in medicine. Ref. 25, Table 1, Figures 6.

Key words: *electron beam deposition; titanium dioxide; microstructure; nanomaterials; phase composition; polymorphous transformations; fractal dimension*

The oxides of transition metals are characterised by a wide range of electrical, optical and structural properties, used widely in electronic, micro- and nanoelectronic technology, optics, metallic, agricultural engineer, cosmetic methods, medicine, etc. The titanium dioxide TiO_2 occupies one of the leading positions, and is produced in many countries of the world.

Titanium dioxide is used widely not only as an individual compound (for example, in the form of powder) but also as a coating deposited to increase the specific surface, mechanical strength, increase heat resistance and the selectivity of the catalysts, produced on the basis of titanium dioxide [1, 2]. Most investigations have been carried out for thin films.

Recently, the special attention of investigators has been attracted by nanocrystalline oxide coatings characterised by a number of unique properties. Undoubtedly, they included the titanium dioxide TiO_2. At the present time, intensively says is carried out into the possibilities of controlling the morphology of this compound on the nanolevel, because the morphology determines the majority of the functional properties of this material. The nanostructured coatings have higher functional properties than identical powder and bulk materials [3–5]. They are also promising for application in materials science and solid-state physics.

The practical application of the nanostructured TiO_2 is not limited to these applications. As previously, special attention is being paid to the non-consolidated structures – nanoparticles of TiO_2. This is due to their extensive application and promising nature in the most important areas of medicine, such as pharmacology, healing cosmetology, development of

biocompatible materials. One of the variants is the formation of the discrete nanoparticles of TiO_2 in the matrix which, if necessary, can be already removed after synthesis [6].

Titanium dioxide can be regarded as a multifunctional material because of its extensive application. Therefore, the attention of the investigators is being concentrated to the development of efficient methods of synthesis of the nanosized titanium dioxide.

TiO_2 can be produced using a large number of deposition methods [1]. The functional characteristics of the TiO_2 coatings (photoactivity, reactivity, etc.), determined by the surface and volume properties of these materials, strongly depend on the methods of production [1, 5], and even small changes in the synthesis condition greatly influence these characteristics.

In this study, investigations were carried out on thick (20...40 μm) condensates of titanium dioxide, produced by electron-beam evaporation followed by vapour phase condensation in vacuum on a subsidy (EB PVD). The physical processes, forming the basis of this technology, the method should be regarded as a nanotechnological method [7, 8].

Unfortunately, far less attention has been paid to the formation of the TiO_2 oxide by the EB PVD method in comparison with other methods. The large number of different structures of TiO_2 represent an additional factor which requires investigation. The understanding of the mechanism of formation of a specific modification of this oxide is also interesting from the scientific viewpoint and useful for developments in practice.

The aim of the present work is the examination of the relationships governing the formation of titanium dioxide condensates in relations the main technological parameters – the substrate temperature and the effect of structural special features on some of the physical characteristics of titanium dioxide.

Production of oxide materials and experimental procedure

Specimens of titanium dioxide were produced by electron-beam evaporation of 50 mm diameter rods of titanium dioxide, produced by coal pressing the titanium dioxide powder of the analytical purity, followed by condensation of the vapour flow on the substrate.

One of the main factors, which determine the structure and properties of the condensates, is the substrate temperature T_s [7, 8]. Experiments were carried out using the methods of deposition of condensates on the substrates with the given temperature gradient along the axis of the substrate [9] which provided in a single experiment information on the condensed materials in the given continues range of deposition temperatures.

The substrate [9] was in the form of a sheet 250 mm long, 22 mm wide, and 2.4 mm thick. The substrate was made of St3 steel. For easy separation of the condensate into individual specimens, transverse grooves 0.9 mm wide were machined on both sides of the substrate; the width of the specimen was 6 mm. Prior to deposition of the condensate the substrate was polished and degreased. The temperature gradient 120...1200°C along the substrate was produced by fixing one end of the substrate in a copper watercooled bar with heating of the opposite edge by the electron-beam. The temperature gradient was measured using five chromel –alumel thermocouples with the accuracy of ±10°C.

The temperature of the other type of the substrate (water-cooled) was maintained in the range 50...100°C. The vacuum in the working chamber during deposition of the vapour flow of titanium dioxide was equal to 1×10^{-2} Pa. The condensation rate in these experiments was constant, the average rate was 1.8...3.0 μm/min. The thickness of the produced condensates reached 20...40 μm.

The structure of the metal of the surface and in the cross-section of the TiO_2 condensates was examined by scanning electron microscopy (SEM) in a CamScan 4D microscope in the mode of secondary and elastically reflected electrons.

The elemental composition of the coatings was determined by an x-ray spectrum microanalyser (attachment EDX to the Cam

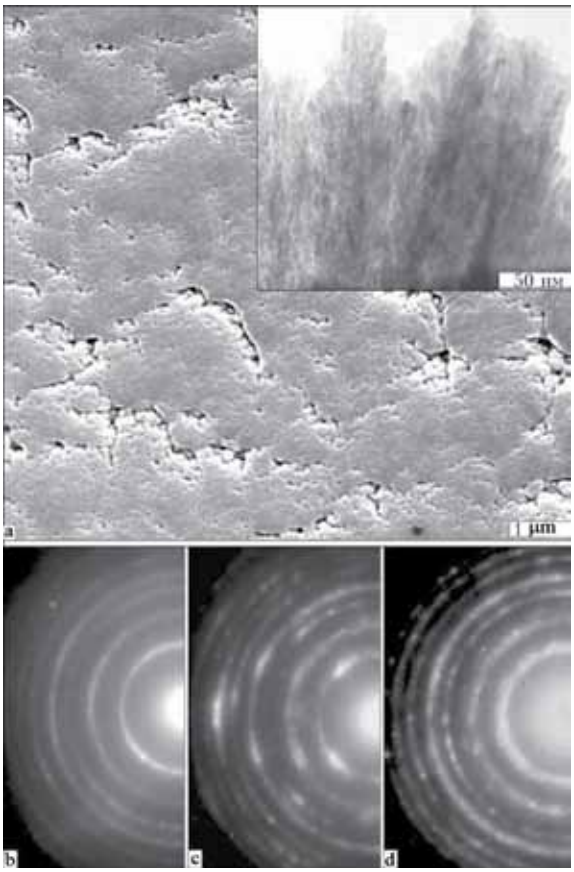

Fig. 1. Microstructure of the TiO_2 condensates and the appropriate electron diffraction diagrams at T_s, oC: a) 120... 300; b) 135; c, d) 300.

Scan 4D microscope); the results were process using the Inca-2000 software. The arrow measurements was ±0.3%.

The phase composition of the produced condensates was investigated by x-ray diffraction in DRON-3M equipment in Cu-Ko Fifa α-radiation (wavelength 0.1542 nm) with the Bragg-Brentano focusing in reflection in the angle range 2θ 10...100°; information was transferred to an automatic printer. X-ray diffraction analysis of the diffractometric data was carried out by refining using the Ritveld method [10] and Maud program [11, 12].

The fine structure of the titanium dioxide condensates was examined by transmission electron microscopy (TEM) in H-800 equipment (Hitachi) at an accelerating voltage of 200 kV. Thick sections, transparent for the electrons, produced by separation from the thick condensates were studied. The electron diffraction and diffraction patterns were identified using the ASTM library.

Electrical strength (breakdown voltage) of the TiO_2 dielectric coating was measured at direct and alternating currents in the conditions of temperature using the procedure described in [13].

Experimental results and discussion

The investigation of the elemental composition shows that the produce condensates corresponded in the composition to the stoichiometric compound TiO_2 (in the range from $TiO_{1.9}$ to $TiO_{2.0}$) in the entire condensation temperature T_s the range examined (120...1200°C). In the condensates, produced by electron-beam technology, the results showed a reduction of the content of impurities in comparison with the initial material, and the overall concentration of the impurities did not exceed 0.1 wt.%.

A sensitive characteristic to a large number of service properties of the coatings is the surface roughness which in the thick coatings usually depends on the size of the volume structure of the material. It is especially important for the planning of the catalytic and optical properties of the oxide to explain the relationships governing the formation of the surface relief of the titanium dioxide condensates. Therefore, in addition to the structure of the sections of the titanium dioxide condensates, the surface morphology of the condensates was also investigated.

The natural surface of the titanium dioxide condensates, produced by EB PVD method at a substrate temperature T_s in the range 120...350°C is smooth, shiny, transparent and glass-like. The microstructure of the surface of this condensates is shown in Fig. 1a. In the cross-section, the structure of the condensates is genius and quite difficult to examine by scanning electron microscopy.

At T_s higher than 350°C, the surface of the condensates shows various growth forms, and the development of the surface increases with increasing temperature. Figure 2 shows the images of the natural surface of the TiO_2

in the plane, normal to the substrate in the temperature range T_s 350...700°C, which correlates with the structure of the surface (Fig. 2).

As a result of condensation at T_s of 350...450°C, the structure contained V-shaped columns with the kinetically favourable orientation with a size of up to 3.0 μm.

The increase of the condensation temperature in the range T_s 450...650°C results in the development of the structure with the fine-column (thin-fibre) texture. All the TiO_2 columns with the diameter of d = 0.3...0.5 μm, up to 30...40 μm long, with the tetragonal tips are oriented in the same vertical direction in relation to the substrate in the direction of incidents of the vapour flow.

The columnar structure is the characteristic special feature of the condensates, produced by the EB PVD method [7, 8] in the range 0.3 $T_m < T_s <$ 0.5 T_m, which is in agreement with the zonal theory of the formation of the structure of the condensed materials [14, 15]. However, the increase of Ts does not result in the expected large increase of the size of the crystals, and the transverse size of the crystals remains almost unchanged. The fine- column structure with d = 0.5...0.7 μm remains unchanged up to T_s (700 ± 10)°C.

The condensates are characterised by textural porosity, i.e., formation of cavities between the crystals. The inter-crystalline porosity is of the open type, size 0.1...0.2 μm with a narrow range of the size distribution of the

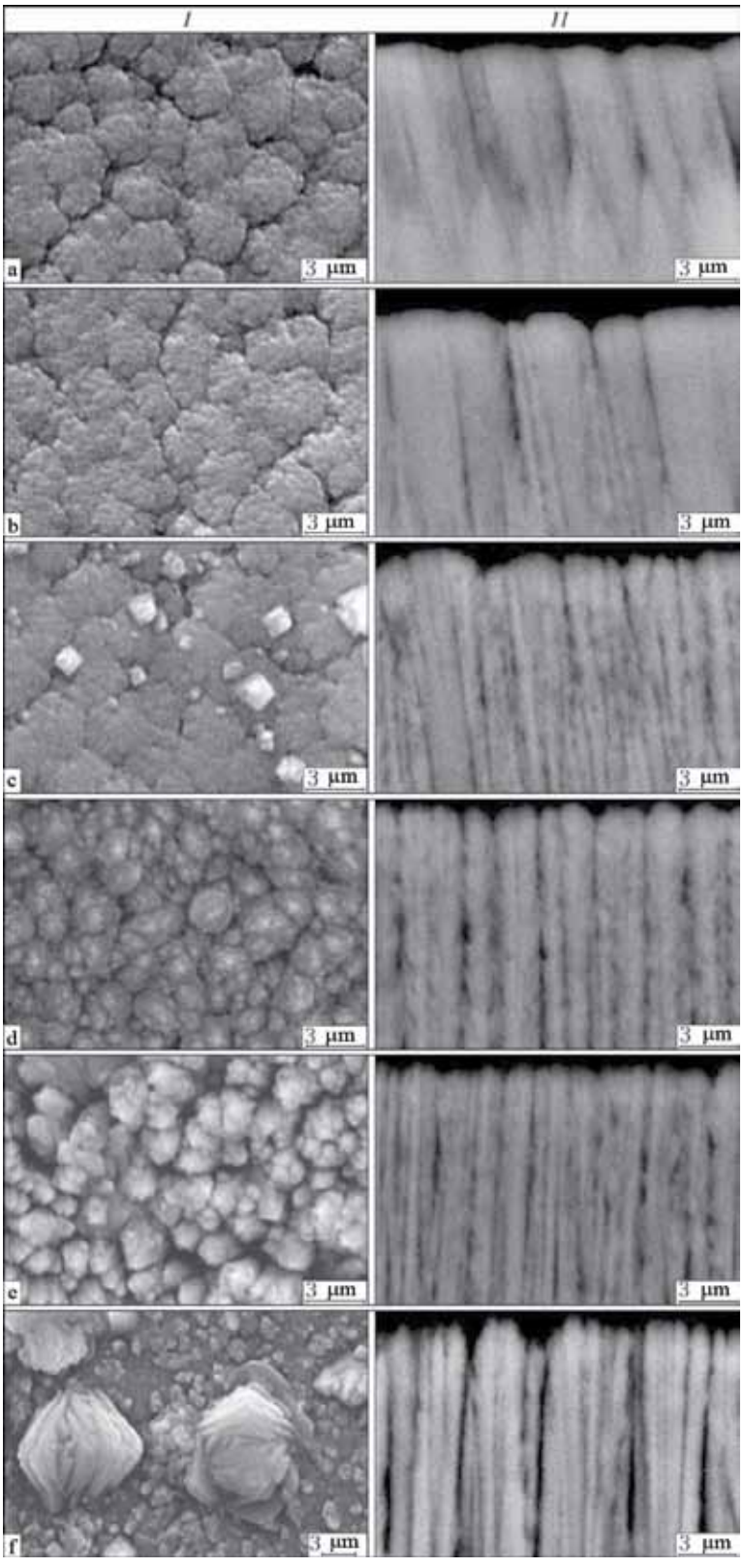

Fig. 2. Microstructure of the TiO_2 condensates at different T_s, °C: *a*) 350; *b*) 430; *c*) 450; *d*) 550; *e*) 650; *f*) 700; I – surface; II – cross-section.

Table 1. Phase composition and structural parameters of titanium dioxide at different values of the condensation temperature

T_s, °C	a-TiO_2			r-TiO_2		
	a, nm	c, nm	Amount of phase, %	a, nm	c, nm	Amount of phase, %
220	0.37853	0.95517	55.0	0.46009	0.29526	43.0
430	0.37853	0.95517	63.8	0.45928	0.29588	36.2
550	0.37908	0.94706	69.4	0.45997	0.29614	30.6
690	0.37812	0.95064	66.9	0.45895	0.26649	34.1
1050	–	–	–	0.46016	0.29640	49.3
Reference	0.37842	0.95146	–	0.4593	0.2959	–

Here a and c are crystal lattice constant of anatase and rutile. Absolute nominal permissible error of measurement of the lattice parameters was +0.00018

pores. The mechanism of formation of porosity is similar to that observed in the majority of condensates of simple substances [15].

Examination of the evolution of the phase composition of the TiO_2 condensates with increase of T_s was carried out by x-ray diffraction phase analysis. Of the three existing crystalline modifications of the titanium dioxide [16], the best-known are the two tetragonal phases: anatase (P4/mnm) and rutile (I41/amd). Regardless of the affiliation to a specific crystal system, they have different crystal lattices and, therefore, form different x-ray diffraction diagrams.

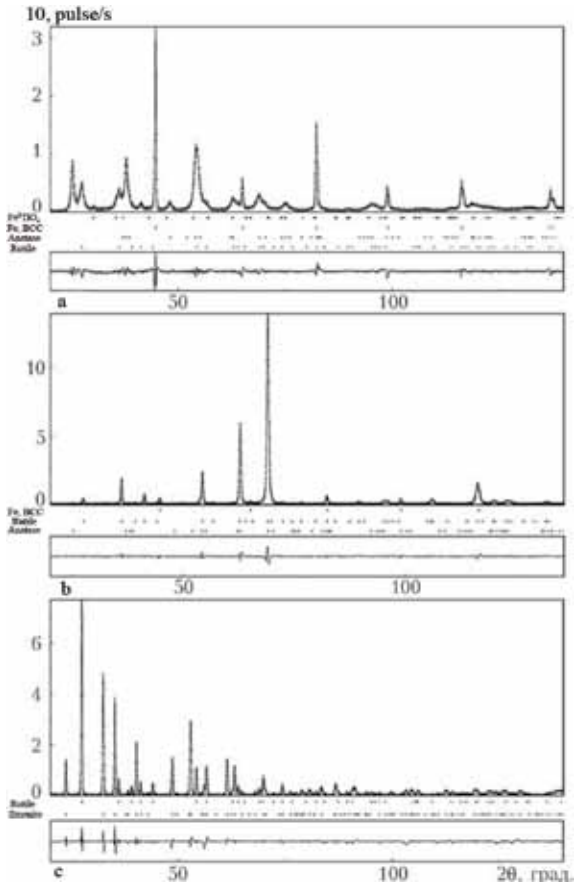

Fig. 3. Refined x-ray diffraction diagrams (by the Ritveld method) for TiO_2, deposited at different T_s, °C: *a*) 220; *b*) 550; *c*) 1050; I – intensity.

According to the results of x-ray diffraction analysis, the specimens, producers T_s lower than 200°C are x-ray amorphous.

The data of the x-ray diffractometry of the specimens, deposited on the substrate at T_s = 220; 430; 550; 690 and 1050°C, were improved by the Ritveld method using a large number of parameters, including the phase scale factors and the components of the background of the x-ray diffraction diagrams; the lattice parameters; deflection of the zero counter; parameters of the profile of the x-ray line and the anisotropy of microstresses and microstrains [12] for both phases; the coordinates of the atoms in the elementary cell and the isotropic thermal parameter for all atoms; the texture parameters. As an example, Fig. 3 shows the results of such improvement for TiO_2, obtained at the temperatures of condensation of 220, 550 and 1050°C. The vertical primes represent the positions of the Bragg reflection's of the given phases. The points indicate the experimental data; the solid line – calculations; the lower curve – the difference between the experimental and

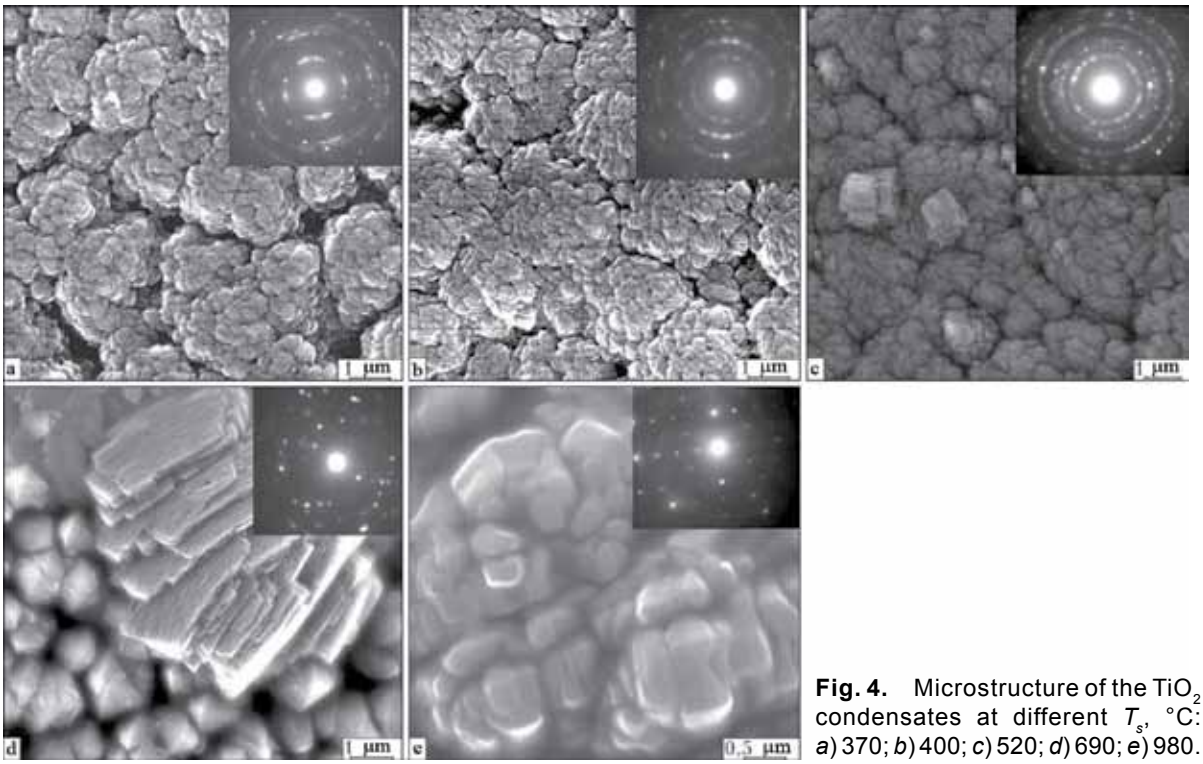

Fig. 4. Microstructure of the TiO_2 condensates at different T_s, °C: *a*) 370; *b*) 400; *c*) 520; *d*) 690; *e*) 980.

calculated values. The reliability factors are also indicated. The volume fractions of the phases are presented without taking the effect of the substrate into account. The phase composition of the condensates and structural parameters of the phases for the investigated specimens are presented in Table 1.

The x-ray diffraction diagrams, shown in Fig. 3, indicate that at T_s = 220°C (Fig. 3a) the background of the reflections from the BCC lattice of the ironic of the substrate show the main characteristic peaks of the anatase (55%), rutile (43%) and a small amount of Fe_2TiO_4 (2%).

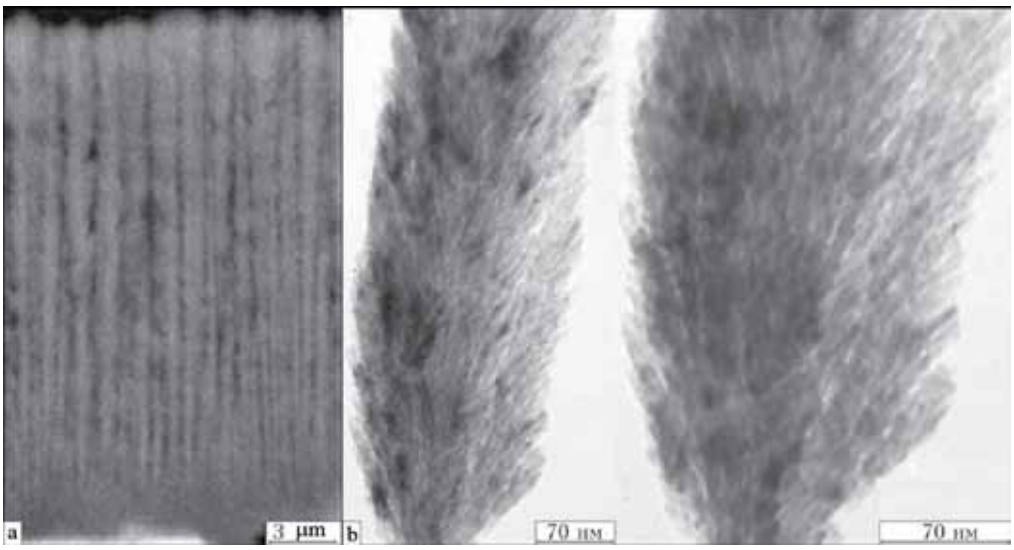

Fig. 5. Examples of the fractal structure of the TiO_2 condensates: *a*) the structure of the condensates; *b*) single object.

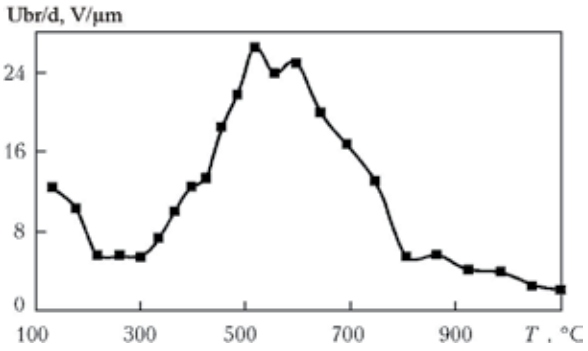

Fig. 6. Electrical properties (breakdown voltage) of the TiO_2 condensates in relation to T_s.

The increase of the deposition temperature in the range up to T_s = 550°C results in the situation in which the structure of the specimens contains of a mixture of only two phases: anatase (a-TiO_2) and rutile (r-TiO_2). The anatase is the main phase in the anatase-rutile mixture, and the intensity of the peaks corresponding to the anatase increases rapidly with the increase of the deposition temperature T_s. Correspondingly, the volume fraction of anatase increases to the maximum value (70% at T_s = 550°C (Fig. 3b). The distinctive texture of growth of a-TiO_2 with the axes of the texture [116] and [110] was detected.

As indicated by Table 1, at the condensation temperature of T_s > 550°C the deposited titanium dioxide consists as previously of a mixture of the stable and metastable modifications (a-TiO_2 and r-TiO_2), by the ratio of the phases changes. The amount of the anatase decreases, and the metastable phase – anatase (a-TiO_2) – gradually transforms to the thermodynamically stable modification – rutile (r-TiO_2). The distinctive gross texture of a-TiO_2 with the [116] and [110] axes remains unchanged also at T_s = 690°C.

Condensation on the substrate, preheated to T_s = 1050°C results in the formation of rutile and ilmenite $FeTiO_3$ in approximately identical amounts (Fig. 3c). In this case, the weak textures of growth of both phases are observed. Thus, for the rutile the axis of the texture is the direction [110], and for ilmenite it is [113].

The parameters of the crystal lattices of anatase and rutile almost completely independent of the condensation temperature Ts and if only slightly from the reference values (Table 1).

More detailed characteristics of the structure of the investigated specimens were obtained using transmission electron microscopy. The images and Michael diffraction patterns of the titanium oxide are shown in Fig. 1, 4.

According to the transmission electron microscopy results, the specimen, produced at 135°C, is characterised by the nano size structure (Fig. 1a, insert), its morphology – needles, columns, with the size of 5...10 nm. The diffraction pattern of the specimen does not contain any sharp reflections, nevertheless, the wider rings, corresponding to the presence of the polycrystalline nanostructure with a size of 5...7 nm are clearly visible (Fig. 1b). All the reflections relate to the anatase structure.

When T_s is increased to 300°C, the size of the crystal structure increases to 40...70 nm (Fig. 1c). Evidently, this process continues with a further increase of T_s. The diffraction patterns of the electrons in condensation in the temperature range 300...400°C (Fig. 1c, 4a, b) are identical and are ring -shaped. The reflections relate to the polycrystalline a-TiO_2, but with increase of T_s they become more intensive and sharper indicating a higher degree of crystallinity of the phase. The size of the structural component is equal to 20...200 nm.

At T_s = 520 and 690°C, according to the results of transmission electron microscopy, the structure consists of aggregates with the size of 0.5 – 0.7 μm, consisting of the individual elements with a size of 0.1...0.2 μm. The results of electron diffraction indicate the presence of both phases, a-TiO_2 and r-TiO_2 (Fig. 4c, d). The electron diffraction pattern, taken from the individual formations on the surface of the condensates of the plate shape form, correspond to the phase r-TiO_2 (the insert in Fig. 4d). The reflections on the electron diffraction pattern, taken from the specimen produced at T_s = 980°C are of the spot shape. They confirm the results obtained in x-ray diffraction analysis regard-

ing the presence of two phases: r-TiO_2 and ilmenite (Fig. 4e).

Electron microscopic studies show that electron-beam deposition results in the formation of a nanostructure homogeneous throughout the entire volume of the condensate with the mean characteristic size of the structural elements smaller than 100 nm. The degree of crystallinity of the thick condensates of TiO_2 using this technology increases with increasing Ts. However, at a condensate thickness greater than 25...30 μm and the condensation temperature of 300...450°C, examination showed the phase inhomogeneity in the thickness of the specimen. For example, according to the electron diffraction patterns, the background of the general structure of a-TiO_2 (Fig. 1c) closer to the surface there were two-phase regions (Fig. 1d) consisting of a mixture of polycrystalline a-TiO_2 and r-TiO_2. Similar structures were already detected in the thick condensates of Al_2O_3 [17].

Additional detailed studies of the TiO_2 condensates, deposited at T_s = 50...100°C, show that they have the amorphous or nano size structure. The transition of titanium dioxide from the amorphous to nanocrystalline structure requires some thermal activation. For example, the specimens of the TiO_2 condensates, produced at T_s (50±10)°C are x-ray amorphous (additional investigations of the specimens by transmission electron microscopy did not show the formation of the grain structure, electron diffraction patterns indicated only diffusion reflections), and the increase of temperature to T_s (100 ± 10)°C resulted only in the formation of condensates with the nanocrystalline phase of titanium dioxide. The degree of transformation of titanium dioxide with the amorphous structure to the nanocrystalline phase (TiO_2 – anatase with the parameters a = 0.3788, b = 0.3788, c = 0.9489) reached 85%, and the size of the regions of coherent scattering was 40...50 nm.

Thus, the analysis of the experimental results shows that the formation of the TiO_2 condensates is governed by the same relationships as those observed in the majority of the inorganic materials [7, 8], produced by EB PVD – formation of the nanosized (5...10 nm) structure up to T_s <0.3 Tm and columnar structures (the size of the crystals 0.5...3.0 μm) in the range $0.3T_m < T_s < 0.5T_m$.

Additional contribution to the size and morphology of the structure is provided by the polymorphic transformations, typical of the TiO_2 oxide. For example, the formation of the stable modification r-TiO_2 based on the metastable modification a-TiO_2, starting at $T_s \sim$ 500°C, is accompanied by the formation of a dispersed-columnar nanostructure (0.5...0.7 μm) (Fig. 2).

An important result is the formation of rutile at T_s = 220°C. In accordance with the phase diagram [18], anatase transforms reversibly to rutile in heating to 700...800°C. There have been only a small number of reports on a transformation at a lower temperature. For example, experiments showed a similar transition in the films at a substrate temperature of 500°C [19]. The appearance of rutile in the thin films at T_s = 220°C in the process of chemical synthesis is associated with the highly non-equilibrium conditions [20]. The phase transition temperature may decrease with the deduction of the size of the structural components of the condensates. There are experimental data [21] showing that TiO_2 with the amorphous structure transforms to a-TiO_2 in heating above 300°C. In the present case, it may only be assumed that the controlling factor is the dimensional factor, but the reasons for this low-temperature transformation require detailed studies.

The specimens of nanocrystalline titanium dioxide, produced in the zone of formation of the columnar structure, have another special feature. According to the scanning electron microscopy data, the columns with the size of 0.5...3.0 μm are aggregates, consisting of small objects (up to 140 nm) of the rod -shaped (columnar) form (Fig. 5).

The qualitative analysis of the morphology makes it possible to classify the structure of the condensate with the thickness of 20...30 μm as a fractal structure, i.e., structure, con-

sisting of individual parts (objects), similar to the integral unit (Fig. 5) [22].

Scanning and transmission electron microscopy techniques were used to investigate a separate object (Fig. 5b). A single column with a size of 140...200 nm is a relatively porous aggregate and consists of a cluster of columns with the size of 5...10 nm. The structure is characterised by fractal geometry of both the volume and the surface. Fractal analysis was carried out to verify this the nominal. The quantitative measure of the geometrical complexity of the object was the fractal dimensions D, indicating the density and uniformity of packing of the space by the elements of the object. The procedures, described in [23], we use for determining the fractal dimensions. The results show that the estimate of D does not depend on the examination scale, the calculation error is ±0.004 and, therefore, D can be used to verify the periodicity of the repetition of the specific structure on the image and compare the structure of different condensates. Analysis of the dependence of the fractal dimensional on the temperature T_s shows that the values of this parameter in the temperature range T_s 120…700°C are almost identical and are distributed in the range 2.92...2.95.

The fractal structures include mostly solids, with the high values of porosity, and, therefore, the fractal dimensional D can be the characteristic of the porous upstairs and determine its adsorption capacity [24]. At the present time it is assumed that the solid-state fractal systems represent a new type of the structural state of matter characterised by cardinal changes of many physical properties and, therefore, the production of substances with the fractal structure and also the search for the relationship between the fractal dimensions, physical and chemical properties is often a very important experimental task [22, 24].

Additional investigation of the electrical properties of the titanium dioxide specimens showed that in the entire condensation temperature range they have the dielectric properties (ρ = 3.0...6.2^{-6}·10 ohm m). The dependence of the curve of the variation of the breakdown voltage on the condensation temperature T_s is shown in Fig. 6. The curve is non-monotonic and correlates with the variation of the microstructure and phase composition of the condensate. Evidently, the peak the curve in Fig. 6 is associated with the preferential formation of the anatase phase in the composition of the condensates with increasing deposition temperature and corresponds to its maximum amount (a-TiO_2 ~ 70%) at T_s 500°C. The formation of the stable modification r-TiO_2 based on the metastable a-TiO_2 in the condensates at T_s > 550°C is accompanied by the formation of a fine columnar structure (0.5...0.7 μm) (Fig. 2) and also by a rapid decreased of the breakdown voltage (Fig. 6).

Since TiO_2 is characterised by the large variety of the morphological and structural forms, it is important to discuss which modification is preferred for industrial production [1–4, 20, 25].

??? Is the phase with the lower stability which is found only seldom in nature and, evidently, for this reason is of no, commercial interest. Anatase has ??? properties, in contrast to rutile which however scatters the light 30% more efficiently. Since r-TiO_2 is a stable phase, it is used quite often in the production of white pigment.

Anatase has a lower atmospheric resistance than r-TiO_2, and protects less efficiently the polymers against ultraviolet radiation. However, many European countries utilise this property of a-TiO_2 for the development of materials (for example, packing materials) which are degraded with time under the effect of solar light and it is important for environmental protection.

Titanium dioxide (not toxic and relatively cheap) is one of the promising for to catalysts and can be used widely for the cleaning of water and air to remove organic substances harmful to health, the formation of self-cleaning antibacterial coatings, et cetera. In most cases, the photocatalytic phase of TiO_2 is assumed to be anatase but reports have already been published according to which

the mixture of the phases r-TiO_2 and a-TiO_2 is characterised by better parameters from the viewpoint of photocatalytic in comparison with single phase materials [1, 25].

Thus, it should be mentioned that the method of EB PVD has a number of advantages in comparison with other synthesis methods, because it makes it possible to produce (design) and based on titanium dioxide with the pre-defined physical-chemical properties. The possibility of the efficient regulation of the structure and phase composition of the condensates for specific applications without additional thermal or other subsequent complicated treatments makes it possible to widen the range of application of this method.

The different forms of TiO_2 (coatings, con the materials, nano particles) with the required morphology and functional properties, produced by EB PVD method, are promising for many applications in technology and medicine, in particular, in the production of highly efficient catalytic systems, membrane catalysts and optical materials.

Conclusions

1. The experimental results show that the formation of the TiO_2 condensates is governed by the same relationships as the majority of inorganic materials, produced by EB PVD method: formation of the nanosized (5–10 nm) to $T_s < 0.3\ T_m$ and columnar (crystal size 0.5 – 3.0 μm) structures in the range the $0.3T_m < T_s < 0.5\ T_m$. The additional contribution to the dimensional morphology of the structure is provided by the polymorphic transformations, characteristic of titanium dioxide.
2. The nanocrystalline titanium dioxide, produced by vacuum deposition, contains phases a-TiO_2 and r-TiO_2, and the type of crystal lattices determined by the synthesis conditions (T_s).
3. It was also established that the polymorphic transformation of a-TiO_2 to r-TiO_2 in the condensates takes place in the temperature range 220°C, which is considerably lower than the phase transition of the thick TiO_2.
4. The experimental results show that the formation of mostly stable modification r-TiO_2 based on the metastable modification a-TiO_2, starting at T_s, equal to (500±10)°C, is accompanied by the formation of the dispersed-columnar structure (0.5...0.7 μm), and also by a rapid decrease of the breakdown voltage.
5. The principal possibility of the formation of the fractal properties of the TiO_2 condensates in a wide temperature range T_s (120...700°C) was established; the fractal dimensions has the values from 2.92 to 2.95, depending on the synthesis conditions (T_s).
6. It was also shown that the materials and and systems based on titanium dioxide, produced by EB PVD method, with the required physical-chemical properties, can be used in many applications in applied material science and alternate energy production, because of the possibilities of controlling the structure and properties.

Submitted 23.2.2014

Advances in Electrometallurgy 2014 ***12*** *(2) 127–135*
Translated from Sovremennaya Elektrometallurgiya 2014 ***12*** *(2) 44–50*

Structure and mechanical properties of vacuum-arc multilayer condensates of nitrides of titanium and its alloys

A.V. Demchishin[1], V.A. Avetisyan[1], A.A. Demchishin[2], L.D. Kulak[1] and V.V. Grabin[3]

[1]*I.N. Frantsevich Institute of Materials Science, Kiev*
[2]*Kiev Polytechnical Institute, NTUU, Kiev*
[3]*E.O. Paton Electric Welding Institute, Kiev*

Studied are the structure, element composition, microhardness and modulus of elasticity of multilayer vacuum-arc condensates of TiN/ZrN, TiN/Ti36AlN, TiN/Ti30CrN systems produced at high rates of condensation (0.3...0.5 μm/min) as a result of decrease in distance between the cathodes and substrates (up to 130...140 A). For comparison, similar characteristics of single-layer condensates TiN, ZrN, Ti36AlN and Ti30CrN, produced under similar conditions, were investigated. Thickness of condensates was 10...15 μm; material of substrates was stainless steel 12Kh17. Dependencies of studied characteristics of condensates on accelerated potential of substrate (U_s = 50...180 V) were found. Values of mechanical characteristics (hardness and modulus of elasticity of nitride single- and multilayer condensates) were determined. Basing on the obtained results, the ratio H^3/E^{*2} was calculated for these coatings, characterizing the level of coating resistance against the plastic deformation. It is shown that the microhardness and ratio H^3/E^{*2} of multilayer nitride condensates are much higher than that in single-layer ones. Microhardness of multilayer condensates is increased with decrease of adjustable thickness of alternating sublayers. Ref. 11, Tables 2, Figures 7.

Key words: *vacuum-arc evaporation; multilayer nitride condensates; high rate of deposition; scanning electron microscopy; microhardness; modulus of elasticity*

One of the priority directions in the development of modern material science is the development and investigation of nanostructured condensed materials for application as wear- and corrosion-resisting coatings for different applications. The most promise for the production of the nanostructured coatings of the interstitial phases is obtained in the case of ion-plasma technology using cathodic vacuum-arc evaporation because this method can be used to produce highly ionised plasma flows in vacuum and in different active gas media, and also exert a strong influence on the reaction of synthesis of different compounds and elementary processes of the growth of metallic and ceramic condensates on the working surfaces of the substrates.

The attention of the experts is attracted by the nitrides of transition metals as a result of the optimum combination of the mechanical and physical properties – a relatively high hardness, high melting point (refractoriness), comparatively low coefficient of heat conductivity and friction, high thermal and chemical stability. In particular, this has made it possible to use these materials as wear-resisting coatings for cutting and pressing tools, important components of machines, for example,

compressor blades of gas turbine engines and piston rings of internal combustion engines.

The possibilities of improving the physical-mechanical properties of the coatings, produced from the simple single-layer nitrides, are already limited. Therefore, the effort of many investigators is directed to the examination of the multicomponent and multilayer structures, produced by vacuum induction-plasma technology [1–4]. The addition of alloying elements to the initial evaporated materials, the transition metals and the formation of multilayer compositions with the regulated thickness of the sublayer makes it possible to reduce the grain size and, consequently, increase the hardness of the produced coatings.

The large number of data for the structure and mechanical properties of the condensed ceramic layers, produced using the ion-plasma technologies and described in the literature, greatly differ. This is explained by the fact that the macrostructure, composition and properties of such objects depend on a large number of technological parameters, including the pressure of the reaction gas in the working chamber, the condition of the vacuum medium, the level of the current of the cathodic arc discharge, the distance between the cathodes and the substrate, the deposition rate of the plasma flows, the material and topographic of the surface of substrates, the values of the negative potential, supplied to the substrate, and the methods of producing consumable cathodes.

The aim of the present work is to obtain further information on the structure and mechanical properties of the alloyed and multilayer condensates based on titanium nitride, produced by vacuum arc deposition.

Experimental procedure

The single-layer binary TiN, ZrN and ternary TiAlN, TiCrN condensates and also multilayer condensates TiN/ZrN, TiN/TiAlN, TiN/TiCrN were produced in the Bulat-3T modified vacuum-arc equipment (Fig. 1). The vacuum chamber contains a system for the automatic maintenance of the pressure of the working gas and is fitted with two evaporating devices, situated against each other. The mechanism for rotation of the substrate contained the console-type substrate holder in which two substrates could be secured simultaneously.

To apply the process of production of the multilayer condensates, experiments were carried out with the conditions of continuous evaporation of the selected metallic materials from two end-type cathodes in combination with the alternating cyclic rotation of the substrate holder by 180°. To ensure the deposition of the plasma flows on the substrates with control duration of holding opposite to the evaporating cathodes, a timer delay was installed in the electrical system for the rotation drive, ensuring the deposition time of the alternating layers of 10, 20, 30, 40, 50 s and longer. Consequently, was possible to produce multilayer ceramic condensates with the thickness of the sublayers in the range 10–1000 nm and the total thickness of up to 20 μm. The cylindrical end-type cathodes with the diameter of 64 mm, produced from pure metals of titanium, zirconium and the Ti–30Zr, Ti–30Cr, Ti–36Al alloys were prepared by electron-beam (pure metals) in vacuum arc

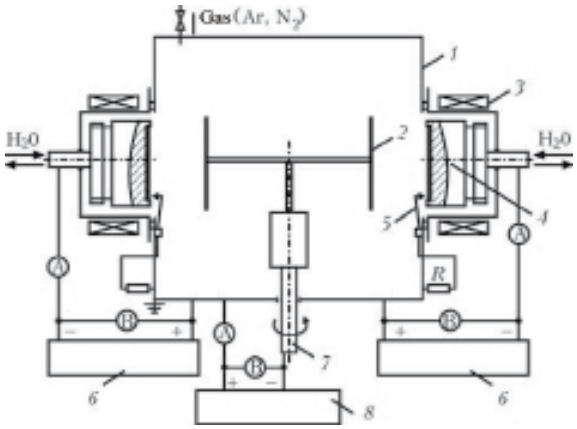

Fig. 1. Diagram of Bulat-3T ion-plasma equipment for producing multilayer condensates: *1*) vacuum chamber; *2*) the substrate; *3*) the stabilising coil; *4*) the end-type cathode; *5*) arc ignition device; *6*) power sources for the arc discharge; *7*) the mechanism for rotation of the substrate; *8*) the sources of the negative potential supply to the substrate.

remelting of the pure initial metals in argon (alloys). The material of the substrates was in the form of sheets of 12Cr17 stainless steel in the form of sheets 100.0×100.0×0.3 mm in size. Prior to loading the substrates into the vacuum chamber, they were subjected to ultrasonic cleaning in acetone and subsequently processed in ethyl alcohol. Prior to depositing the condensates on the substrates, the vacuum of $5 \cdot 10^{-3}$ Pa was produced in the working chamber. Subsequently, a negative potential of 1 kV was supplied to the substrate, the evaporators were activated and the working surfaces of the substrates were cleaned by bombardment with the ions of evaporated cathode materials for 5 min. The formation of the condensates of nitrides of titanium and its alloys with zirconium, chromium and aluminium was carried out in a nitrogen gas medium at a pressure of $4 \ldots 6 \cdot 10^{-1}$ Pa. The arc current in the deposition process was 90...140 A, and the negative bias potential on the substrate varied in the range from–50 to –180 V. The distance between the substrate and the cathodes was 125 mm. The substrate temperature reached 350...400°C. The deposition time of the sublayers τ was 10, 20 and 30s, the total duration of production of the composite was 30...40 min; the total thickness of the produced coatings was 15...20 μm at the deposition rate of up to 0.5 μm/min. The hardness of the coatings was measured in Mikron-Gamma equipment with a Berkovich pyramid at a load of 10, 20, 30 g and Fischer equipment at a load of 10 g. The mean values of the hardness were determined from 5...7 measurements for each condensates. The phase composition and the

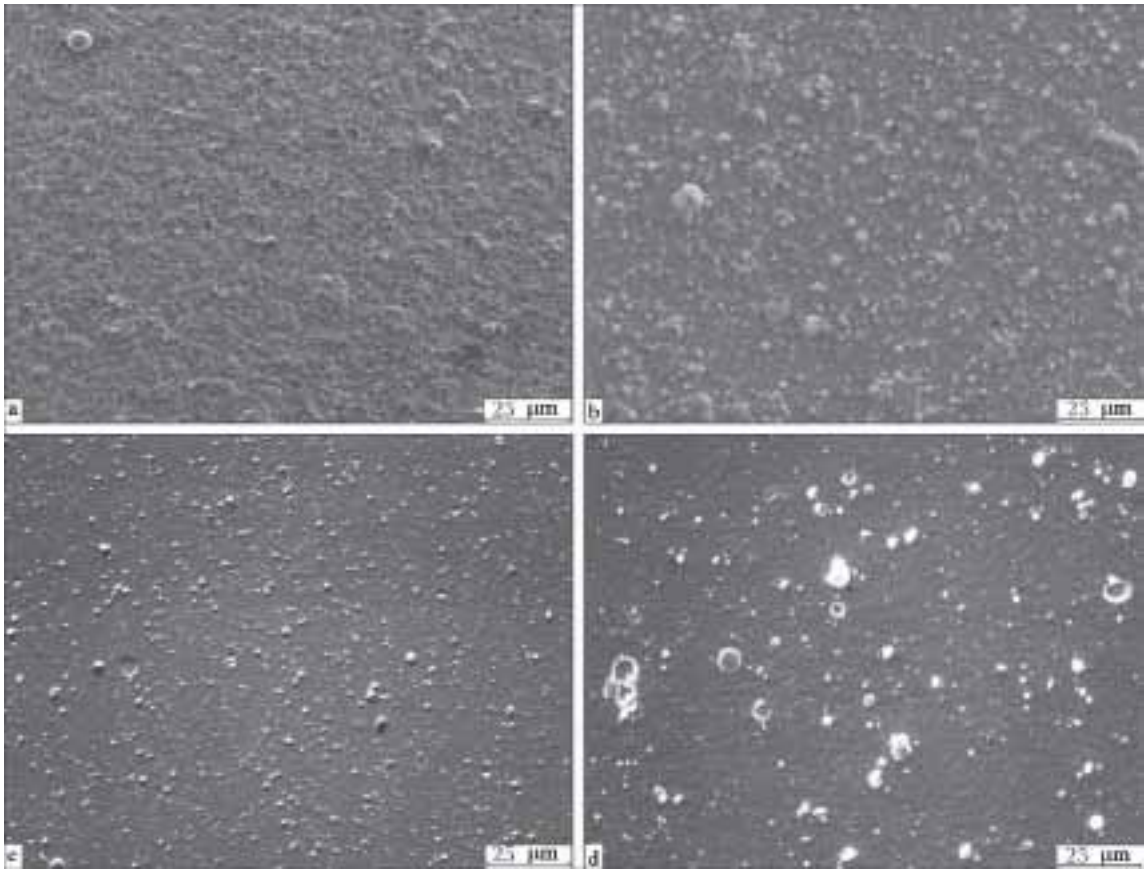

Fig. 2. Topography of the surface of the titanium nitride of the multilayer TiN/ZrN condensates at different values of the voltage on the substrate – 50 (*a*, *b*), – 180 V (*c*, *d*), and also the arc current of 90 A (*a*, *c*) and 140 A (*b*, *d*).

predominant orientation of the crystals in the deposited layers wave estimated using 50XVP scanning electron microscopes. The latter was fitted with an INCA 450 analyser of x-ray spectra.

Experimental results and discussion

The typical topography of the surface of the titanium nitride of the multilayer TiN/ZrN condensates, deposited at different substrate voltages and arc currents, is shown in Fig. 2 which indicates that the increase of the arc discharge current increases the amount and dimensions of the microdroplet phase in the nitride coating. At the same time, the higher electrical potential, applied to the substrate, results in the formation of a higher density of the condensates. Spectrometric studies of the charge composition of the plasma of the vacuum arc with the titanium, zirconium, aluminium and chromium cathodes [1] indicate the presence of single-, two-, and three-charge ions of metals together with the neutral metallic atoms in the plasma flow. The ratio of these components depends on the arc discharge current, the pressure of the reaction gas in the working chamber and the chemical composition of the cathodes. The increase of the accelerating potential of the substrates increases the energy of the positive ions, deposited on the surface of the substrates, the temperature of the substrates and, consequently, increases the density of the produced coatings.

Investigations of the structure of the fracture surfaces of the condensates of the single-layer nitrides indicate that the condensed layers in the cross sections consist of columnar crystals, positioned on the normal to the surface of the substrate, and the width of the crystals increases with increasing substrate potential. For example, the width of the columnar crystals of the TiM condensates increases from 500 to 1000 nm with the increase of the bias voltage and the substrate from –50 to –180 V. This result is explained by the increase of the ion energy in the plasma flow in relation to the increase of the value of the electrical potential, supplied to the substrates, leading to the increase of the local temperature on the surface of the substrate. In these conditions, the intensity of surface diffusion increases and becomes the dominant factor with otherwise identical deposition parameters, and also determines the final structure of the coating.

The typical structures of the multilayer TiN/ZrN condensates in the cross-section, produced by scanning electron microscopy, are shown in Fig. 3. The buyers voltage on the substrates was –100 (Fig. 3*a*) and –180V

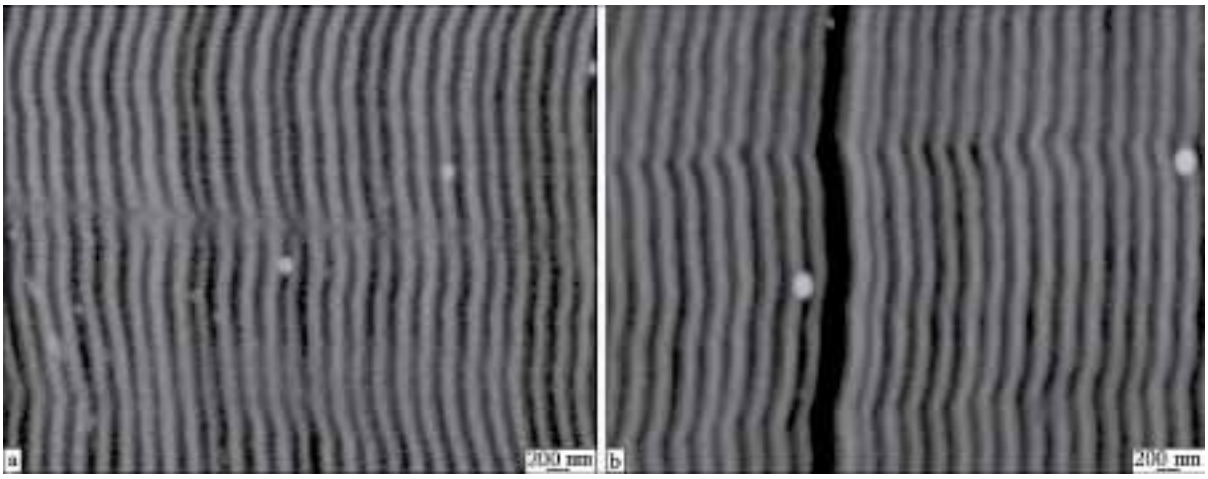

Fig. 3. Scanning electron micrographs of the structure of the TiN/ZrN condensates in the cross-section; the substrate potential – 100 (*a*), – 180 (*b*); τ = 30 s; arc current for the titanium and zirconium cathodes was 130 A.

(Fig. 3*b*). As indicated by the microstructures, the condensed composites are characterised by a laminated structure with the mean thickness of the sublayers of 150...180 nm. However, the boundaries between the layers do not have sharp contours, indicating the mutual dissolution of the components of the compositions at the interlayer boundaries during deposition. Actually, according to the data published in [5], the FCC cubic nitrides of the transition metals of the groups IV–UI form in the majority of cases continuous solid solutions.

As indicated by the presented microstructures, the variation of the negative bias voltage in the substrate in the range –100…180 V has almost no effect on the nature of the microstructure. However, the microhardness of the condensed composite reflects the effect of the electrical potential. The higher values of the voltage result in the formation of multilayer condensates of refractory compounds with a lower hardness. For example, the microhardness of the TiN/ZrN condensates, which were produced at the substrate voltage of –180 and –100V, was 42 and 45 GPa, which is associated with the presence of a large number of the effects in the condensates, obtained at lower deposition temperatures.

Figure 4 shows the distribution of the elements of the TiN/ZrN coating in the thickness of the condensates.

As indicated by the results, the thickness of the alternating sublayers at τ = 30s is 150...180 nm, and the curves of the distribution of the chemical elements are characterised by the presence of sharp peaks, indicating the interaction between the sublayers in the given deposition conditions. The presence of iron in the condensates at a depth of more than 2 μm on the side of the steel substrate indicates that the cleaning, heating conditions and the values of the negative potential of the substrate, selected in the study, result in a reliable bonding of the coating with the substrate.

X-ray diffraction studies of the phase composition of the coatings show that the multilayer condensates of the TiN/ZrN system with the thickness of the sublayers of 150...180 nm (τ = 30s) consist of nitrides of titanium and zirconium with a cubic lattice (Figure 5*c*), and the TiN and ZrN condensates

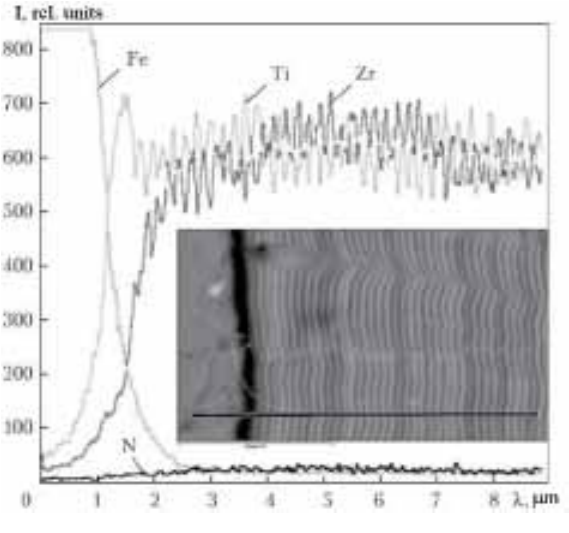

Fig. 4. Distribution of elements in the thickness of the TiN/ZrN coating: *1*) intensity; 2) the thickness of the sublayer.

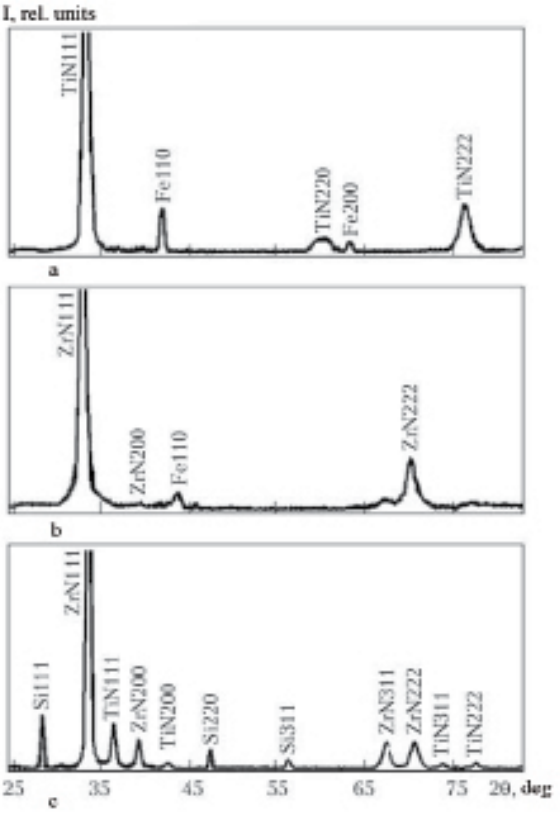

Fig. 5. X-ray diffraction of the specimens: *a*) TiN; *b*) ZrN; *c*) TiN/ZrN; τ = 30 s.

Table 1. X-ray spectral analysis of the multilayer TiN/ZrN condensate (reference specimens: C – SiC, N – BN, Ti – Ti, Zr – Zr, Fe – Fe)

Element	Conditional concentration	Corrected intensity	Content of elements	
			wt %	At. %
C	10.1	1.8628	5.09	14.51
	5.0			
N	18.0	0.8879	18.96	46.31
	0			
Ti	29.3	0.8793	31.25	22.32
	9.0			
Fe	0.39	0.9019	0.41	0.25
Zr	42.5	0.8973	44.30	15.62
	2.0	–	–	–
Total		100.0		

(Fig. 5*a*, *b*) have a cubic lattice and mainly the (111) orientation. The peak characteristics of the x-ray diffraction for these multilayer TiN/ZrM condensates indicate the presence of a dense nanocrystalline structure in the sublayers with the mean size of the crystals of 55...70 nm. The reduction of the thickness of the alternating sublayers to 50...60 nm (τ = 10 s) results in the formation of a small peak of the (TiZr)N solid solution, indicating the presence of a large fraction of the interlayer transition zones in the volume of the condensates.

The x-ray spectrum analysis of the multilayer TiN/ZrN compositions shows that, in addition to titanium, zirconium and nitrogen, the condensates contain a relatively large amount of carbon (5 wt.%) (Table 1). This is explained by the effect of the gas atmosphere of the oil vacuum in the working chamber of the equipment. The experimental results also show that the coatings are characterised by a shortage of nitrogen which is compensated by the presence of carbon, indicating the formation in the condensates, in addition to TiN, Ti_2N, ZrN, of also a certain amount of the interstitial phases TiCN and ZrCN. In [6] this was reported that the effect of the nitrogen and carbon atoms on the hardness of this condensates is approximately additive.

The typical structures of the multilayer TiN/TiAlN and TiN/TiCrN condensates in the cross-section are shown in Fig. 6. The bias voltage in the substrates was –180V. As indicated by the scanning electron micro-graphs of the structures, the condensed compositions have a 80 structure with the mean thickness of the alternating sublayers of 80–100 nm, at τ = 30s. The boundaries between the layers also do not have sharp contours, as in the case of the TiN/ZrN condensates, indicating the mutual dissolution of the components of the compositions at the interlayer boundaries in the process of vacuum arc deposition.

The diffraction diagrams of these multilayer condensates, produced at the bias voltage in the substrate of –50 and –100 V, indicate the presence of the (111) and (200) diffraction peaks, the ratio of these speaks depends on the level of the electrical potential, applied to the substrate.

Investigations of the distribution of the components of these condensates in the thick-

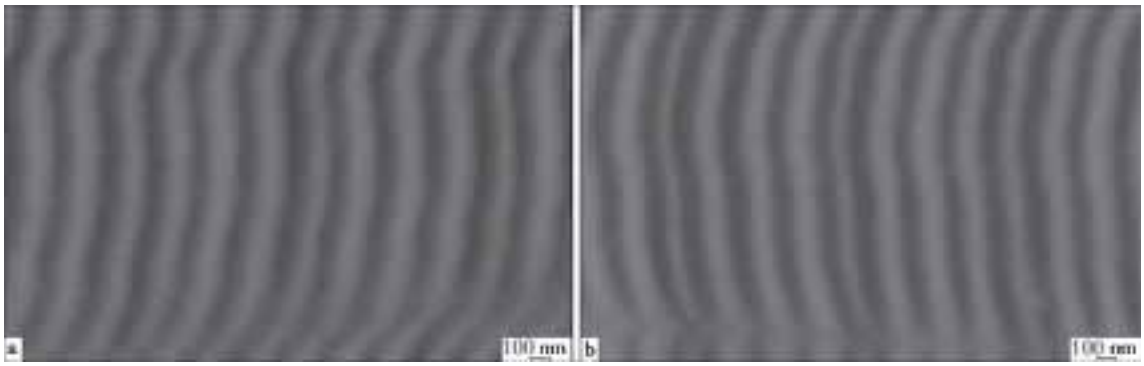

Fig. 6. Scanning electron micrographs of the structure of the multilayer TiN/TiAlN (a) and TiN/TiCrN (b) condensates in the cross-section, the substrate potential – 180 V, τ = 30 s.

Table 2. Mechanical characteristics of the nitride condensates, produced at a bias voltage on the substrate of – 100 V and the deposition time of the sublayers 10 s (the total condensation time of the plasma flows 30 min)

Type of condensate	H, GPa	E, GPa	H_3/E^{*2}
TiN	23	350	0.076
ZrN	21	295	0.082
Ti36AIN	28	270	0.232
Ti30CrN	25	290	0.143
TiN/ZrN	45	320	0.685
TiN/Ti36AlN	42	365	0.428
TiN/Ti30CrN	40	340	0.426

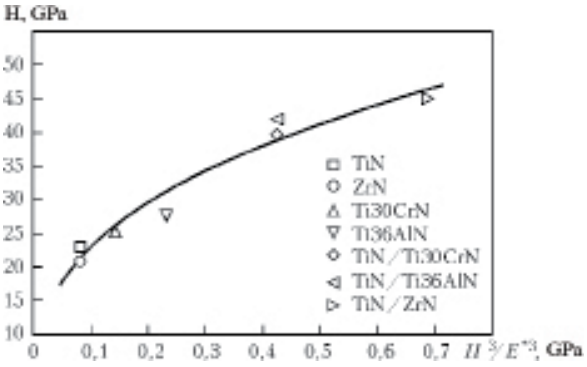

Fig. 7. Relationship of the ratio H^3/E^{*2} and H for the single- and multilayer condensates of nitrides based on titanium and its alloys, produced by vacuum-act deposition on stainless steel substrates.

ness of the coatings indicate that the chemical elements of this compositions are distributed selectively uniformly in the cross-section of the condensates, but the content of the following additions in them differs from the chemical composition of the cathode materials. For example, the mass fraction of aluminium and chromium in the coatings is 1.3...1.5 times smaller than the amount of these elements in the evaporated cathode is in relation to the substrate potential. The enquiries of the electrical bias results in a reduction of the content of the following elements in the coating as a result of the different degrees of ionisation in the evaporation of the cathode materials.

The values of the mechanical characteristics, such as hardness *H* and elasticity modulus *E*, of the nitride single and multilayer condensates, were determined by microhardness measurements. The qualitative comparative characteristics of the formation resistance of the material is the ratio H^3/H^{*2} [7], which was also determined for the investigated condensates. Here E^* is the reduced Young modulus, equal to $E/(1 - \nu^2)$; E is the Young modulus; is the Poisson coefficient. This ratio shows that to increase the plastic deformation resistance, it is necessary to try to obtain the minimum possible elasticity modulus at a high hardness. The results are presented in Table 2.

The bias voltage for the condensates in this case was –100 V, the duration of deposition of the sublayers was 10s. In these conditions, the thickness of the produce sublayers in the multilayer TiN/ZrN condensates was equal to 50...60 nm, and in the condensates alloyed with chromium and aluminium it was 25...30 nm.

As indicated by the data presented in Table 2, the values of the hardness and the H^3/E^{*2} ratio of the alloyed single-layer condensates based on the titanium nitride are higher than the identical parameters of the single-layer nitrides of the binary systems as a result of the formation of solid solutions, additional phases and grain refining. In turn, the values of the hardness and the H^3/E^{*2} ratio of the multilayer condensates are considerably higher than the values for the single-layer condensates.

The reason for the large increase of the hardness of the nanostructured multilayer compositions is the presence of a large number of interfaces between the nano layers, blocking of these interfaces by the movement of the linear defects during deformation of the condensates and the formation of the solid solutions of different elements at the interlayer boundaries.

In addition, it may be the result of differences in the elasticity moduli of the alternating sublayers, forming the condensed compositions, and also because of the presence of large compressive macrostresses in the resultant condensates. An additional factor

for increasing the hardness is the presence in the condensates of carbon, arriving from the gas atmosphere of the working chamber, which results in the formation of the titanium-based carbonitrides. The experimental results indicate the advantages of the multilayer condensates in comparison with the single-layer alloyed and unalloyed condensates.

The increase of the substrate potential to –180 V results in a reduction of hardness of older condensates by 10...15%, which is associated with a reduction of the number of defects in the condensates, produced at higher deposition temperatures, and also with a reduction of the amount of the alloy elements in titanium. For example, vacuum-arc evaporation of Ti–36% Al cathode in nitrogen with subsequent deposition of its plasma flow on the substrates made of stainless steel with the bias potentials of –100 and –180 V results in a reduction of the aluminium content of the condensate by respectively 28 and 23%. The similar results were obtained in the case of vacuum-arc evaporation of a Ti–30% Cr cathode. In this case, the condensate produced at a bias voltage of –100 V, contained 23% of chromium. A reduction in the amount of aluminium and chromium in the coating in vacuum-deposition was reported in [8, 9].

According to [7], the dependence $H^3/E^{*2} = f(H)$ characterises the relationship between the mechanical properties of the deposited layers. A similar dependence, constructed on the basis of the experimental data obtained in the present study, is shown in Fig. 7. This dependence is described efficiently by the parabolic curve, drawn through the experimental points. It was reported in [10] that the H^3/E^{*2} ratio can be used for evaluating the impact toughness of the nanostructured ceramic coatings.

It should be mentioned that the vacuum-arc -like at coatings, produced at high condensation rates, are relatively non-equilibrium. Therefore, the result of the relaxation processes, the hardness of these coating decreases with time. The measurements of the microhardness of the multilayer nitride condensates after stories for 10 months at room temperature showed that the hardness of the coatings decreased by 30...40%. The presence of the relaxation effect in the nitride coatings was also reported in [6, 11].

The experimental results, obtained in the present study, confirmed the effect of a large number of technological factors on the structure, phase composition and mechanical properties of the nitride condensates. This requires a constant control of the conditions of formation of these compositions in order to ensure the reproducibility of their characteristics.

Conclusions

1. The investigations were carried out into the structure of the vacuum-arc single- and multilayer condensates of nitrides based on titanium and its alloys with aluminium and chromium, produced at high deposition rates (0.3...0.5 μm/min), in relation to the values of the accelerating voltage of the potential (–50…–180V). The multilayer condensates had a laminated structure with the mean thickness of the alternating layers from 150...180 nm to 50...60 nm for the TiN/ZrN system, and from 80...100 nm to 25...35 nm for the TiN/TiAlN and TiN/TiCrN systems.
2. The experimental results also show that the multilayer condensates of the TiN/ZrN system have mostly the crystal orientation (111), as in the case of the single-layer TiN and ZrN condensates, whereas the TiN/TiAlN and TiN/TiCrN compositions showed the presence of the textures (111) and (200), and the ratio of these textures depends on the level of the electrical potential of the substrate.
3. It is also shown that the aluminium and chromium content of the TiN/TiAlN and TiN/TiCrN condensates depends on the substrate potential. The increase of the potential reduces the content of the alloying elements in the coating.
4. The hardness, elasticity modulus and the H^3/E^{*2} ratio were determined for all investigated nitrides. The results show that the values of hardness and the H^3/E^{*2} ratio of

the alloyed single-layer condensates based on titanium nitride Are higher than the identical parameters of the single-layer nitrides of the binary systems. In turn, the hardness and the H^3/E^{*2} ratio of the multilayer condensates are considerably higher than the values for the single-layer nitride coatings.

References

1. Andreev, A.A., Vacuum-arc equipment and coatings, Khar'kov Physico-Technical Institute, 2005.
2. Ducros, C., et al., Journal of surface and coatings technology, 2003, **163**, **164**, 681–688.
3. Reshetnyak, E.N., Strel'nitskii, V.E., In: Prof. the Second International scientific and technical conference: Nanostructured functional coatings and materials for the industry, volume 1: Nanostructured materials, Khar'kov, vol. 1, 2007, 6–15.
4. Shulaev, V.M., et al., in: Equipment and technologies of heat treatment of metals analysis, in: Equipment and technology of heat treatment of metals and alloys, vol. 2, Khar'kov, 2008, 6–9.
5. Hollek, Ch., Binary and ternary carbide in nitride systems of the transition metals, a handbook, Metallurgiya, Moscow, 1988.
6. Andrievskii, R.A., Usp. Khimii, 1997, vol. 66, 57–76.
7. Musil, J., et al., Journal of Surface and Coatings Technology, 2002, **154**, 304–315.
8. Wang Da-Yung, et al., ibid, 1999, **114**, 109–113.
9. Vetter, J., et al., ibid, 1995, **74**, **75**, 286–291.
10. Musil, J., Jirout, M., ibid, 2007, **201**, 5148 – 5152.
11. Shulaev, V.M., et al., In: Equipment and technology for heat treatment of metals analysis, volume 2, Kharkov, 2008, 11 – 15.

Submitted 14.3.2014

Advances in Electrometallurgy 2014 ***12*** *(2) 136–144*
Translated from Sovremennaya Elektrometallurgiya 2014 ***12*** *(2) 51–57*

ELECTROMETALLURGY OF STEEL AND ALLOYS

Investigation of the effect of calcium fluoride on the energy and technological parameters of treatment of rail steel in the ladle – furnace system

[1]G.A. Esaulov, [2]M.I. Gasik, [2]A.P. Gorobets and [1]Yu.V. Klimchik
[1]Dneprostal' Metallurgical Plant, Dnepropetrovsk
[2]National Metallurgical Academy of Ukraine, Dnepropetrovsk

Described are the physical-chemical premises of use of rational conditions of additions of solid slag-forming materials into the ladle and problems of formation of oxide-fluoride slag melt are discussed, the diagrams of meltability of the binary system $CaO–CaF_2$, ternary oxide- fluoride-calcium system $CaO–Al_2O_3–SiO_2$ with 10 % CaF_2 were analyzed. It was noted that content of CaF_2 in the composition of basic slag does not influence the thermodynamic conditions of formation of associates, but defines the chemical characteristics of oxide-fluoride melt and kinetics of mass-exchange processes in metal–slag system. It was found that the presence of fluorspar at the stage of slag formation from filler hard materials accelerates the assimilation of lime by slag melt and, thus, provides the increased desulphurisation ability of slag. Results of pilot-industrial application of fluorspar in ladle treatment of wheel steel St2 (GOST 10791–2011) in ladle-furnace system (LFS) are given. In accordance with the program of investigation the filler of fluorspar was added into steel-pouring ladle during yield of 160 t of metal–semi-product from furnace DSP-190. The scientifically-grounded control of condition of formation of refining slag by fillers of fluorspar allows 30...35 % reducing the power consumption at the stage of LFS and providing the high quality of continuously-cast billet for manufacture of all-rolled railway wheels. Ref. 10, Tables 4, Figures 3.

Key words: *wheel steel; arc electric furnace; metal-semi-product; deoxidizers; alloying elements; slag-forming materials; fluorspar; ladle-furnace installation; saving of electric power*

Importance of the investigations. Formulation of the experimental task and main assumption of the currently used technology of melting electric steel

The technology of refining the metal in the ladle–furnace systems by slag with the controlled physical-chemical characteristics is of practical and scientific interest from the viewpoint of ensuring the standard requirements on the quality of metal for railway wheels. The continuous technological scheme of production of electric steel for producing continuously cast blanks for all-rolled railway wheels in the conditions of the Dneprospetstal' Plant includes the following stages: melting of the metal–semifinished product in the DSP-190 electric arc furnace, with discharge of 160 t

of metal into a steel casting ladle, additions of deoxidation agents during filling the ladle, together with alloying additions, carburisation agents and slag-forming materials. In the subsequent stages, the rail steel is subjected to treatment in the ladle–furnace system (LFS) for desulphurisation and deoxidation with further transfer of the ladle to vacuum treatment and final deoxidation. The continuous casting of steel is carried out in a four-strand continues casting radial installation with the production of blanks of rail steel with a diameter of 450 mm [1].

The processing and analysis of the data for the melts and ladle treatment of the rail steel show that as a result of the imperfections in the conditions of adding materials to the ladle in the discharge of the metal-semifinished product from the DSP-190 into the ladle of the LFS and the ladle prior to vacuum treatment the specific consumption of electric energy in the treatment of the rail steel in the LFS increases.

In the currently available technology, the consumption of the materials added to the ladle during discharge of the metal–semifinished product from the furnace into the ladle is on average (kilograms per 1 melt): 1300 MnS17, 600 FS65, 700 carbon, 45 aluminium, 1200 limestone (previously, roasted dolomite or imported bauxite were added). Further additions to the ladle included 120 kg of material (45...47% MgO, 37...39% SiO_2, 9% Fe_2O_3) for the covering of the outlet orifice of the discharge window, and 0.1 kg/t of the starting mixture (19% SiO_2, 37.5% Cr_2O_3, 21.1% Fe_2O_3, 11.9% Al_2O_3, 8% MgO) for the channel of the slide valve of the steel casting ladle. For melting the given amount of the ferroalloys and slag-forming materials, the metal–semifinished product is superheated to ensure that prior to discharge from the DSP-190 furnace to the ladle its temperature is 1625...1630°C.

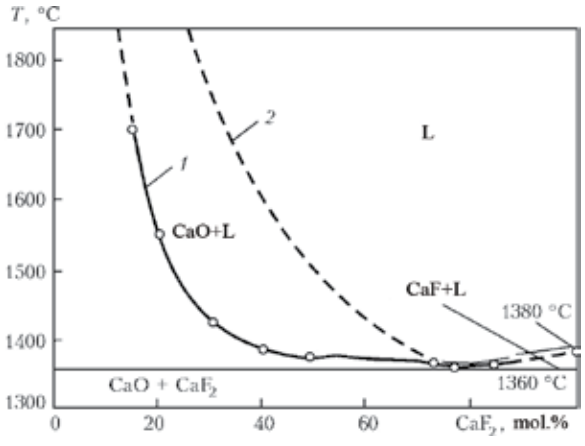

Fig. 1. Diagram of the fusibility of the $CaO–CaF_2$ system: 1) according to Budnikov [3]; 2) according to Eytel [4].

As a result of the reactions of the oxidation of the metal in the ladle with aluminium and alloying with silicon in the slag formed from the limestone, the materials for covering the window, and the channel of the slide valve of the ladle, it is necessary to increase the content of Al_2O_3 and SiO_2. However, the amount of the slag melt, formed in the first stage, is not sufficient for the simulation of limestone by the slag. Therefore, during holding of the metal in the ladle and prior to supplying it to the LFS, part of the added limestone is in the slag form.

The LFS is used for collecting the chemical composition of the steel by the additions of high carbon ferromanganese FMn78 and ferrosilicium FS65.

In order to ensure melting of the limestone in the slag form, compensate the heat used for the melting of the correcting additions (FMn 78, FS65), the metal in the LFS is heated to the temperatures of 1615...1620°C prior to sending it for vacuum treatment. The consumption of electric energy in the treatment of the metal in the ladle–furnace system is equal to approximately 7000 kW h per 1 melt. According to the standard conditions, it is necessary to add 1.4 kg/t of steel (225 kg per 160 t melt) of fluorspar [2]. The fluorspar can be added to the ladle after treatment of the rail steel in the LFS, i.e., prior to vacuum treatment of the metal. The shortcoming of this variant is not only the fact that its ‘diluting’ properties are not utilised in the initial stages of treatment of the metal in the ladle, but also the large reduction of the viscosity of the slide in vacuum treatment which is accompanied by

extensive splashing of the slag to the edge of the ladle during vacuum treatment.

Physical-chemical prerequisite for the selection of the rational conditions of additions of fluorspar in ladle treatment of the rail steel

One of the main tasks of the ladle treatment of the metal is the desulphurisation of the metal with the slag melts on the basis of the oxide-fluoride $CaO–CaF_2$ (Fig. 1).

The presented fusibility diagrams indicate the existence at the temperatures of the steel melting process (≤1600°C) of the homogeneous slag melt with the mass content of CaO/CaF_2 of 3:1. This content of the components and shows the phase composition of the oxide-fluoride melt, approaching the temperature conditions of the formation of the eutectic in the $CaO–CaF_2$ (T_m = 1360°C at 80 mol.% CaF_2).

In comparison of the thermochemical characteristics of the $CaO–Al_2O_3$ used as the desulphurisation slag system, and the slag melt of the $CaO–CaF_2$ the lower energy requirement for the formation of the slag refining system is observed when using the fluorspar with the melting enthalpy ΔH_m, equal to 30 kJ/mole, in comparison with 117.15 for Al_2O_3. As a result of the interaction of the slag with the refractory materials of the lining of the ladle, and partial oxidation of the alloying components, the basic composition of the slag of the $CaO–CaF_2$ is transformed to the multicomponent $CaO–MgO–Al_2O_3–SiO_2–CaF_2$ system.

The values of the melting point of the slags of this system can be estimated in the analysis of the primary solidification fields of the $CaO–Al_2O_3–SiO_2–CaF_2$ system (Fig. 2).

The experimental result show the ambiguous effect of the additions of CaF_2 on the

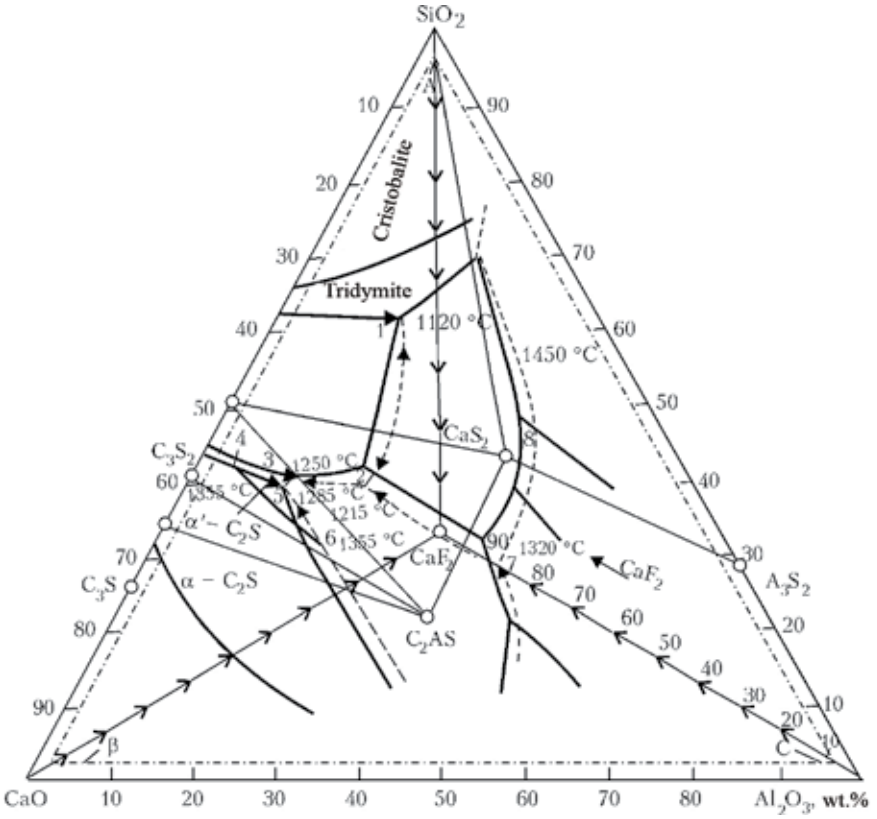

Fig. 2. Phase equilibrium and the temperature concentration fields of the $CaO–Al_2O_3–SiO_2$ ternary system with 10% CaF2 [5].

composition of these systems – presence of up to 1.5% CaF_2 results in the mineral formation of the primary slacks, when the CaF_2 content is higher than 5% that is not only a reduction of the temperature by 70...120°C for the points of the ion-variant equilibria, but also the displacement of the crystallisation fields of the helenite $2CaOAl_2O_3SiO_2$ in the direction of the Al_2O_3–CaF_2 side of the concentration triangle, reducing the size of the field of stability of the calcium metasilicate $CaO{\cdot}SiO_2$, rankinite $3CaO–2SiO_2$ and anortite $CaO{\cdot}Al_2O_3{\cdot}2SiO_2$ [5].

The $CaO–Al_2O_3–SiO_2$ three-component system with 10% CaF_2 is characterised by the large increase of the concentration field of existence of two non-mixing liquids, restricted by the curve with the origin, corresponding to 5% Al_2O_3 on the Al_2O_3–SiO_2 side with determination at the point 27.6% CaO on the $CaO–SiO_2$ side of the concentration triangle (Fig. 2).

The chemical and mineralogical analysis of the composition of the phases, formed as primary slags in the initial stages of solidification of the melt, indicates that CaF_2 does not take part in the mineral formation reactions and shows (especially in the high silica melt) the depolimerizing properties, breaking the chain structures of Si:O:Si and increasing the content of oxygen onions in the melt in accordance with the following reaction:

$$(–Si–O–Si–) + 2F = 2(–Si–F) + O^2 \qquad (1)$$

Evidently, the reaction (1) changes not only the physical properties of the melt but also the oxidation potential of the slag system, which has the direct effect on the activity of oxygen and sulphur dissolved in the metal. The occurrence of the reaction of desulphurisation by the slag systems is determined by the establishment of the balance between the metal and the slag, the activity of oxygen in the metal, the composition of the slag and the metal and taking into account the relative mass of the slag:

$$[S_{KOH}] = \frac{{}^{\alpha}[O]\left[(S)_{sl} + \frac{[S]_{Hay}}{m}\right]}{f_S C_S + \frac{{}^{\alpha}[O]}{m}}, \qquad (2)$$

where $[S_{in}]$, $[S_{fin}]$ is the sulphur content in the metal prior to and at the end of the desulphurisation process; $\alpha_{[O]}$ is the activity of oxygen in the metal; f_S is the activity coefficient of sulphur; C_S is the sulphide capacity of the slag; m is the relative mass of the slag 1 kg of steel.

The thermodynamic model of the behaviour of CaF_2 in the binary systems and insistence with a more complicated composition makes it possible to investigate their properties on the basis of the theory of ionic solutions, assuming that the activity of the element is equal to its ionic fraction. Developing the serial structure of the slags as the associated solutions, in [6] the authors noted the low intensity into particle interaction of CaF_2 with the melt of the $CaO–Al_2O_3–SiO_2$ melt, thus excluding the participation of CaF_2 in the process of formation of slag melts, and approximated the properties of the liquid melt by the presence in their composition of the complexes (associates) $CaO{\cdot}Al_2O_3$,

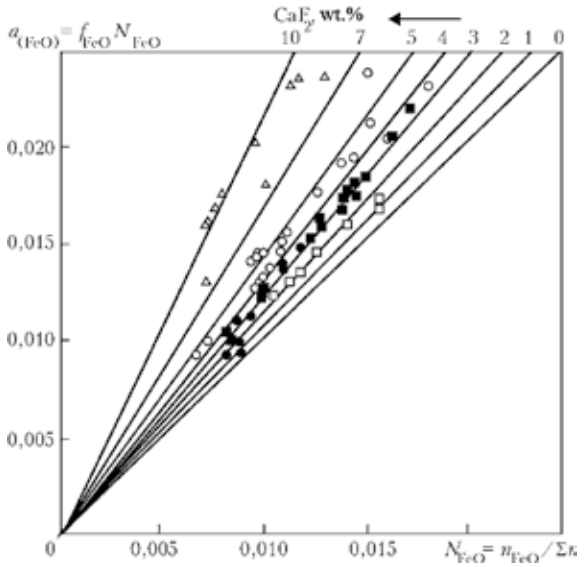

Fig. 3. Effect of calcium fluoride on the activity of iron oxide α(FeO) in the ladle slags; the numbers 0…10 indicate the CaF_2 content [8].

$2CaO{\cdot}Al_2O_3$ and the SiO_2 networks. In this theory, we assume the absence of modelling structures such as fluorine-containing molecules and complexes of the type Me–F (CaF, SiF). At the same time, spectroscopic studies of the solidified compositions of the $CaO–Al_2O_3–CaF_2$ system showed the presence of the complexes Al_x [AlF_6^{3-}, AlF_3^{2-}), indicating the participation of the fluorine ions in the deformation of the crystal chemical structures of Al_2O_3. In the $CaO–CaF_2$ system, showing the positive deviations of the activity α_{CaF2} in the range of higher content of CaF_2, there is the inter-molecular interaction of the components so that it is possible to estimate the value of the excess mixing energy ΔG^E in terms of the theory of regular solutions (the heat of formation of the solution differs from zero ($\Delta H^E \neq 0$), the mixing entropy is equal to the entropy of the ideal solution ($\Delta S^E = -R\Sigma_i \ln x_i$) [7]:

$$\Delta G^E = L_{1x}(CaO)\left[1 - x(CaO)\right] + \\ + L_2\left[x(CaO)\right]^2\left[1 - x(CaO)\right]^2, \quad (3)$$

where L_i the parameter characterising the temperature dependence of the mixing energy ΔG^E; x(CaO) is the molar fraction of CaO; $L_1 = RT(3.84 - 0.00\ 1087T$; $L_2 = -RT\ (11.87–0.00472T)$ [J].

Analysis of the dependence (3) indicates that the effect of the temperature of the slag melt on the value of the mixing energy of the components ΔG^E is small, and the maximum value of ΔG^E is obtained for the compositions with the high calcium fluoride content. For example, in the final stages of solidification of the mother solution, enriched with fluoride as the component of the $CaO – Al_2O_3 – SiO_2 – CaF_2$ system with the lowest melting point, the results show the formation of the ordered phase structures, containing fluoride components $2CaO\ SiO_2\ CaF_2$ (cuspidine), $12CaO{\cdot}7\ Al_2O_3{\cdot}CaF_2$.

According to the practical experience in the companies with the refining of the metal by the slag with the composition $CaO/CaF_2 = 3/1$ with the mass fraction of CaF_2 in the range 20… 10%) of first value is the initial contend of CaF_2, the second value during the treatment of the metal), the calcium fluoride increases the number of the oxygen anions in the melt as a result of the reaction of depolymerization of the structures (SiO_4^{4-}) by the reaction (1) and increases the basicity of the slag during the following reaction:

$$3CaF_2 + Al_2O_3 = 3CaO + 2AlF_{3\,ras}, \\ \lg K_p = -\frac{14677}{T} + 4.2296 \quad (4)$$

In [8] the authors described investigations of the effect of CaF_2 on the activity of FeO and the oxygen content in ball bearings carbon steel ShKh15. On the basis of statistical processing of the results obtained for the industrial melts it was established for the first time that the increase of the mass fraction of CaF_2 in the furnace basic slags (from 0.5 to 5%) increases the oxygen concentration of the steel, wt.%.

(CaF_2)	$[O]_{Fe}$	Number of melts
$\frac{0.5...2.0}{1.2}$	0.0023	46
$\frac{2.0...4.0}{3.0}$	0.0027	27
>5	0.0031	14

As explained in [8], the calcium fluoride greatly reduces the solubility of iron oxides in the slag, i.e., increases the activity of the slags and, at the same time, increases the content of the oxygen dissolved in the steel.

On the basis of the experimental results obtained for the industrial melts of ShKh15 steel in the conditions of Dneprostal' Co. with refining in the ladle using furnace slags (without LFS) in different content of CaF_2 it was established that we can use the empirical dependence of the coefficient of activity of iron in the slag f_{FeO} on the CaF_2 content of the slag [8].

$$f_{FeO} = 1 + 5.18 \cdot 10^{-2}\ (CaF_2) + 6.32 \cdot 10^{-3}(CaF_2) \quad (5)$$

The dependence $\alpha_{FeO} = f_{FeO} N'_{FeO}$ at the CaF_2

Table 1. Consumption of deoxidation agents, alloying elements, carburisation and slack forming materials in the melting of the metal–semifinished products in the DSP-190 ladle in the stages of ladle treatment of the rail steel St2 according to GOST 10791 – 2011

Melt No.	Sampling area	Materials of additions per 160 t melt, kg								T, °C
		MnS17	FS65	Al	C	Lime-stone	Dolo-mite	Window charge	Fused fluorspar	
1134863 (basic)	Furnace	–	–	150	–	–	–	–	–	1665
	Ladle	1300	600	45	705	900	102	120	–	–
	LFS	FMn78 139	55	–	150	800	–	–	–	–
1134865 (exper.)*	Furnace	–	–	150	–	–	–	–	–	1628
	Ladle	1305	600	–	702	1200	–	120	154	–
	LFS	FMn78 104	–	45	162	162	–	–	–	–
1134867 (exper.)*	Furnace	–	–	150	–	–	–	–	–	1633
	Ladle	1300	599	–	699	1200	–	120	150	–
	LFS	FMn78 156	65	45	157	800	–	–	–	1652

*In experimental melts at the end of vacuum treatment the metal was deoxidized with ferrosilicocalcium SK30 in the amount of 22 kg per melt.

Table 2. The chemical composition of the metal–semifinished products prior to discharge from the DSP-190 furnace, the rail steel of the experimental melt No. 1134865 in treatment in the LSF and vacuum equipment (sample No. 1 – prior to start, No. 2 – after treatment of the steel). N/D – not determined

Method	Sample No.	Mass fraction of elements, %								
		C	Si	Mn	P	S	Al_{total}		Ca	Cr
							Al_{solub}	Al_{ox}		
Furnace prior to disch.	1	0.08	0.007	0.071	0.007	0.048	–	–	0.0036	N/D
LFS	1	0.47	0.366	0.698	0.014	0.026	0.0190		0.0016	0.088
							0.017	0.002		
	2	0.585	0.346	0.745	0.015	0.004	0.0100		0.0070	0.089
							0.009	0.0016		
Vacuum system	1	0.583	0.350	0.747	0.015	0.004	0.009		0.0014	0.088
							0.008	0.001		
	2	0.581	0.337	0.729	0.014	0.002	0.008		0.0012	0.089
							0.007	0.001		
MNLZ-2	1	0.581	0.347	0.726	0.014	0.002	0.007		0.007	0.089
							N/D			

Table 3. Change of the chemical composition of the slag in the refining of the rail steel in the LSF

Slag sample in treatment	CaO	Mass fraction of component, %								Slag mass, t
		SiO_2	Al_2O_3	MgO	Fe_2O_3	Cr_2O_3	MnO	S	CaF_2	
Start	50.0	18.0	18.0	8.0	0.50	0.30	0.20	1.09	2.3	–
End	46.47	11.50	32.20	14.87	0.07	1.58	0.34	1.73	1.9	3.73

Table 4. Technological parameters of the individual stages of ladle treatment of St2 rail steel in the LSF

Ladle treatment stage						Total parameters of stage A and B			Mass of slag, t
Formation of slag (A)			Alloying of metal (B)			Duration, min: s		Electric energy consumption	
Duration, min: s		Electric energy consumption	Duration, min: s		Electric energy consumption				
Stage A	Work under current		Stage B	Work under current		Stage A and B	Work under current		
Current technology, melt. 1134863									
25:03	10.07	3430	29:00	10:14	3620	54:02	20:21	7050	2.71
Experimental melt No. 1134865									
5:06	3:09	1140	40:24	10:59	3520	47:49	14:08	4660	3.73
Experimental melt No. 1134867									
8:56	3:00	1060	46:41	13:06	3460	55:37	16:06	4520	3.76

concentration in the slag from 0 to 10% is shown in Fig. 3 which gives the experimental values of α_{FeO} taking into account f_{FeO} for the individual samples of the ladle slag of 70 melts with different contend of CaF_2. The molar fraction of FeO in the slag (N'_{FeO}) is calculated using the method proposed by N.M. Chuiko, based on the serial structure of the slags is a system with partially associated molecules [9].

Figure 3 shows that the activity of the iron oxide of the slags with CaF_2 of less than 2.5% is 1.5...2.0 times lower than in the slags with the high concentration of CaF_2 (5…10%). On the basis of the experimental studies and processing of the results in [8] it was concluded that it is not necessary to use the fluorspar for the audacity of the slag, especially prior to discharging the steel, and that the slags, containing calcium fluoride, should be the oxidised more thoroughly to obtain the FeO content 0.2%.

The increase of the amount of CaF_2 in the composition of the refining slags in the LFS to 15...20% (the conditions used in many plants for ladle treatment) create suitable conditions for the development of the processes of evaporation of CaF_2, fluorides SiF_4, AlF_3, which results not only in the unstable composition of the slag and during ladle treatment [4], but also increases the number of the ionised particles in the parking channel thus increasing the length of the arc with the possible melting of the slag belt of the lining of the ladle. The minimisation of the content of CaF_2 to 2...5% reduces the ionic component of the specific electrical conductivity of the slag melt of the CaO–Al_2O_3–MgO–SiO_2–Ca_2, so that it is possible to increase the thermal power, generated in the slag and, consequently, the heating rate of the steel.

Thus, the analysis of the experimental results shows that the presence of CaF_2 in the composition of the refining slags does not lead to the formation of the fluoride-containing associates at the temperature of the steel melting process, but increases the

fluidity of the slag melt with the thermal 10 expansion of the concentration fields of the existence of CaO-containing phases of the $CaO–Al_2O_3–SiO_2$ systems, which accelerates the simulation of the limestone by the melt already in the early stages of slag formation.

The results of pilot plant melts of rail steel produced with changes in the conditions of adding fluorspar

Two experimental melts of electric steel St2 (GOST 10791–2011) were produced using the currently available technology of melting the metal-semifinished product in the DSP-190 furnace with ladle treatment of 160 t of metal in the LFS with vacuum treatment. The difference between these experimental melts in the existing technology is the addition of fluorspar (approximately 1 kg per melt) to the steel casting ladle during discharge of the metal-semifinished product from the ladle, but not after treatment in the LFS. The temperature of the metal-semifinished product prior to discharge from the furnace was 1665 (basic), 1628 and 1633°C (experimental melts number 1134865 and 1134867. The amount of the deoxidation, alloying and carburisation agents in each melt was approximately the same (Table 1).

The mass of the slag in the ladle in the LFS was approximately 3.7 t or 2.3%. At the given basicity of the slag the amount of the slag influences the final sulphur content of the steel. The chemical composition of the metal–semifinished product prior to discharge from the furnace and the rail steel in the stages of LFS and in vacuum treatment are presented in Table 2.

The furnace slag prior to discharge of the metal–semifinished products from the furnace is characterised by a high content of iron oxides (34.2% calculated for Fe_2O_3). The metal with 0.08% C and 0.007% Si prior to discharge from the furnace was characterised by a high content of oxygen dissolved in it (0.096%). Preliminary deoxidation of the metal–semifinished product with aluminium in the amount of 0.9 kg per 1 t in the DSP 190 furnace prior to discharge resulted in a decrease of the degree of oxidation of the metal and a high degree of pickup of the elements in the alloying of the metal in the ladle prior to treatment in the LFS: the burn-out of silicon and manganese was respectively 10 and 5%.

The aluminium, added to the ladle in the LFS in the amount of 45 kg (0.3 kg/t) was almost completely used for the deoxidation of the slag, as confirmed by the increase of the content of Al_2O_3 in the slag during treatment of the metal in the LFS (Table 3).

It should be mentioned that the requirements of the GOST 10971–2011 inter-governmental standard do not control the aluminium content in the rail steel and, at the same time, the application of aluminium in final deoxidation of the steel is greatly restricted because of the probability of formation of corundum band inclusions in the metal which initiate the propagation of fatigue cracks as a result of alternating cyclic loading during service of the railway wheels.

After discharge of the metal–semifinished products into the steel casting ladle, the sulphur content of the metal of the melt No. 1134865 decreased from 0.048 to 0.026% prior to placing the ladle in the LSF, and after completing the treatment it again decreased to 0.00 4%. In treatment of the steel in vacuum equipment below the LFS slags, the sulphur content decreased from 0.004 to 0.002%.

The degree of desulphurisation in these stages of treatment was 45.8 (the furnace – reception ladle); 84.6 (treatment in LSF); 50% (vacuum treatment). The final indicator of the degree of desulphurisation of the metal with a change of the conditions of adding fluorspar in this melt was equal to 95.8% which corresponds to the parameters of this technology.

The content of CaF_2 in the refining slags for ladle treatment in the experimental melts was 3%. The change of the conditions of adding the fluorspar, regardless of the increase of the mass of the refining slag in

the LFS by 37%, in comparison with the current technology parameters decreased by 34% of the specific consumption of electric energy in the LFS stage from 43.7 to 28.7 kW·h/t (Table 4).

As indicated by the data in Table 4, a significant contribution to the decrease of the energy losses is provided in the stage of slag formation, resulting in a decrease of the total operating time of the LFS under current.

The resultant reduction of the specific consumption of electric energy is explained by the formation of a homogeneous slag already in the stage of discharge of the metal–semifinished products from the furnace as a result of the addition of fluorspar resulting in the dissolution and assimilation of limestone by the slag melt of the $CaO–Al_2O_3–MgO–SiO_2–CaF_2$ system.

Conclusions

1. The structure of the continuous technological procedure of production of the rail steel in the conditions of the electric steel melting of the Dneprostal' plant was analysed with special attention paid to the main assumptions of the technology for each stage: melting of the metal–semifinished products in the DSP-190 furnace, deoxidation, alloying and carburisation of the metal in the steel casting ladle, additions of slag-forming elements in the formation of the primary ladle slag with subsequent treatment of the metal in the LFS and vacuum treatment.

2. The physical-chemical assumptions of the rational regime of adding solid materials to the ladle are discussed and special attention is given to the problems of formation of the oxide–fluoride slag melt. The fusibility diagrams of the $CaO–CaF_2$, $Al_2O_3–CaO$ binary systems are analysed. It is shown that the content of CaF_2 in the composition of the basic slag does not influence the thermodynamic conditions of the desulphurisation reaction, but determines the physical-chemical characteristics of the oxide-fluoride melt and the kinetics of mass-exchange processes in the metal–slag system.

3. The $CaO–Al_2O_3–SiO_2$ oxide–fluoride-calcium system with 10% CaF_2 is analysed, and the results show that the presence of the fluorspar in the stage of formation in the steel casting ladle of the slag from the added solid materials results in the assimilation of limestone and, consequently, increases the desulphurisation capacity of the slag.

4. Experimental melts of the rail steel were produced and the processes of slag formation with the addition of the fractionated limestone, combined with the fluorspar in the steel casting ladle and during the discharge of the metal–semifinished product with a mass of 160 t from the DSP-190 furnace were investigated.

5. The experimental results show that the change to conditions of treatment of the metal–semifinished product with solid materials in the ladle using approximately 1 kg/t of the fluorspar results in accelerated assimilation of the limestone and early formation of the homogeneous slag prior to placing the ladle in the LSF, together with the active process of desulphurisation with a 30–35% decrease of the specific consumption of electric energy in the LSF stage.

References

1. Esaulov, G.A., et al., Metallurg. Gornorud. Promst', 2013, No. 4, 20–28.
2. Kravchenko, Yu.S., et al., Elektrometallurgiya, 2008, No. 1, 38–44.
3. B udnikov, P.P., Tresvetskii, S.G., DAN SSSR, 1953, **89**, No. 3, 479–482.
4. Eitel, W., Physical chemistry of silicates, IL, Moscow, 1962.
5. Toropov, N.I., Barzakovskii, V.P., Izv. AN SSSR, Moscow, 1963, 258.
6. Zaitsev, A.I., et al., Neorg. Mater., 1998, **34**, No. 1, 80–88.
7. Zaitsev, A.I., Mogutnov, B.M., In: Fundamental studies of physical chemistry of metallic melts, Akademkniga, Moscow, 2002.
8. Chuiko, N.M., Rutkovskii, V.B., Izv. VUZ, Chern. Metall., 1960, No. 6, 14–16.
9. Chuiko, N.M., Chuko, A.N., Theory and technology of electric melting of steel, Golovnoe Izd., Kiev, Donetsk, 1983.
10. Gasik, M.I., et al., Metallurg. Gornorud. Promst', 2011, No. 5, 20–29.

Submitted 2.12.2013